Master Thesis

Schematisation of discharge time series in morphodynamic river models

S.J.H.A. Gradussen

TU Delft

;

Cover photograph: View of the 'Ooijpoort' pedestrian bridge located in a floodplain area near Nijmegen. The photograph is taken during a high water period in January 2018. Courtesy: Sam Peeters, Nieuwsredactie

Schematisation of discharge time series in morphodynamic river models

by

Sebastiaan Johannes Henricus Andreas Gradussen

Master thesis
to obtain the degree of Master of Science
at the Delft University of Technology
to be defended publicly on the 21st of June, 2019

Student number: 4523393

Graduation committee

dr.ir. A. Blom	Delft University of Technology	*Chairman*
dr.ir. R.J. Labeur	Delft University of Technology	
dr.ir. C.J. Sloff	Delft University of Technology / Deltares	
ir. H.J. Barneveld	HKV Consultants	

Preface

The 3rd of August 1994 I crossed the river Waal for the first time in my life. Going home after being born in the hospital in Nijmegen, I must have catched a glimpse of the river Waal. Perhaps that was the moment where my fascination for rivers began. In the years that followed, I have always been amazed by the impact of rivers and impressed by how these natural features might form a threat, but on the other hand how rivers can be extremely valuable for society. This was one of the main reasons why I made the decision to devote my master's study to the field of river engineering. I am very fortunate that by means of this thesis, I finalise a precious period of my life. I would not have been able to succeed without the help of many people that have been supportive, suggestive, carrying and always optimistic. Therefore, I want to express my gratitude to a number of people in personal.

Firstly, I would like to thank my graduation committee. Their knowledge and field experience is extremely valuable. Astrid Blom, Hermjan Barneveld, Kees Sloff and Robert Jan Labeur have been an inexhaustible source of inspiration, insight and useful feedback. I want to thank Astrid Blom for being my daily supervisor, the many reviews of my work, her patience and the personal support during the past year. Finally, Liselot Arkesteijn inspired me during the first months of the project.

Deltares provided me with all the tools and coffee I needed. Especially, the access to their Linux cluster was very useful. Willem Ottevanger helped me during the first months with setting up the numerical model and saved me from many headaches. Besides, several people from the research group of river engineering at the TU Delft were always open for conversation. I want to thank Meles Tewolde and Victor Chavarrías for their insights and resources.

During my study in Delft, my family, friends and roommates have been indispensable. In particular, Max Capelle and Wouter van Adrichem helped me with text reviews and provided necessary feedback on my work. I want to thank my parents Hans and Marjo and my sisters Manon and Marlou for their involvement. I cannot imagine a better home. Finally, I am very grateful to Merel. Your optimism and everlasting support kept me going.

Bas Gradussen
Delft, June 8, 2019

Courtesy: waterpeilen.nl

Abstract

River discharge is an essential parameter in morphodynamic modelling. It proves to be highly variable in both time and space. In this thesis the impact of the schematisation of time-dependent discharge series on morphodynamic change is studied. The impact is governed by several factors such as the long-term discharge statistics, and both short- and long-term sequences of discharge stages. A variable river discharge itself does not necessarily result in morphodynamic change. Changes in conveyance area and roughness are dominant sources of bed fluctuations and bed waves. Moreover, backwater dominated segments are subject to mild fluctuations in the river bed.

The combination of natural variation of hydrological processes in the upstream river catchment and the absence of a significant correlation among statistical characteristics of subsequent years makes it hard for river engineers to construct discharge time series for river models that simulate morphodynamic development. The limited predictability of future discharge time series is an important source of uncertainty in model predictions. A way to estimate this uncertainty is by means of a time-consuming Monte Carlo approach, resulting in a mean long-term morphodynamic trend and the associated uncertainty. An alternative method is the application of a deterministic series for which the long-term discharge statistics are translated into a cycled annual hydrograph (CAH). It is expected to yield similar morphodynamic changes with respect to the mean trend from the Monte Carlo approach without the need for a large number of computations. However, as is demonstrated in this study, the CAH-method lacks in performance in simulating average long-term development and the amplitude of fluctuations in the river bed, especially at locations where strong sediment transport gradients are experienced.

Using a simplified two-dimensional model that represents a locally widened floodplain, the impact of the included bandwidth, short-term and long-term sequences on morphodynamic change is investigated. The aim is to improve the deterministic hydrograph schematisation and to find a more convenient way to get insight into uncertainty in simulated morphodynamics. These findings result in a set of recommendations for future schematisations of discharge time series in morphodynamic river models.

An improved deterministic approach is proposed. Using historical measurements of daily discharge data, years with a similar statistical maximum, mean and standard deviation can be classified. The classified years are translated into multiple cycled annual hydrographs (MCAH). By using these hydrographs, synthetic time series are constructed. Compared to the CAH-approach, the proposed MCAH-method yields a significant reduction of the root mean square error with respect to the long-term average morphodynamic trend from the Monte Carlo simulations. Moreover, the MCAH-series result in amplitudes of bed fluctuations that are closer to the response to natural discharge time series. Finally, the MCAH-series can be used to give a rough indication of the uncertainty in future morphodynamics.

Contents

CHAPTER 1

Introduction

1.1 Context and problem statement

Computational models are becoming increasingly important for the assessment of morphodynamic evolution of river systems all over the world. These models are simplified, mathematical representations of geometries and natural processes. Since the very first morphodynamic models were created in the 1980's, their application has been intensified. According to H.J. Barneveld (personal communication, 2019), the urge for using morphodynamic models increased among Dutch river managers and engineers mainly after experiencing the need for making forecasts related to inland navigation and after experiencing ongoing erosion problems in Dutch rivers. Bed degradation of 1-2 cm/year along the Dutch parts of the river Rhine is the consequence of training works that were constructed to provide amongst others suitable conditions for inland shipping (Blom, 2016).

Recently, multiple large river interventions were executed in the Dutch river system, under the collective name of Room for the River (RfR) projects. These projects were designed with the aim to increase flood conveyance and to provide high spatial quality (Ruimte voor de Rivier, 2018). A large number of measures in combination with their spatial scales is expected to induce a significant impact on the river system (e.g. Van Vuren et al., 2015). This impact manifests in terms of amongst others long-term trends in bed level change and short-term fluctuations around these trends. The possible large-scale impact of river interventions emphasises the need for reliable morphodynamic models to evaluate future effects on the river system. This thesis focusses on the application of time-dependent discharge boundary conditions on morphodynamic models of engineered rivers. The considered processes are purely longitudinal. The studied timescales are of orders of years up to decades and the associated spatial scales are of orders of $10^3 - 10^5$ m.

River discharge is of major influence on the morphological evolution of a river. River managers and engineers therefore face the challenge of composing a well-considered representation of the river discharge when performing morphodynamic simulations. The discharge proves to be variable in both space and time (Figure 1.1). The natural variation of hydrological processes in the river catchment and the absence of a significant correlation among

subsequent years of discharge observations (Van Gelder et al., 2000), are dominant causes of the limited predictability of future discharge time series. Consequently, the inclusion of discharge time series contributes to uncertainty in modelling future morphodynamics.

(a) **(b)**

Figure 1.1: (a) View of the river Waal at the Bemmelse Waard (top) and at Nijmegen (bottom) during a discharge stage of 3030 m^3/s that just exceeded bankfull discharge; Date: March 23., 2019. **(b)** View of the same locations, during a discharge stage of 1100 m^3/s; Date: April 22., 2019 [courtesy: personal collection].

In fact, uncertainty in model input (and model output) has many origins. Van Asselt and Rotmans (2002) distinguish between the following categories: 1) variability, which is inherent to the highly random character of nature and 2) limited knowledge, which is related to amongst others quality and frequency of measurements, model simplifications and empirical relations. This thesis focusses only on the uncertainty that is induced by the limited predictability of future river discharge time series on longitudinal morphodynamic evolution. Moreover, this study only addresses the influence of discharge time series without considering the impact of climate change.

In order to compose future discharge time series, the river engineer must be fully aware of the model impact of parameters that define time-dependent variability of river discharge, such as the long-term statistics of discharge, and the influence of short-term and long-term sequences of flow stages. Depending on the expected morphodynamic change and the time scales one is interested in, multiple approaches exist for imposing the upstream discharge boundary condition. For example, one often imposes a dominant, or *forming* discharge when modelling equilibrium states of rivers (e.g. Wolman and Miller, 1960). However, many studies (e.g. De Vries, 1965) disapprove the use of a constant discharge being representative for the variable discharge when simulating river morphodynamics. The main reason for that is the fact that a wide variety of time scales of morphodynamic processes prevails in river systems. Consequently, a single discharge cannot yield similar morphodynamic change of all these different processes as would be found with a variable discharge (Buffington, 2012; Blom et al., 2017).

Instead of a constant discharge, discharge time series are more commonly applied. Several approaches exist for composing discharge series: 1) cycled or repeated historical series (e.g. Ottevanger et al., 2015); 2) synthetically generated series (e.g. Van Vuren, 2005) and 3) the deterministic approach (e.g. Yossef and Sloff, 2012) for which one cycled annual hydrograph (CAH) is used that is based on the long-term discharge statistics.

Besides imposing a single time series, a probabilistic Monte Carlo method has become a frequently used concept (e.g. Van Vuren et al., 2015). This method requires a large number of historical or synthetic discharge time series (realisations). The advantage of the Monte Carlo method is that it results in an *average* long-term morphodynamic trend of all the imposed realisations. Moreover, it provides an indication of the uncertainty around this long-term trend in terms of a confidence interval. Uncertainty in future river morphodynamics can be of large interest for river managers: it might contribute to the planning of maintenance strategies for the upcoming future (Van Vuren et al., 2015), or support risk assessments on the impact of river interventions. The main disadvantage of a probabilistic Monte Carlo method is the required computational effort, since many computations have to be performed. Therefore, in order to get an indication of only the long-term morphodynamic trends, engineers often use the deterministic CAH-approach, which aims to result into a similar long-term morphodynamic development as the *average* long-term trend that yields from a probabilistic Monte Carlo simulation. However, as Huthoff et al. (2010) demonstrate, this similarity in long-term morphodynamic development is not necessarily observed in model simulations. The typical problem river engineers encounter is schematised in Figure 1.2.

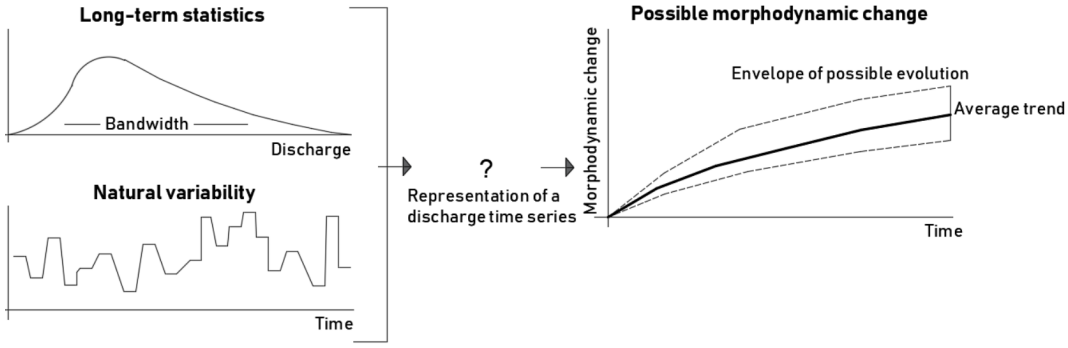

Figure 1.2: Schematised challenge for river engineers when constructing discharge time series in morphodynamic river models.

In general, it is not just variability in river discharge that governs morphodynamic change. Other important features are necessary for these dynamics: variability in sediment flux, (sudden) spatial changes in cross-sectional properties (geometry and roughness) and the presence of backwaters, inducing gradients in sediment transport. Bolla Pittaluga et al. (2014) discuss that, besides the forcing by river discharge and sediment flux, non-homogeinities in the cross-section along the longitudinal direction are essential forcing mechanisms with respect to morphodynamic change. River interventions, such as RfR-projects, often introduce such changes in the cross-sectional geometry that cause long-term trends, fluctuations and propagating bed waves under the influence of unsteady forcing.

Problem statement

River discharge is a complex parameter in river modelling. It induces uncertainty in modelled morphodynamics due to its limited predictability. A robust way to get insight on the *expected* long-term morphodynamic change as well as the associated uncertainty, is the use of a Monte Carlo simulation. This approach is time-consuming due to the required number of realisations. The deterministic cycled annual hydrograph (CAH) is a method that requires less effort as only one realisation is needed. It aims to model similar long-term morphodynamic development as would be obtained with the Monte Carlo simulations. However, the similarity between the average trends from both the probabilistic Monte Carlo simulation and the deterministic CAH-approach is not necessarily observed in morphodynamic simulations. Since the deterministic approach is a convenient concept due to its limited computational effort compared to the Monte Carlo simulation, finding an improved deterministic approach is desirable. Moreover, finding a convenient model strategy that yields insight on the uncertainty in modelled morphodynamics is valuable. In order to do so, insight on the various factors that define the variability of river discharge, such as long-term and short-term sequences, and their implication on morphodynamics has to be increased.

1.2 Objective and research questions

This study aims to study the performance of the CAH-approach compared to the modelled morphodynamics with the Monte Carlo method. With the goal of improving the CAH-approach, factors that define discharge variability and their impact on medium- to large-scale morphodynamics are studied. This insight will be used to setup improvements and recommendations for future application and schematisation of discharge time series in morphodynamic models of engineered rivers on timescales of years up to decades and according spatial scales of $10^3 - 10^5$ m.

The following four research questions will be answered during this thesis:

1. What is the origin of variability in river discharge and what is its relevance with respect to morphodynamic change?
2. Which approaches exist in the current practice for imposing the upstream discharge boundary condition?
3. To what extent does discharge variability, as well as the model approach for upstream discharge time series, impact medium- to large-scale morphodynamics?
4. Which recommendations can be made for future application and schematisation of the upstream discharge time series in morphodynamic river models on timescales of years up to decades?

1.3 Approach and thesis structure

The structure of this report builds on the structure of the research questions. Chapter 2 focusses on the first research question and gives an introduction into variability in river discharge and its theoretical implications on river morphodynamics. The study is substantiated with several statistical analyses of data sets of daily discharge observations at measuring stations along the German Rhine. For answering the second research question

in Chapter 3, an overview will be given of a set of common approaches that are used to impose upstream discharge boundary conditions, based on literature research and the evaluation of earlier studies and reports. The essential considerations that have to be taken into account when composing the upstream discharge boundary condition will be discussed. In Chapter 4, a conceptual study is conducted to find answers to research question 3. A typical RfR-intervention is modelled by means of a conceptual model setup: a locally widened floodplain, resulting in a spatial change in width of the floodplain over a length of 3 kilometers. A simplified two-dimensional model is constructed of which the geometry, discharge data and sediment characteristics are roughly based on the Dutch Upper Rhine. A Monte Carlo simulation consisting of 20 realisations is performed. The morphodynamic change that results from the deterministic cycled annual hydrograph (CAH) is compared to the results from the Monte Carlo simulation and the differences are discussed. Several factors that define time-dependent variability in river discharge are investigated. Based on the findings from Chapter 4, an improved deterministic approach (the multiple cycled annual hydrographs (MCAH-) method) is proposed in Chapter 5 and its performance is studied and compared to the results from the Monte Carlo simulations. Chapter 6 provides a discussion. Finally, in Chapter 7, the findings of Chapters 2, 3, 4 and 5 are combined into a synthesis and recommendations for the schematisation of discharge time series in river models that simulate morphodynamics on time scales of years up to decades. The structure of this thesis is schematised into Figure 1.3.

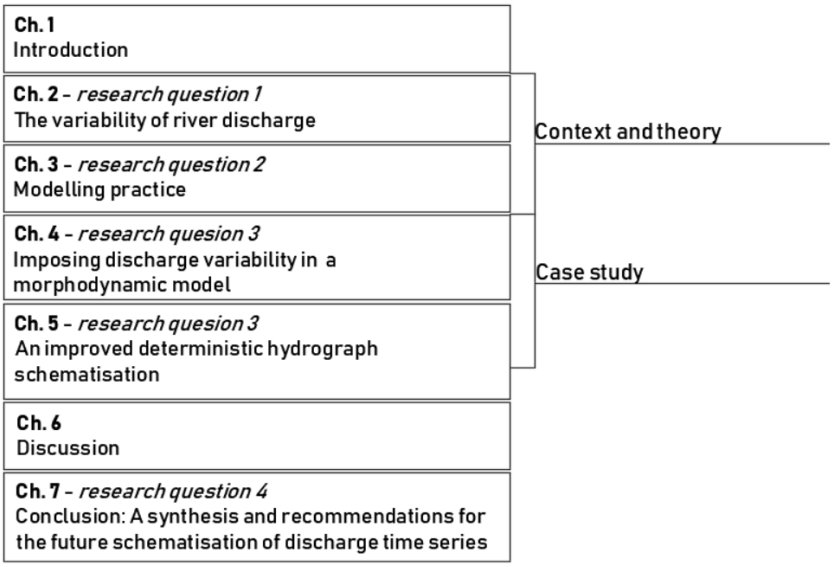

Figure 1.3: Structure of this thesis

CHAPTER 2

The variability of river discharge

This chapter addresses the context of variability in river discharge. It discusses the origin of variability in river discharge, the (statistical) properties and the implications on morphodynamic change in rivers.

2.1 The origin of variability in river discharge

River discharge is dependent on both natural and anthropogenic sources in the upstream catchment area of the river system. It depends on time and space (Montanari, 2012; Poff et al., 1997). An important contribution to the variability is delivered by upstream tributaries and natural processes such as the melting of snow and glaciers, precipitation, evapotranspiration and groundwater flows. Human-induced hydrological processes such as civil and industrial water use, irrigation and groundwater exchange are of influence on the variability of discharge as well (Montanari, 2012). Figure 2.1 illustrates the major processes and fluxes that influence river discharge.

Many time scales can be observed regarding the variability of discharge. Montanari (2012) distinguishes between intra-annual and inter-annual periodicities, indicating that not all discharge events show periodic behaviour within one year of discharge observations. Intra-annual cycles are seasonal variations. Inter-annual sequences cover multiple years. Wolman and Miller (1960) already noticed discharge events with a recurrence frequency of once in 50-100 years, calling them 'catastrophic flood events'. Other long-term persistent hydrological events that currently still lack a physical explanation are so-called Hurst-Kolmogorov events (e.g. Hurst, 1951). Regarding the latter, it is questionable whether one can speak of actual periodic events, or one rather observes long term autocorrelation of discharge sequences that resembles all statistical fluctuations that can be found on the time scale of the order of 50-100 years. These Hurst-Kolmogorov events represent the high uncertainty of various hydrological processes that influence river discharge such as temperature, precipitation, humidity and atmospheric pressure (Dimitriadis, 2017). Since there is not much data on hydrological and discharge features of river systems for periods longer than 100 years, validation of this theory is hardly available.

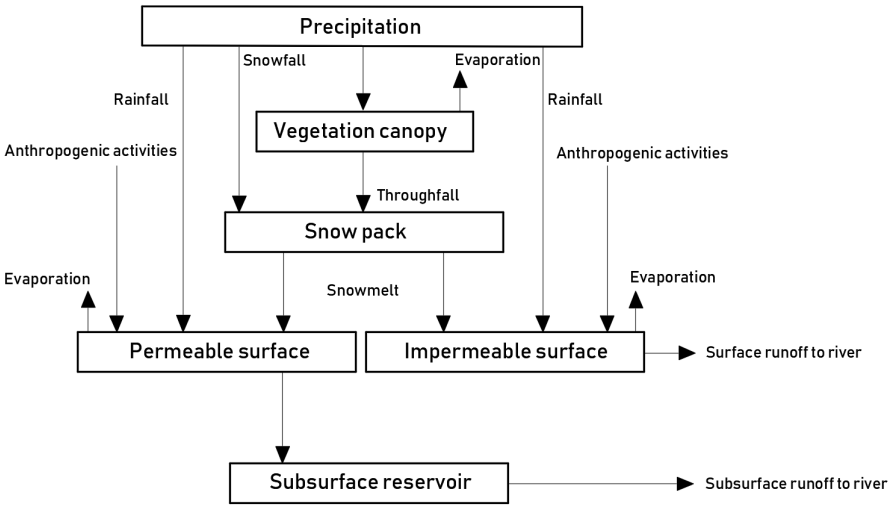

Figure 2.1: Processes and fluxes that govern runoff in a basin (after Bowers et al., 2011)

Besides the hydrological processes, geological features have an impact on the time-dependent variability of discharge as well. Amongst others, Wolman and Miller (1960) mention that river discharge is likely to become increasingly variable if the catchment area decreases and less tributaries deliver water to the main stem. The more tributaries are connected to the main stem, the more likely it is that during dry low-flow periods of some tributaries, other tributaries will compensate for this low discharge and make the discharge in the main stem less variable.

The timing of the typical annual discharge cycle also varies spatially. Hegnauer et al. (2014) mention the shift of annual cycles and peaks in time when moving from the upper basin to lower reaches. The yearly averaged peaks at the observation stations in the upper basin are dictated by the spring snow melts. These melting events dominate contribution due to local precipitation events. In the lower reaches of the river, these yearly averaged peaks are dominated by (more local) autumn-winter precipitation events. Reaches in between often show on average two yearly peaks, in which both the melting of snow and ice upstream and more local precipitation are distinguishable. Hence, once can speak of a combination of geological and meteorological factors that are responsible for this spatial variation. This is demonstrated for the German part of the river Rhine. Figure 2.2 illustrates 9 locations for which daily discharge observations from 1950-2013 (Global Runoff Data Center (GRDC), 2018) are used.

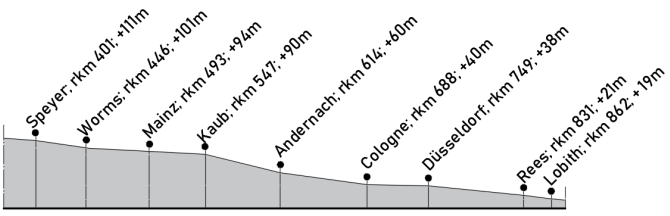

Figure 2.2: Longitudinal section of the German Rhine with the studied observation stations [source data: NL Rijnpatent; USGS, 2018].

Figure 2.3 shows a contour plot that illustrates the normalised mean daily discharge over the years 1950-2013 for the nine observations stations from Figure 2.2. The data is normalised with respect to the maximum mean daily discharge over 1950-2013 at that specific station. This illustrates the different timing of high and low water periods between the observation stations. The peaks in mean daily discharge in the downstream reach of the German Rhine (Rees, Lobith) are indeed found in the late autumn and winter season, whereas the largest average flow rates upstream (Speyer, Worms) were measured during the late summer season. At intermediate stations (Mainz, Kaub, Andernach) peaks are observed during both the early spring and summer season.

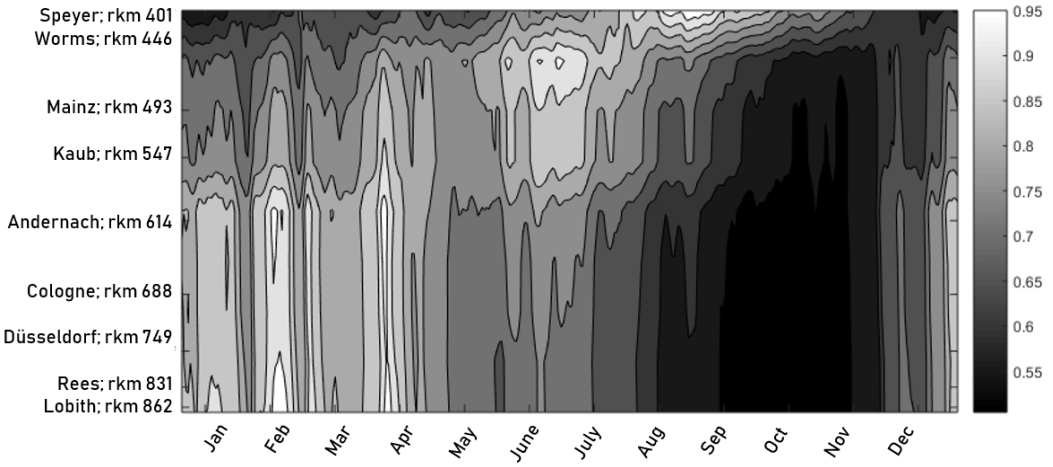

Figure 2.3: The mean daily discharge throughout the year over the period 1950-2013 is normalised with respect to the maximum of the mean daily discharges at that specific location. This normalisation is performed for all observation stations along the German Rhine that are presented in Figure 2.2. A Gauss filter is applied to smoothen the contours, explaining why the maxima are not found at 1.0, but at 0.95 [source data: GRDC, 2018].

2.2 The statistical properties of river discharge

This section considers the long-term time series, seasonal variability, long-term statistics and the daily statistics for the discharge data of the river Rhine as measured at Lobith.

2.2.1 Obtaining discharge data

In the previous section the daily discharge data of the river Rhine that is obtained during the past decades is used for several analyses. It is important to state that it is not the river discharge itself that is measured at those observation stations. That would be a complicated and costly operation. Several practical alternatives exist. The two most common methods are addressed here. 1) The *velocity-area* method. By measuring both the flow velocity and water levels at one location, an estimation can be made of the according discharge by multiplying the (estimated) average flow velocity (U_{av}) with the cross-sectional area (A_{cross}) that follows from the water level and cross-sectional profile ($Q = U_{av} * A_{cross}$). 2) Another common method is the use of a *Q(h)*-relationship. This relationship can be constructed by using scale models or using direct calibration measurements from the field. By measuring

only the water levels, one can read the matching discharge from the *Q(h)*-relationship (Van den Houten et al., 2010). Both methods need to be updated and re-calibrated continuously as the river cross-section changes in time.

The fact that different river management authorities use different measurement techniques and model calibration results in non-uniformity among data sets. An example of these differences is observed in the GRDC (2018) discharge data set when comparing the long-term discharge statistics over the period of 1951-2010 for the observation stations at Rees (located in Germany) and at Lobith (located in the Netherlands). Lobith is located approximately 30 kilometers downstream of Rees. In between, no confluences or bifurcations are present. It is remarkable that according to this data set a mean daily discharge of 2324 m^3/s can be derived at Rees, whereas the mean daily discharge at Lobith is lower, based on the GRDC-data set: 2245 m^3/s.

Moreover, inaccuracies in measurements and calibration procedures, make the translation of measurements of water levels and flow velocities into a discharge magnitude a source of uncertainties.

2.2.2 Daily statistics and seasonal variability

Many hydrological processes in the upstream basin show time-dependent variations due to the inherent natural variability. Despite the (not entirely) random nature of these processes, periods of low and high water can often be characterised throughout the year, as is shown in Figure 2.3. The yearly, statistical structure of the river Rhine at Lobith is shown Figure 2.4.

The daily mean shows a gentle fluctuation throughout the year, implying the yearly, seasonal variability of the river. The extreme observations show a lot more variation. The 90%-confidence interval around the daily mean is wider in the wet season (late autumn up until the end of the winter), than during the dry season. From this, the river flow appears to be more variable during the wet season than during the dry season.

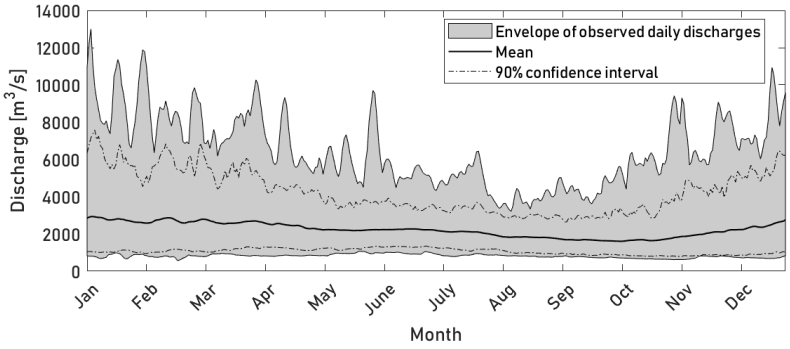

Figure 2.4: Daily statistics for the daily discharge observations at Lobith from 1901-2010, including the daily mean, the 90% confidence interval and the envelope of all observations [source data: GRDC, 2018].

2.2.3 The long-term statistics

The collection of discharge data for a long period results in the long-term discharge statistics, characterised by heavy-tailed distributions such as exponentional-, but more often, lognormal-type of probability distributions (e.g. Chow, 1954). Lognormal distributions have the feature that they contain only non-negative valued variables. These distributions

are skewed and can be fully described by two parameters: 1) a statistical mean, and 2) the standard deviation (Lane, 2013).

The daily discharge observations at Lobith from 1901-2010 result in the lognormal probabilistic distribution as presented in Figure 2.5.

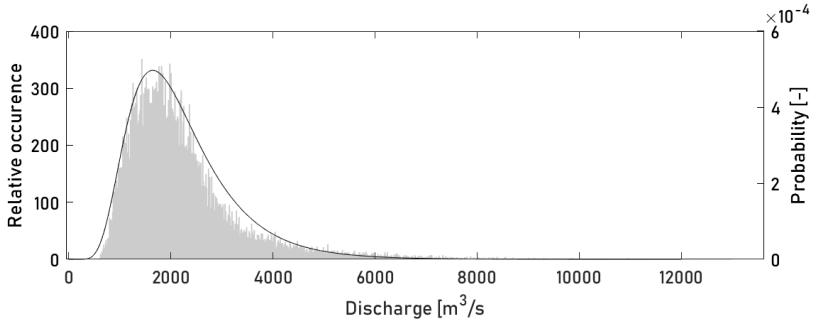

Figure 2.5: Histogram (gray) and the empirically fitted lognormal distribution (black) for the discharge data of the river Rhine, measured at Lobith from 1901-2010; Mean: 2222 m^3/s, standard deviation: 1139 m^3/s [source data: GRDC, 2018].

This distribution is obtained for daily discharge measurements. In many cases, such a rich collection of measurements is not available, and the discharge is measured less frequently. This leads to a decrease in resolution of the distribution as (extreme) discharge events with a relatively short duration might not be observed. To understand how this might affect the long-term statistics, the discharge data set as measured at Lobith 1901-2010 is modified. This is demonstrated as follows. Table 2.1 summarises the statistical parameters of four different probabilistic distributions of the river Rhine, all measured at Lobith. The first collection is described by the daily measurements, similar to Figure 2.5. The second, third and fourth are composed from discharge measurements intervals of one week, one month and two months respectively. For the studied data set, it appears that a decrease of the measuring frequency causes a slight shift in the statistical mean. The difference in standard deviation is however more significant. This can be related to the observations from Figure 2.5. The daily mean shows a gentle fluctuation throughout the year, whereas the 90%-confidence interval shows more significant variations throughout the year. Another explanation is the fact that by decreasing the measuring frequency, it is more likely that extreme (either high or low) discharge events are excluded in the data set, since the typical time scale of these events is in the order of days to weeks. As Huthoff et al. (2010) describe that the standard deviation of a data set is more sensitive to rare events than the mean.

Table 2.1: Statistical parameters for four different measurement frequencies at Lobith for the years 1901-2010 [source data: GRDC, 2018].

Measurement frequency	**Long-term mean** [m^3/s]	**Long-term std.dv.** [m^3/s]
Daily	2222	1139
Weekly	2220	1136
Monthly	2236	1164
Two-monthly	2285	1239

Establishment of the long-term statistics

An important consideration when composing a statistical data set, is the number of observations needed to obtain a well-established long-term mean and standard deviation that do not change significantly due to the influence of individual, extreme events. This is investigated for the daily discharge data for the river Rhine as measured at Lobith over the period 1901-2010. When starting in 1901, the establishment of the mean and standard deviation is presented in Figure 2.6. The red lines represent the 5% interval around the long-term mean and standard deviation of daily discharge measurements.

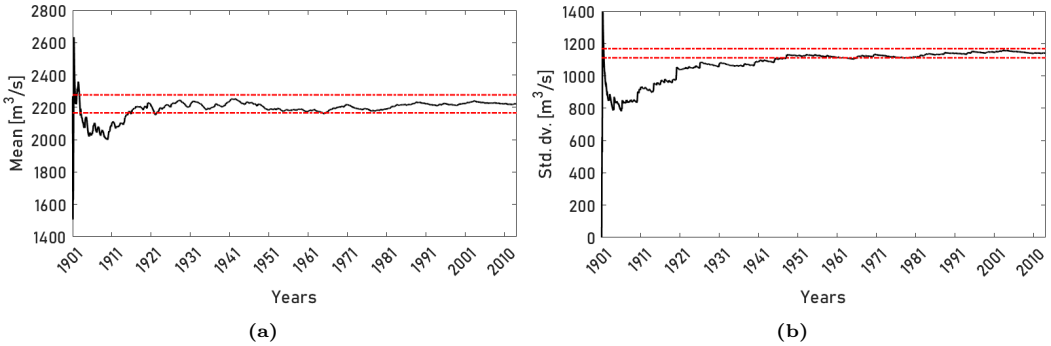

Figure 2.6: Establishment of **(a)**the mean and **(b)** the standard deviation of the discharge series at Lobith (black solid line) with respect to the 5%-interval around the long-term value for the period 1901-2010 (red dashed lines) [source data: GRDC, 2018].

The mean tends towards a fairly constant value already after 10-20 years. For the standard deviation, it takes longer to reach a value that falls within the 5%-interval: 40-50 years. The standard deviation of the statistical record is more sensitive to extreme, individual events (Huthoff et al., 2010), which might explain the longer time needed to establish to a fairly constant value within the 5%-interval. The establishment is studied when starting at 1901 as well to text whether the selection of years influences the duration of the establishment of the long-term statistical parameters. Similar results are found if the same procedure would be executed, but starting from another year. More information can be found in Appendix A.

2.3 Characteristics that define discharge variability

In a mathematical sense, variability is defined as the extent to which statistical data is distributed around the mean (Lane, 2013). The statistical long-term variability of discharge is represented by its probability density function (PDF) as is shown in the previous section. However, the long-term statistics do not provide information on the sequences of subsequent events and years. As morphodynamics is dictated by bed material load (Jansen, 1979; Frings et al., 2014) and the interaction between river discharge and the associated variability in sediment transport (and therefore the river morphodynamics as well) is non-linear ($S \propto Q^b$), the sequence is regarded as an essential factor when studying morphodynamics. Sequences are build from discharge events with a certain magnitude and duration. Sequences can be observed on both intra-annual (within one year) and inter-annual (spanning multiple years) time scales (Montanari, 2012). These features will be discussed here briefly.

2.3.1 Discharge magnitude

In many studies it has been discussed that there is a relation between magnitude of discharge stages and morphodynamic evolution of the river system (e.g. Stall and Fok, 1967; Pizzuto, 1994). Both studies are based upon medium-term (20-40 years) discharge records in combination with data on morphological changes. General findings were that the relatively high discharges (by Stall and Fok (1967) defined as the 10 percent highest discharges of the record) are mainly responsible for the morphological development of the stream. Pizzuto (1994) drew the same conclusion for the highest discharges in the records, but extended the theory by stating that lower discharges have the property of restoring the morphology after rare, extreme discharge events. Van Denderen (2014) demonstrated this as well by using field data and numerical experiments and refers to this restoring feature as the *refilling* of local erosion pits that resulted from a flood event.

2.3.2 Duration of events

Costa and O'Connor (1995) state that it is not merely the magnitude of discharge and the associated sediment transport that impact morphological changes. They state that it is rather the amount of work performed by the stream that governs this development. This suggests that the duration of a discharge stage is expected to be of influence as well. Accordingly, not the highest discharges or transport rates are of main influence on morphological change, but rather the events with medium to large duration and magnitude (Wolman and Miller, 1960). This implies that morphodynamic change is mostly dictated by the mid-range of discharges in the probability density spectrum (Buffington, 2012; Costa and O'Connor, 1995; Blom et al., 2017). On the left side of the lognormal probabilistic distribution, there are low discharges with a relatively large probability of exceedance. Their impact on morphodynamic evolution is mainly limited by their relatively low transport capacity. On the right side of the spectrum, there are extreme discharges with a relatively large transport capacity that have a limited recurrence frequency. The latter causes the overall contribution of these extreme discharges to be of less significance.

2.3.3 Intra-annual and inter-annual sequences

In Figure 2.4 a moderate yearly fluctuation can be observed considering the daily mean throughout the year for the case of the river Rhine at Lobith. Besides this yearly cycle, other events can be distinguished in the discharge observations with a smaller periodicity than one year (intra-annual, such as floods and droughts, with a typical time scale of several days to weeks). According to Montanari (2012), events with a larger periodicity can be observed as well (inter-annual, such as long-term meteorological cycles).

In order to study whether repetitive patterns, dependency structures or whether a correlation can be traced among subsequent short- and long-term discharge sequences, additional analyses are conducted using the discharge data set as measured at Lobith from 1901-2010. The autocorrelation function[1] is a useful concept for this purpose. Van Vuren (2005) found hardly any significant autocorrelation in discharge events on periods larger than 10 days in case of the river Rhine (Van Vuren, 2005). Figure 2.7 shows the autocorrelation function with respect to the considered time lag in terms of days. A significant autocorrelation can

[1] Autocorrelation is the cross-correlation of a signal with respect to itself, but one of the two compared signals is shifted over a certain time-lag. The concept is especially useful to evaluate correlations of events shortly after each other, or to find repetitive patterns.

be observed for a relatively short time-lag, as discussed by Van Vuren (2005). If the autocorrelation function is evaluated for a larger time-lag up to several years of discharge data, a repetitive pattern can be observed with peaks and troughs that occur approximately every 365 days. This indicates the repetitive pattern that is caused by the seasonal yearly cycle. It illustrates that the timing of high and low water periods shows similarities among the years. The autocorrelation is however rather weak, implying that the exact timing, magnitude and duration of events shows hardly any similarities between the yearly observations in the discharge data set.

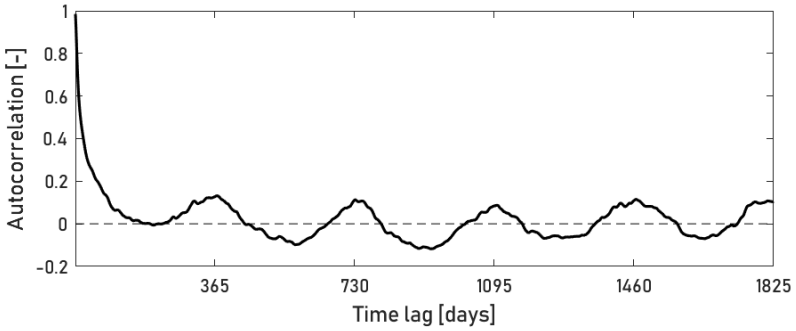

Figure 2.7: Autocorrelation function applied on the daily discharge data at Lobith for the years 1901-2010 [source data: GRDC, 2018].

To substantiate the finding that no significant autocorrelation can be traced between consecutive discharge hydrographs, the dependency and correlation of characteristic statistical parameters of subsequent years is evaluated. This is exhibited in Figure 2.8. The plots show the dependency and correlation of the yearly mean discharge (Figure 2.8a), the yearly maximum discharge (Figure 2.8b) and the yearly standard deviation (Figure 2.8c) of the of year i related to the subsequent year $i+1$. No dependency or significant correlation can be found for the three yearly statistical parameters between subsequent years. Van Gelder et al. (2000) also stated that no significant correlation is found for subsequent hydrographs at Lobith. This implies that one cannot make a prediction of the characteristics of the year $i+1$ based on the observations from year i. This emphasises the complication of composing discharge time series in morphodynamic models.

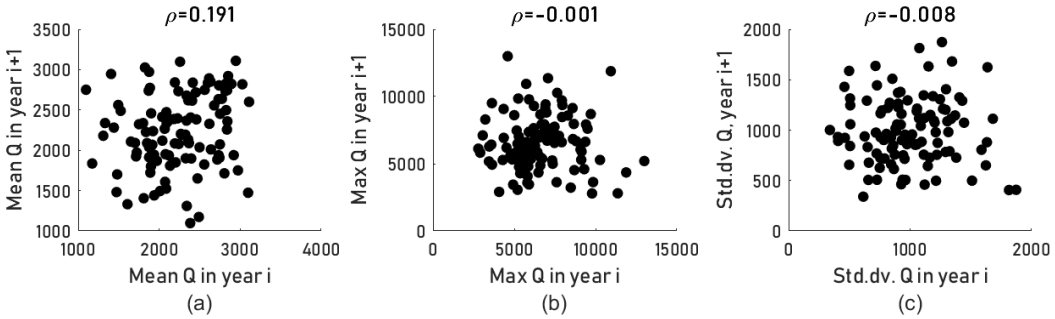

Figure 2.8: Dependency structures and the correlation of the **(a)** yearly mean discharge, **(b)** yearly maximum discharge and **(c)** yearly standard deviations of discharge between subsequent years i and $i+1$ for the discharge data set at Lobith for the years 1901-2010 [source data: GRDC, 2018].

Due to the non-linear interaction between discharge and morphodynamics, the sequence of subsequent events and years is a key characteristic for the morphology. This can be demonstrated with the following example. Assume the different years $Y_1, Y_2, ...Y_n$. Due to the absence of a dependency or significant correlation between statistical parameters among subsequent years, these years can occur in any sequence, without changing the statistical properties of the collection of years. Still, the different sequence leads to a different realisation of morphodynamic evolution. An important concept to explain this property is defined as the memory effect (e.g. Pickup and Rieger, 1979; Bolla Pittaluga et al., 2014). Pickup and Rieger (1979) explain this concept mathematically by stating that a future morphodynamic state is a convolution of the result of historical flow (flood) events. This implies that the future morphodynamic state is not only determined by the current forcing but also depends on the current morphodynamic state which has been formed by previous years of forcing. The contribution of a historical flow state has a decreasing weight in time, meaning that the memory effect of a discharge event fades away in time. Bolla Pittaluga et al. (2014) investigated a similar theory using a model study of the Magra river. They studied the fading impact of floods that disturbed the bed topography locally. The effects of the previous floods were still noticeable several years later, but the impact of the historical floods indeed showed a fading character.

Due to the time needed for the memory of previous flood events to vanish completely, the morphodynamics does not always restore completely after a flood event, as was observed in the study by Bolla Pittaluga et al. (2014) as well. After several floods passed in the record, the morphodynamics was a (non-linear) superposition of the impact by multiple floods that occurred.

2.4 The impact of variable discharge on longitudinal processes

In this section, an overview will be given of the characteristics that define the influence of variability in river discharge on morphodynamic change.

2.4.1 Time scales of morphodynamic processes

Morphodynamic processes occur on a wide variety of spatiotemporal scales throughout the river system. Buffington (2012) states that the extent to which different scales of processes respond to flow events with a certain timescale, depends on the overlap of frequency distributions of driving forces (river discharge, sediment transport) and resistance on the different scales of morphological response. The smallest scales are associated with individual grains. Moving to larger scales, changes in bed forms, river cross section and longitudinal changes can be found subsequently. The processes that prevail on relatively small spatiotemporal scales are mainly dominated by individual events such as floods, whereas the largest scales are dominated by the long-term statistics of the upstream boundary conditions.

2.4.2 Longitudinal morphodynamics

River morphodynamics in the main stem is mostly dictated by bed material load (Jansen et al., 1979), expressed by S. In longitudinal direction x, this bedload sediment transport might change due to either sudden or gradual changes in transport capacity or changes in the availability of erodible bed material. In case of unisize sediments, the morphology reacts

in terms of changes in bed level according to the Exner mass balance, which is expressed by Equation 2.1 (Exner, 1925).

$$\frac{dS}{dx} \propto -\frac{dz}{dt} \tag{2.1}$$

In case of mixed sediments, the morphology reacts both in terms of change in bed level and bed material composition. The coupled response depends on the thickness of the active layer of the stream bed (Mosselman and Sloff, 2008). In case the active layer thickness is much smaller than the water depth, the changes in morphodynamics are mainly manifested in changes in bed texture. When both the active layer thickness and the water depth are of the same order of magnitude (as is the case for the Upper Dutch Rhine system; Mosselman and Sloff, 2008), a combination of bed texture and bed level can be expected. In modelling practice, this active layer thickness is often kept constant, linked to the river bed dune height (e.g. Mosselman and Sloff, 2008) or is coupled to the water depth (e.g. Ottevanger et al., 2015).

In general, a variable discharge, in combination with the according gradients in sediment transport, results in continuous fluctuations of the river bed level and bed texture. The effects of unsteady forcing on morphodynamics can be classified into three zones (e.g. Blom et al., 2017; Arkesteijn et al., 2018a). These three zones are presented in Figure 2.9. The three zones will be discussed briefly.

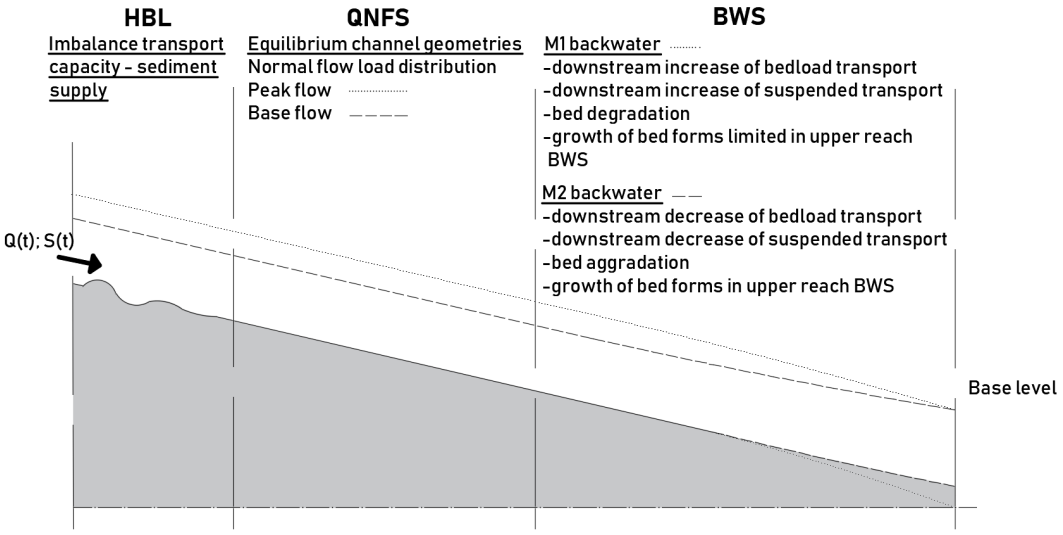

Figure 2.9: Three distinguishable zones in the longitudinal river profile (after Blom et al., 2017; Arkesteijn et al., 2018a)

The backwater segment (BWS)

Starting with the backwater segment (BWS), induced by a downstream water level that does not match the normal flow depth. At the downstream boundary of the BWS, sea level might cause these upstream backwaters. Besides, amongst others water-controlling structures, bifurcations and changes in the geometry of the cross-section might initiate upstream backwaters.

A variable discharge causes constantly fluctuating backwaters. The bed surface texture and bed elevation fluctuate according to these alternating backwaters (Arkesteijn et al.,

2018a; Nittrouer et al., 2011). In case no long-term trends are observed, small fluctuations occur around a mean state that is called the dynamic equilibrium state (e.g. De Vries, 1993).

The quasi-normal flow segment (QNFS)

Secondly, in the quasi-normal flow segment (QNFS) the equilibrium channel geometry and bed texture have adapted in such a way, that the sediment load varies with the prevailing discharge according to the *normal flow load distribution* (Blom et al., 2017) and gradients in sediment transport will be present. Consequently, hardly any effects due to short-term variations in sediment fluxes are noticeable in the river bed.

The hydrograph boundary layer (HBL)

Finally, there is the so-called hydrograph boundary layer (HBL), which is the river section where propagating bed waves in terms of bed level, slope and texture are experienced (Parker, 2004). The induced fluctuations are generally of larger intensity when compared to the fluctuation due to backwater influence in the BWS (Arkesteijn et al., 2018a). At the upstream boundary of the HBL, bed waves are generated due to several causes. First of all, there is the artificial generation of bed waves at the upstream boundary of a morphodynamic model, as a consequence of an incoming sediment load and a composition that do not meet the normal flow load conditions. Besides this artificial cause, these bed waves might have a physical origin as well. The most common cause is a sudden change in cross-sectional area of the river (e.g. Bolla Pittaluga et al., 2014; Van Denderen, 2014). The unsteady forcing due to a variable discharge in combination with sudden changes in cross-sectional geometry causes constant fluctuations and the generation of bed waves. Bolla Pittaluga et al. (2014) address the width of the engineered river as a source of *external forcing* on the river morphology. Besides the width of the cross-section, Blom et al. (2017) mention sudden changes in friction and the presence of confluences and tributaries as common sources for HBL-waves.

The length of the HBL-zone and the amplitude of the waves are dependent on multiple factors such as the duration of the hydrograph cycle compared to the morphodynamic timescale (Parker et al., 2008), the sediment grain size distribution and the degree of discordance between transport capacity and actual transport (Wong and Parker, 2006). Bed waves move downstream and dampen because of sediment exchange between the water and the bed. The waves are fully damped eventually when the sediment conditions are adapted to normal flow load conditions (Blom et al., 2017). In case of graded conditions, the waves in bed level and bed composition do not necessarily have the same propagation speed (Suzuki, 1976; Mosselman and Sloff, 2008). Ribberink (1987) derived the propagation velocity of waves in bed level c_{bed} analytically (Equation 2.2). For a river bed with mixed sediments and under the assumption that the active layer thickness is constant in time, Mosselman and Sloff (2008) derived the analytical celerity of a bed sediment composition wave c_{mix} (Equation 2.3).

$$c_{bed} = \frac{bs}{(1-\epsilon)(1-Fr^2)d} \tag{2.2}$$

$$c_{mix} = \frac{\mu s}{\delta(1-\epsilon)} \tag{2.3}$$

In which b is the non-linearity parameter between discharge and sediment transport, s is the volumetric sediment transport per unit width, ϵ is the porosity of the bed sediment, Fr is the Froude number, d is the water depth, μ is the ratio between the bedload grain size and

the average grain size in the active layer and δ is the active layer thickness. In case of mixed sediments, the river bed reacts in a coupled way in terms of changes in bed level and bed texture. The extent to which they both change as a reaction to a certain forcing depends on the ratio of timescales of both bed waves. In case of the Dutch Upper Rhine, Mosselman and Sloff (2008) find that the ratio c_{bed}/c_{mix} equals $5\delta/d$. This emphasises the influence of the active layer thickness in morphodynamic river models.

2.4.3 Implications on the river engineering practice

The classification of the longitudinal profile into three zones is an idealisation of the river practice. In natural rivers, the HBL and the BWS may overlap and a QNFS may be absent. When the HBL- and BWS-zones overlap, the momentary morphology is a superposition of all local changes and traveling waves through the system. Both the effects in the HBL and the BWS are of importance in terms of functionality of the river. One important aspect of these fluctuations is the impact on navigability. Fluctuations in the bed level can temporarily limit the draught of an inland vessel as the navigational depth might decrease locally. This asks for well-considered maintenance strategies and designs of river interventions that might induce these fluctuations.

In engineered rivers such as the river Rhine, the width of the morphodynamically active channel is more or less confined by the presence of engineering structures such as groynes, fixed banks and quay walls. The main irregularities along the active channel are caused by inland ports (Figure 2.10a), tributaries and side channels.

The configuration of the floodplain areas shows much more spatial irregularities in longitudinal direction (Figure 2.10b). At places where the floodplain area is confined or widens, the flow experiences local acceleration and deceleration respectively and mild upstream backwaters are initiated. This occurs during discharge stages when the floodplains are inundated. These local changes in flow velocity induce sharp gradients in sediment transport and result in changes in bed level and composition and generate HBL-bed waves that propagate downstream. Relatively low discharge stages that do not exceed bankfull discharge force the river morphology back to its state prior to the inundation of the floodplains (Van der Klis, 2003, Van Denderen, 2014).

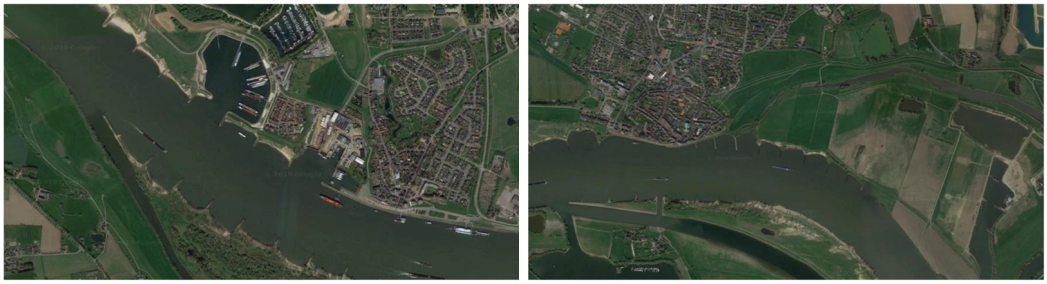

(a) **(b)**

Figure 2.10: (a) An inland port ('vluchthaven') along the Dutch Upper Rhine near Lobith and **(b)** a sudden confinement of the floodplain width along the German Niederrhein at Rees. [source: Google Earth]

Relevance on river interventions

The Room for the River (RfR-) programme has led to numerous interventions in the Dutch river system. One aim of the programme was to increase the conveyance capacity of the rivers

(Van Vuren et al., 2015). Typical examples of measures that formed part of the programme were the construction of side channels, and the lowering and widening of floodplain areas. These measures can be seen as added irregularities of the river cross-section. These measures introduce (strong) gradients in sediment transport. Besides the associated fluctuations, these measures result in long-term trends as well since these measures disturb the river morphology prior to the intervention. The adaptation of the river morphology to river interventions is often a long-term process prevailing on timescales of decades to centuries (Van der Klis, 2003), whereas associated fluctuations around these trends take place on timescales of floods up to years.

Studies that involve the application of a variable discharge on cases that are similar to RfR-interventions (e.g. Van der Klis, 2003; Van Vuren, 2005) show that the long-term response to a variable discharge results in different morphodynamics compared to the case with a steady discharge. Especially in the zones where the flow rapidly accelerates or decelerates, the (dynamic) equilibrium morphology is not necessarily governed by the long-term statistics of discharge and sediment transport, as would be the case for reaches with large-scale sediment transport gradients. The local morphodynamic features are rather governed by the variation of durations and magnitudes (sequences) of discharge events. The largest uncertainty can be expected near these zones with strong sediment transport gradients. This will be demonstrated and elaborated further in Section 4.3.

Due to the large number of RfR-related projects and their associated spatial scales, the interventions may lead to combined effects (Sloff et al., 2014). Morphodynamic models can be used to make predictions on the evolution of such long-term trends and associated fluctuations. Predictions are important to understand consequences of river interventions. These models can be used to support the development of amongst others management strategies that might be needed to maintain the functionality of the river (e.g. Van Vuren et al., 2015). Furthermore, models can support risk analyses on future impact of river interventions.

2.5 Sources of uncertainty in morphodynamic modelling

Modelling river morphology involves many interpretations of measurements, simplifications, variable parameters and empirical relations. All these components are sources of uncertainty as hardly any of these parameters can be considered to be purely deterministic (Van der Klis, 2003). Many studies are conducted to classify types and sources of uncertainty. Van Asselt and Rotmans (2002) distinguish between two dominant sources of uncertainty. These are: 1) variability, meaning that the model input parameter has a highly random character. An important contribution is delivered by the fact that future discharge time series and the influence of climate change on future discharge are to a large extent unpredictable as is shown with the use of the (auto-) correlation and dependency structures of the discharge data set as measured at Lobith (Section 2.3.3), and 2) limitations of knowledge, depending on *i*) unreliability, being the result of amongst others incomplete, infrequent or inexact measurements. Examples are the measurement of grain size distributions and the *Q(h)*-relations that are used to transform water levels into river discharge; *ii*) structural uncertainty, caused by the fact that some parameters cannot be measured, modelled, or processes that are not yet observed or understood completely (Van der Klis, 2003). Important examples for such sources of uncertainty in morphodynamic models are sediment transport models, numerical schematisations and model calibration.

Van Vuren (2005) mentions that estimating the main source of uncertainty in modelling

river morphodynamics is complex due to the non-linear interactions, and the signature that is connected to space and time. The main findings of an uncertainty analysis proved that the tuning parameters of the sediment transport model might have a significant contribution to model uncertainty. The uncertainty of grain size in bed material is hardly of influence on uncertainty associated with modelled morphodynamics. The induced uncertainty in model outcomes that is caused by river discharge was found to be dependent on the non-uniformity of the flow cross-section, such as the width of floodplains, presence of bifurcations and side harbours along the main stream.

Throughout the remaining of this thesis, only the uncertainty that is induced by the limited predictability of discharge time series will be considered. This study only addresses the influence of discharge time series, without considering the impact of climate change.

CHAPTER 3

Modelling practice

This chapter discusses the most common methods to represent the river discharge in morphodynamic river models.

3.1 Constant discharge

Many studies propose a single discharge that represents the effects of an entire hydrograph and the related sediment fluxes. It aims to yield similar morphodynamic development of a river channel as the entire hydrograph would do (e.g. Wolman and Miller, 1960; Copeland et al., 2000; Doyle and Shields, 2008). The idea is that a single *formative* discharge (Crosato, 2008) is often associated with the equilibrium state of a channel, or the static component of the dynamic equilibrium state of the river system (Arkesteijn et al., 2018a; Blom et al., 2017). Even though this concept might be a useful tool for qualitative assessments, many studies claim that a single discharge cannot be representative for all morphological processes that prevail in a river system. De Vries (1974) states that different morphodynamic processes are dominated by different statistical moments of the discharge probability distribution and can therefore not be governed by a single discharge.

3.2 Hydrograph time series

An approach to pursue the natural variation of the discharge time series is by imposing a discharge time series represented by hydrographs. In order to save computational time, the hydrograph is often discretised into a piecewise constant hydrograph. This simplification is schematised in Figure 3.1. Wiersma (1997) briefly discusses that such a piecewise constant hydrograph schematisation still yields accurate model results, if not too coarse. The coarser the schematisation, the more detail is lost in both the discharge time series and the resulting morphodynamics.

Such a stepwise, or piecewise constant simplification can be considered as a quasi-steady approach (e.g. De Vries, 1974). The hydrograph is represented by an alternation of steady

flow states. This theory can be justified because of the large difference in time scales of changes in discharge and morphology, due to the large difference in propagation speed of bed waves and gravity waves of the water level. The quasi-steady approach implies that any disturbance in the water level travels infinitely fast. Furthermore, the dynamics of flood waves cannot be represented (Arkesteijn et al., 2018a).

The amount of detail of fluctuations that has to be conserved in the hydrograph depends on the purpose and time scale of the studied morphodynamics. An important consideration when discretising the hydrograph, is that both the discharge (and sediment transport) statistics should remain similar to the original series.

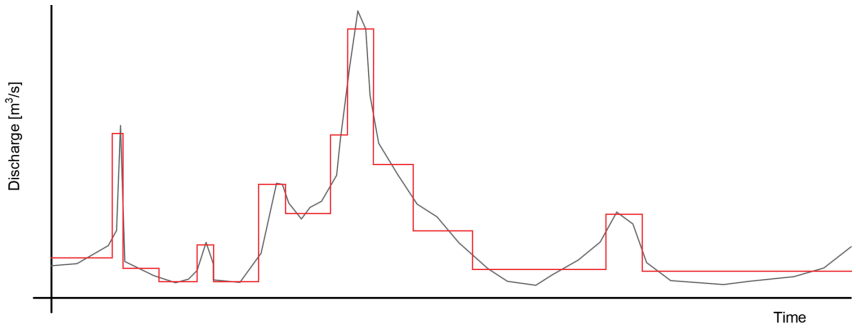

Figure 3.1: The actual discharge time series (black) and a discretised, piecewise constant schematisation (red).

This piecewise constant representation of the discharge time series leads to noticeable effects. The sharp transitions in between discharge stages, results in gravity waves in the water level that propagate downstream as well as model instabilities (Yossef et al., 2008). These gravity waves are not necessarily artificial effects, since sudden changes in (natural) flow conditions result in gravity waves in the water surface as well. However, the quasi-steady approach assumes that the hydrodynamics within the model domain ignores gravity water level waves.

Several ways exist to obtain steady flow situations in models. For simple, one-dimensionsal models, one could direct apply the backwater-Exner equations (e.g. Arkesteijn et al., 2018a). For more complex, two-dimensional models, an approach has been developed that was applied for the *Duurzame Vaardiepte Rijndelta* (DVR) model[1]. This method requires preparation before the actual model is started. First, the flow fields are run until a steady flow state is established, for each individual discharge magnitude that occurs in the time series. During these simulations, the morphology is not updated. The steady flow field for each individual discharge stage is then stored in a database. After this preparation, the actual simulation can be started. Each time a discharge stage occurs during the actual simulation, the steady flow field from the database is retrieved instead of recalculating the flow field for every discharge step so that only little spin-up time is required (e.g. Yossef et al., 2008). This reduces the required computation time significantly. The steady flow field from the database is updated with the new steady flow field that belongs to the updated morphology. This method is effective in case the morphodynamic changes are not too large during each

[1]The DVR toolbox was constructed over the past decade with the aim of making predictions on the morphodynamic response of the Dutch Rhine system to river interventions, to make diagnoses of historic trends and to simulate future long-term trends (Van Vuren et al., 2006). It includes a two-dimensional model representation of the entire Dutch Rhine system. The tool is especially useful for designing (long-term) maintenance strategies to ensure navigation on the Dutch Rhine branches.

discharge stage.

The concept of piecewise constant hydrographs can be used to construct discharge time series as model input. As was stated in Chapter 2, the main complexity when setting up future time series is caused by the limited predictability of future discharge time series due to the absence of a significant correlation. In practice, methods are developed to deal with this complication. The following paragraphs introduce methods to construct discharge time series for the model input.

3.2.1 Cycling historical series

A straightforward method is the use of measured historical discharge series. By either using a long-term record (e.g. Ottevanger et al., 2015) or cycling shorter measured time series (e.g. Van Heijningen, 2017), the natural variability of the river discharge can be maintained. The main drawback of this method is that it assumes that the future river discharge events and sequences will be exactly the same as the historical discharge series. The range of modelled sequences is limited by the observed series. Furthermore, especially on short-term simulations, one must be careful which years of observations are used since the yearly statistics among subsequent years vary. An advantage of this method is that yearly structures (and therewith the mutual daily correlation) are maintained.

3.2.2 Synthetic series

A way to overcome the shortcomings of cycling historical observations, is the construction of synthetic time series. Various methods to construct synthetic discharge time series can be found in literature (e.g. Van der Klis, 2003; Van Vuren, 2005). A selection of these methods is described here. 1) The first uses the marginal probability density function (PDF) of 10-day discharge intervals. In Chapter 2 it was already mentioned that observations of successive days show significant correlation up to 10 days. The marginal PDF and the autocorrelation function for the 10-daily intervals are combined into a multivariate lognormal distribution. From this distribution, random time series can be generated. 2) Based on historical observations, a new time series can be constructed by bootstrapping coherent periods from this data set[2]. An option is to maintain the yearly structure and hence draw complete years from the historical data set. Despite the fact that the new sequences differ, the time series are still limited by historical observations just as for the cycling of historical series. 3) Van der Klis (2003) proposes a method in which future discharge time series are constructed based on four parameters: *i*) the magnitude of floods and *ii*) base discharges, *iii*) the flood duration and *iv*) the time until the middle of the flood peak with respect to the start of the hydrological year. In this method, each year is simplified into one-yearly floods. Each of these parameters can be described by a probability density function, based on long-term discharge measurements. By randomly sampling from these distributions, synthetic time series can be constructed.

3.2.3 Deterministic series

The deterministic approach to compose discharge series is the introduction of a cycled annual hydrograph (CAH). Sloff (2011) shows a procedure of composing such hydrographs. The duration curve of the river discharge that follows from the long-term discharge statistics,

[2]Bootstrapping refers to a resampling method with replacement of drawn samples from a data set. Resample procedures can also be executed without the replacement of drawn samples.

can be discretised and translated into a single, yearly hydrograph. The total duration of each discharge magnitude in the yearly cycled hydrograph matches the relative probability of occurrence that is retrieved from the discretised flow duration curve, multiplied with the number of days in a year. Typically, the CAH has a symmetrical or slightly skewed shape with one high water event in each year. By this means, the long-term statistics is repeated with a yearly frequency in terms of a CAH. The idea about imposing the long-term discharge statistics in combination with a yearly frequency, is that this would result in morphodynamic development that is similar to the average long-term trend as would be obtained when applying a probabilistic method such as a Monte Carlo analysis. Hence, it can be considered as a *best guess* regarding a future discharge time series and aims to produce similar long-term morphodynamic development as would be obtained by the mean development from a Monte Carlo analysis. More details on the construction of the CAH can be found in Sloff (2011). In Section 4.4, the CAH will be constructed for the long-term discharge statistics of the Dutch Upper Rhine.

3.2.4 Uncertainty in morphodynamics

The presented time series all result into a single morphodynamic realisation. However, in Chapter 2, it is discussed that due to the non-linear interaction of river discharge and morphology, the sequence of subsequent events and years is manifested in the end state of the simulation. This means that different time series potentially yield different morphodynamic realisations. Together with the fact that discharge time series are highly unpredictable, this causes uncertainty in future morphodynamics. Insight on this uncertainty can be gained with the aid of a probabilistic method such as a Monte Carlo simulation. This means that a large number of time series is simulated, resulting in an average long-term morphodynamic trend, as well as the related uncertainty around the trend.

Such a probabilistic method proves to be a useful tool in case of modelling future river morphodynamics. Moreover, Huthoff et al. (2010) demonstrate that the use of a deterministic discharge time series does not necessarily result in similar morphodynamic development as would be obtained with a Monte Carlo approach. A schematic overview of both a deterministic simulations and a Monte Carlo procedure is presented in Figure 3.2.

There are several important drawbacks for the Monte-Carlo method. First of all, a large number of computations is needed to obtain an established mean and standard deviation in morphodynamic response (Huthoff et al., 2010). Another important disadvantage is the fact that for an increasing number of stochastic input variables, the number of required model runs grows exponentially. For morphodynamic river models, more space- and time-dependent factors such as variable sediment fluxes, roughness and grain size are important contributors to modelled uncertainty as well (Van Vuren, 2005). Still, in many studies that apply Monte Carlo simulations for studying river morphodynamics, discharge time series are considered to be the only stochastic input variable (e.g. Van Vuren et al., 2015).

3.3 Probabilistic input

In Arkesteijn et al. (2018b) it is proposed to move from discharge time series towards probabilistic distribution functions as input for long-term morphodynamic river models. Instead of imposing one single discharge magnitude at each time instant, a range of possible discharge stages is imposed at the same time during each time step. In fact, this is similar to imposing hydrographs that are compressed infinitely during each time step. A set of

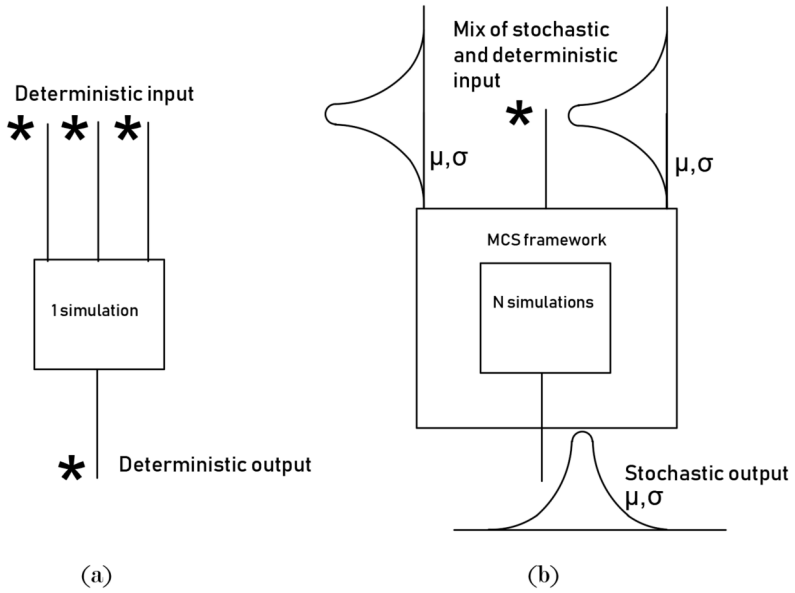

Figure 3.2: An overview of the structure of **(a)** a deterministic simulation and **(b)** a Monte Carlo procedure.

hydrodynamic modes is computed throughout the entire domain in a parallel way. For all these modes the sediment transport gradients are calculated. The weighted average is taken over these transport gradients using the probability of occurrence of each hydrodynamic mode. Ultimately, this results in a bed level update. This cycle is run each time step. This type of modelling is mainly applicable for long-term trends and studies with less detailed results. This method disregards the influence of sequences. The model results coincide well with the mean of the Monte Carlo approach, but smoothens out details.

CHAPTER 4

Imposing discharge variability in a morphodynamic model

This chapter consists of five parts. In the first part (Section 4.1), the conceptual study is introduced and the morphodynamic response to a steady discharge is evaluated. Secondly, in Section 4.2, a variable discharge time series is imposed to study the effects of a variable discharge on the modelled morphodynamics. In Section 4.3, a Monte Carlo simulation is conducted and the results are compared to a morphodynamic response to the deterministic cycled annual hydrograph (CAH) in Section 4.4 to increase insight on the lacking performance of the CAH-series. With the aim of improving the CAH-method, the impact of short-term sequences, long-term sequences and the included bandwidth of the long-term discharge statistics will be studied in fifth part of this chapter (Section 4.5). The findings from this chapter contribute to the proposal of an improved deterministic method in Chapter 5.

4.1 Model description

A strongly idealised two-dimensional numerical model is used to study a conceptual case. The main advantage of a conceptual study is that the complexity and the dependency on parameters other than river discharge is limited compared to complex model studies. A river intervention is modelled that can be considered as a typical example of a Room for the River measure. The case involves a local widened floodplain. The morphodynamic response to this intervention under the influence of a steady discharge is evaluated to increase the physical understanding of the model behaviour. Thereafter, the morphodynamic change due to a variable discharge will be studied.

Especially the case in which the floodplains have an impact on the river morphology, the contribution of discharge stages above and below bankfull discharge will become clear, making it an interesting case. In this thesis, the bankfull discharge (Q_{bf}) is defined according to Williams (1978), who describes it as *the flow stage that just fills the active channel to the top of its banks.* It marks the flow condition of incipient floodplain inundation. The bankfull discharge stage is schematised in Figure 4.1a.

For the model simulation, Delft3D is used. The river is modelled as a straight, prismatic

compound channel. The layout is presented in Figure 4.1b. The main channel has a width of 300 m, as well as the floodplains. The elevation of the floodplains is selected such, that bankfull discharge stages is 4000 m^3/s. The floodplain is widened by 300 meters at one side of the river over a trajectory of 3 km. The floodplains are morphologically inactive. Only the main channel is morphologically active. Only longitudinal morphodynamics will be studied. The main channel is one grid cell wide, as well as the floodplain and the widened floodplain.

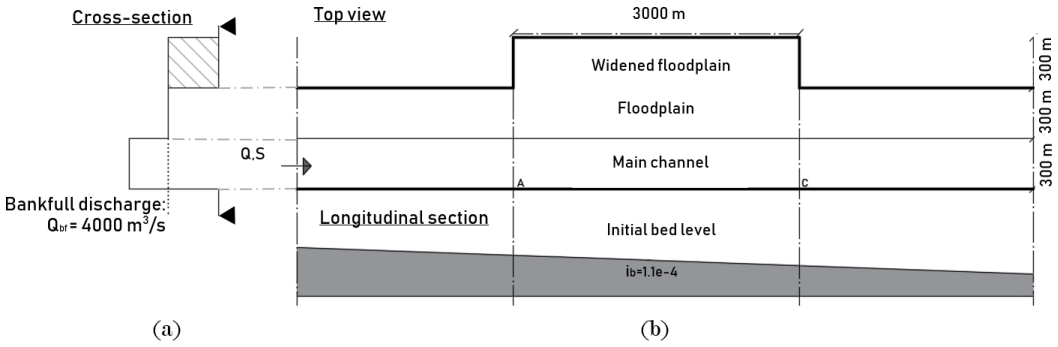

Figure 4.1: (a) The cross-section of the case study, indicating the bankfull discharge stage and the layout of the floodplains and **(b)** the top view (top) and the longitudinal section (bottom) of the model layout of the conceptual study.

The model makes use of a simple, two-dimensional domain decomposition. This means that the widened floodplain is not a widened grid cell (as would be the case with a one-dimensional model), but an extra row of cells is added locally. The domain decomposition allows for lateral exchange of momentum between the floodplain and the main channel. The two-dimensional domain composition is selected because it results in more realistic behaviour in case of a sudden expansion of a floodplain (Proust et al., 2006). Another reason why the two-dimensional representation is selected, is the fact that this study aims to extend earlier findings of one-dimensional studies (such as Van der Klis, 2003; Van Vuren; 2005) towards more practical two-dimensional model applications, such as the DVR-model that is introduced in Chapter 3.

The initial sediment characteristics are roughly based on measurements of the Dutch Upper Rhine (BfG-SedDB, 2016). The grain size distribution of the river bed is divided into four sediment fractions. The active layer thickness is set at 1.0 m. The threshold-based Meyer-Peter Muller formulation with the inclusion of the Ashida and Michue hiding and exposure schematisation is selected as transport model. The critical bed shear stress is set at 0.025 N/mm, based on reference studies of the Dutch Upper Rhine (Ottevanger et al., 2015).

At the upstream boundary, the bed level and bed composition are fixed in time. Indirectly, the model imposes equilibrium transport at the upstream boundary. An important consequence is that the equilibrium concentration of the sediment flux at the upstream model boundary is hence defined by the initial grain size distribution of the bed surface sediment. The combination of the long-term discharge statistics, together with the resulting equilibrium sediment transport results in an equilibrium slope (Blom et al., 2017) that might differ from the initial slope of the model. Consequently, a bed slope disturbance is expected to travel from the upstream boundary into the domain. Therefore, the upstream model boundary is located 50 km upstream of the studied river section.

In modelling channels with floodplains, an important feature is the distribution of discharge over the main channel and the floodplains. In the model, the water discharge is distributed such, that outside of the backwater influence zone (BWS), a zone of normal flow (QNFS) prevails both in the main channel and on the floodplains. The depths in the model are similar to the depths as calculated with the Chezy equations for a compound channel. The distribution of flow velocity and the water depths at the main channel and at the floodplains can be found in Appendix B.1.

Chapter 3 introduces a method how to create a database of spun-up steady flow states for two-dimensional model configurations that apply the quasi-steady piecewise constant hydrograph schematisation to limit computational time. This approach is used for this case study as well.

4.1.1 Model response to a steady discharge

In this section it is aimed for to understand how the model responds to a steady discharge and to check whether the model results match the expectations from a theoretical analysis. To increase the understanding of the model behaviour, first a one-dimensional theoretical analysis is performed to study both the initial morphodynamic response and the equilibrium state to the widened floodplain. For this analysis, the morphodynamic response to a steady discharge of 6000 m^3/s is considered. This discharge stage exceeds the bankfull discharge stage. Consequently, the floodplains convey water discharge as well and hence the morphodynamics of the main channel is affected. A one-dimensional analysis of the initial and equilibrium response of the bed level inside the main channel is presented in Figure 4.2. It is assumed that the flow velocity is uniform throughout the cross-section.

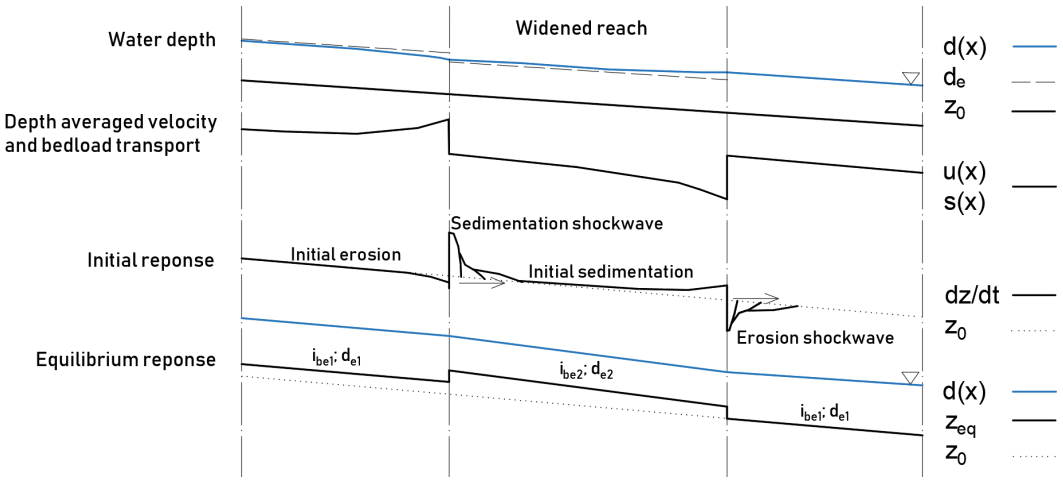

Figure 4.2: Morphodynamic response of the bed level inside the main channel to the widened floodplain. The symbols represent the longitudinal water level $d(x)$, the equilibrium water level d_e, the initial bed level z_0, the streamwise flow velocity $u(x)$, the streamwise sediment transport $s(x)$, the rate of change in bed level dz/dt, the equilibrium bed level z_{eq} and the equilibrium bed slope i_{be}.

The widened floodplain initiates backwater effects within the widened reach itself, and upstream of the widened reach. Upstream of the widened reach, a large-scale positive sediment transport gradient will prevail due to the gradual drop of the water surface and an according increase in flow velocity and sediment transport in longitudinal direction.

According to the Exner sediment mass balance (Equation 2.1, initial erosion will be induced upstream of the reach with the widened floodplain. The opposite occurs inside the widened reach where the flow decelerates and positive large-scale sediment gradients result in initial sedimentation.

The zones where the cross-sectional area suddenly increases at the start of the widening, an sedimentation shock wave will be observed during the initial response. This is the result of a sudden decrease of longitudinal flow velocity and sediment transport. The sharp negative gradient in sediment transport causes local sedimentation, according to the Exner sediment mass balance. The opposite occurs at the location where the widened floodplain suddenly ends and where the flow experiences sudden acceleration: an erosion wave will be initiated.

Initial morphodynamic response

To understand how the simplified two-dimensional model behaves compared to the one-dimensional theoretical analysis, the morphodynamic response of the active channel to a constant discharge of 6000 m^3/s will be studied at different moments in time. First, the initial response during the first year is presented in Figure 4.3a.

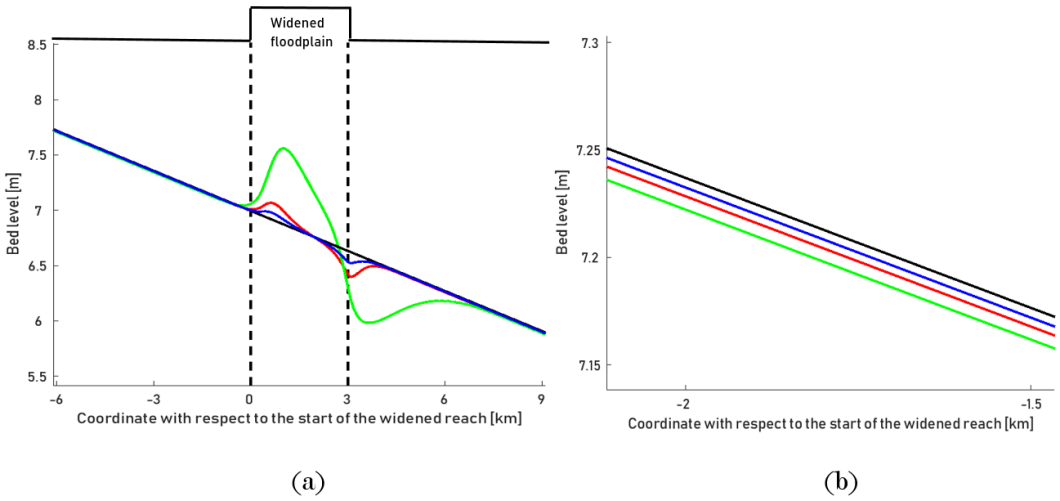

Figure 4.3: **(a)** Initial morphodynamic response to a steady discharge of 6000 m^3/s after 10 days (blue), 1 month (red) and 1 year (green); **(b)** A detail of the initial erosion upstream of the reach with the widened floodplain. The solid black line represents the morphodynamic state prior to when the floodplain was widened.

Upstream of the reach with the widened floodplain, erosion can be observed during the initial response as a consequence of the upstream backwater effects that are induced by the widened floodplain. This erosion increases during the first year of initial response but is however not significant (Figure 4.3b) compared to the change in bed level at the locations where the cross-sectional area suddenly changes and rapid acceleration and deceleration of the flow is observed. The widened floodplain induces only mild upstream backwater effects compared to the morphodynamic change that is caused at the rapid change in flow cross-section at the expansion and contraction zones (see Appendix B.2 for more information about the backwater effects).

When the flow suddenly expands at the start of the widened reach, a zone of relatively strong sedimentation is induced. Moreover, a shock wave travels downstream. Contrar-

ily to the one-dimensional analysis, this does not occur directly when the cross-sectional geometry changes. This is a consequence of the flow expansion that is the result of the two-dimensional flow decomposition. The difference between the purely one-dimensional analysis (in which the flow velocity is assumed uniform throughout the cross-sectino) and the used two-dimensional model decomposition is schematised in Figure 4.4. By introducing the two-dimensional domain decomposition, horizontal flow expansion and contraction are accounted for. Additionally, flow velocities that are not constant throughout the cross-section. This enables the lateral exchange of momentum between the main channel and the (widened) floodplain. For a case with that includes floodplains, two-dimensional flow effects become important as these effects govern the distribution of discharge over the main channel and the floodplain to a more realistic extent compared to one-dimensional representations (Proust et al., 2006). The model allows for a transverse flow component contributing to the discharge distributions over the main channel and the floodplain. The exchange of momentum results in smoother gradients in flow velocity and sediment transport (V. Chavarrias, personal communication; May 1, 2019). The difference between the longitudinal flow velocities for both the one-dimensional analysis and the two-dimensional representation is included in Figure 4.4 as well.

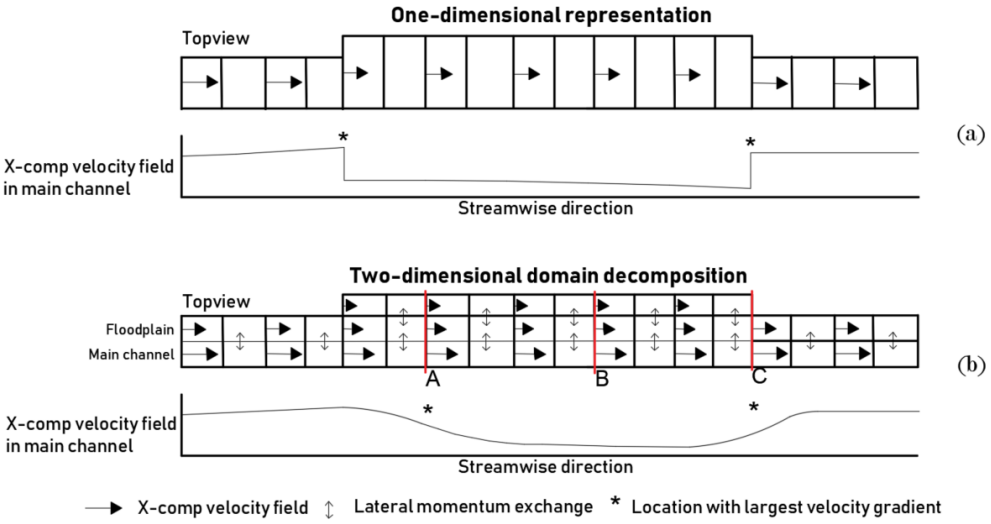

Figure 4.4: Difference between **(a)** the purely one-dimensional model representation and **(b)** the applied two-dimensional domain decomposition in case of modelling a sudden change in floodplain width. The largest flow velocity gradients are found at A (largest negative transport gradient) and at C (largest positive sediment transport gradient).

The flow gradient is smeared out over a distance that can be defined as the adaptation length of the flow after a sudden change in flow conditions. It is a measure of the distance it takes the flow to adapt to a sudden change in cross-sectional geometry. According to Struiksma et al. (1985), this adaptation length λ_w can be described by Equation 4.1, in which C is the Chezy roughness coefficient, d is the water depth and g represents the gravitational acceleration.

$$\lambda_w = \frac{C^2 d}{2g} \tag{4.1}$$

Using the model parameters, this leads to an adaptation length in the order of 800-1000

m. The streamwise component of the flow velocity inside the main channel is plotted in Figure 4.5. The flow adaptation length λ_w is marked as well. This adaptation length reasonably coincides with the calculated adaptation length.

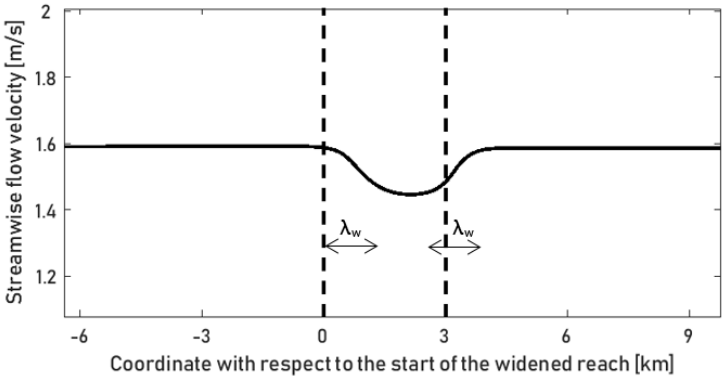

Figure 4.5: The streamwise flow-velocity inside the main channel. The flow adaption length λ_w is marked as well. The dashed lines indicate the reach with the widened floodplain.

Besides this theoretical explanation of the smoothened flow- and sediment transport gradients (and the resulting smoothened initial bed level change compared to the one-dimensional theoretical analysis from Figure 4.2), Sloff (personal communication; June 3, 2019) mentions the (relatively small) influence of both numerical diffusion and a (slightly overpredicted) molecular viscosity inside the model as well. A consequence of this smoothening of sediment transport gradients due to two-dimensional flow effects, is the fact that the largest negative sediment transport gradient is not found right at the sudden change is cross-sectional geometry, but slightly downstream.

Similar as for the zone where the flow expands, a more smooth morphodynamic response is observed at the zone where the flow contracts. An erosion wave is initiated that travels downstream. During the initial phase, an erosion pits develops at the location where the flow contracts and an erosion wave starts propagating downstream. The location of the erosion pit during the initial days to months is found at approximately the same location as what is expected from the one-dimensional theoretical analysis. The reason for this is the fact that flow decelerates (negative flow gradient) shortly after the flow expansion whereas the flow experiences acceleration (positive flow gradient) already before the contraction with a maximum close to the contraction itself (Ray et al., 2012). See Appendix B.3 for more information about the velocity field around the widened floodplain for a steady discharge of 6000 m^3/s.

Overall, the initial response shows many similarities with respect to the theoretical one-dimensional analysis. However, the morphodynamic change is much smoother for the case of a two-dimensional representation and the location of the zone where the sedimentation shock wave is initiated is found slightly downstream of the widened floodplain.

The influence of grid size on this effect is also investigated. The velocity fields are compared, as well as the resulting sediment transport. The computed bed level changes are similar for a streamwise grid cell size of 100 m compared to the results from the used model with a streamwise grid cell size of $300m$. A comparison can be found in Appendix B.4 for the case of a steady discharge of 6000 m^3/s after one year.

Equilibrium morphodynamic response

After several decades, a new morphodynamic equilibrium establishes. How this compares to the morphodynamic equilibrium from a one-dimensional analysis is presented in Figure 4.6.

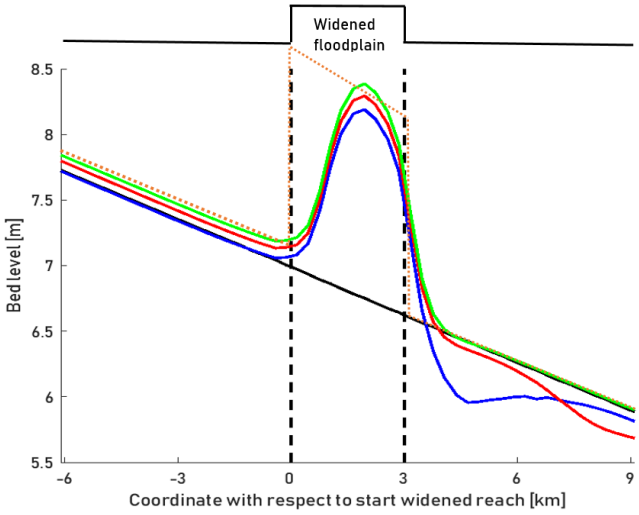

Figure 4.6: The long-term morphodynamic response to a constant discharge of 6000 m^3/s after 10 years (blue), 20 years (red) and 40 years (green). The expected (qualitative) morphodynamic equilibrium (see Figure 4.2) is represented by the orange dashed line. The morphodynamic state before the floodplain was widened is depicted by the black line.

The equilibrium response with the two-dimensional representation is smoother compared to the one-dimensional analysis as well. Moreover, the morphology is also affected just downstream of the reach with the widened floodplain in case of the two-dimensional model. Still, it is fundamentally similar to the one-dimensional analysis.

4.2 Morphodynamic response to the natural discharge time series 1971-2010

The model response to a steady discharge is evaluated in the previous section. In this section, the morphodynamic response to a variable discharge time series will be discussed. The aim is to understand the morphodynamic response and the differences in bed level response compared to the case with a constant discharge.

As a source for the river discharge, the discharge time series of 1971-2010 as observed in the Upper Rhine (GRDC, 2018) will be imposed at the upper boundary of the model. The discharge time series is discretised into piecewise constant hydrographs consisting of 13 discrete discharge levels. Both the measured and the discretised series are shown in Figure 4.7. The minimum duration of a discharge stage is 3 days, hence discharge events in the order of days are included.

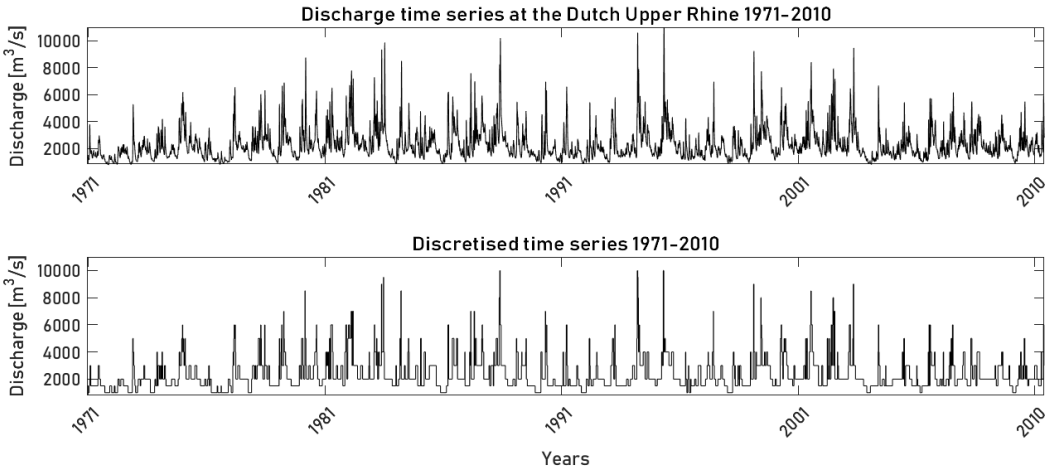

Figure 4.7: Observed and discretised time series of the river discharge at the Dutch Upper Rhine from 1971-2010 [source data: GRDC, 2018].

In Chapter 2 it is mentioned that morphodynamic change is mainly governed by bed material load transport. Therefore an analysis of the sediment transport is made to analyse how the different discharges stages contribute to the yearly averaged sediment flux. Figure 4.8 presents the contribution of discharges on the horizontal axis to the total volume of bed load transport for the years 1971-2010. This relationship is presented in terms of the cumulative density function (CDF) of bedload transport as a function of the water discharge.

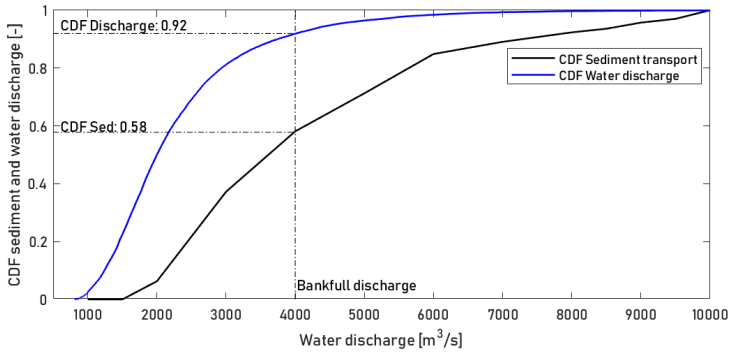

Figure 4.8: CDF of sediment transport (black) and river discharge (blue), both as a function of water discharge. The properties for the bankfull discharge are marked with the dashed line.

From Figure 4.8 it follows that the discharge stages below bankfull discharge (Q_{bf}=4000 m^3/s) are responsible for almost 60% of the total sediment transport during the years 1971-2010, whereas these discharges are exceeded only 8% of the total time. Another observation is that for discharge stages up to 1500 m^3/s no sediment transport is observed. This is the consequence of the selected bedload transport model, since it is threshold-based.

As a consequence of the smoothened longitudinal flow gradients, the sediment transport gradients are smoothened as well, when compared to the one-dimensional theoretical analysis. See Appendix B.5 for more information about the sediment transport for several

discrete discharge stages.

The morphodynamic state at the end of the 1971-2010 series (hence after 40 years) is shown in Figure 4.9a. This is not the dynamic equilibrium state. A model run is executed with a duration of 70 years as well, by repeating the natural discharge time series 1971-2010. This leads to the dynamic equilibrium state of the morphology. The morphodynamic state after 70 years is presented in Figure 4.9b. Throughout this thesis, the morphodynamic development during the first 40 years will be elaborated. Therefore, the dynamic equilibrium state after 70 years will only be discussed briefly.

The dynamic equilibrium state that is observed in Section 4.1.1 for the case of a constant discharge is established sooner due to the fact that the selected discharges has a magnitude of 6000 m^3/s. The yearly average sediment flux is much larger compared to the yearly average sediment flux that results from the variable discharge time series 1971-2010. Consequently, bed waves travel faster and hence the morphodynamic time scale of the studied reach is shorter. Another consequence of the relatively high yearly average sediment flux in the case with the constant discharge, is the larger observed changes in bed level in the (dynamic) equilibrium state with respect to the bed level response to the variable discharge time series 1971-2010. Therefore, only a qualitative comparison is made between the model results with a constant discharge and the simulation with a variable discharge time series in this section.

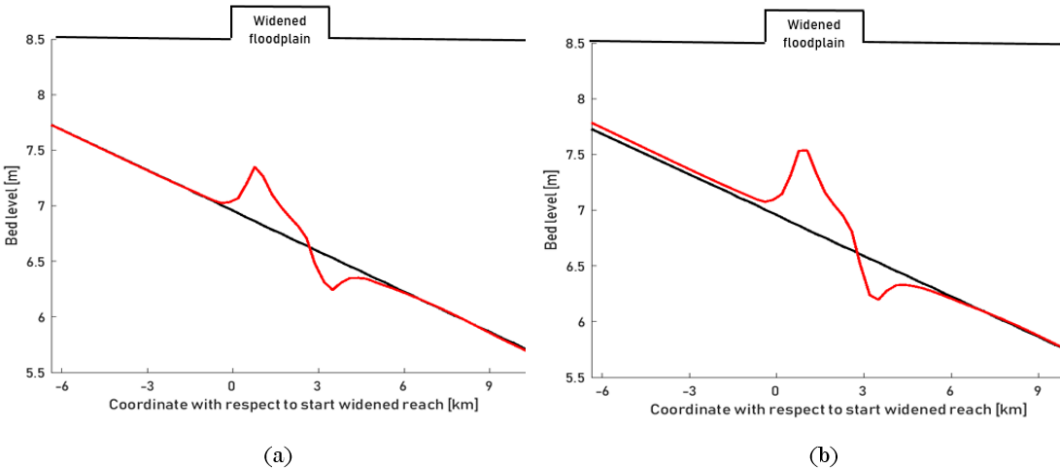

Figure 4.9: (a) The simulated morphodynamics after 40 years and **(b)** after 70 years (by repeating the series 1971-2010).

Under the influence of a variable discharge, a zone of relatively strong sedimentation develops right after the flow expansion at the widened floodplain. Additionally, an erosion pit develops at the zone where the flow contracts and accelerates. Both the sedimentation zone and erosion pits are still present in the dynamic equilibrium state, whereas these morphodynamic features are absent for the case with a steady discharge as observed in Section 4.1.1. This can be explained as follows. For the case of a constant discharge, only one shock wave will be generated both at the expansion and contraction initially. The shock waves propagate out of the studied domain and dampen out gradually due to mass exchange with the river bed. Hence, the influence of the shock wave vanishes over time. On the contrary, in case of a variable discharge, waves will be constantly generated at the sudden flow expansion and contraction. In Chapter 2, these waves are introduced as hydrograph boundary layer (HBL-) waves. As long as the discharge remains variable in time and the

discharge frequently exceeds the bankfull discharge, these waves will be generated in the river bed. These HBL-waves travel downstream. Their amplitude decreases due to mass exchange with the river bed, but also due to discharge stages below bankfull discharge that force the morphology back to its initial state (Van der Klis, 2003). Despite the fact that the persistence of a single HBL-wave decreases in time (due to the downstream propagation, their diffusive nature and the dampening during relatively low discharge stages), their influence might not be completely vanished as soon as a new HBL-wave is generated at the sudden change in conveyance area at the widened floodplain. As a consequence, the influence of both the previous and the new HBL-waves is combined.

This superposition of waves is schematised in Figure 4.10. This effect results in the development of a local sedimentation zone and erosion pit at the locations where the flow experiences sudden expansion and contraction respectively. The trend towards a local dynamic equilibrium at the flow expansion and contraction is hence not merely governed by the long-term discharge statistics, as would be the case for reaches that are dominated by large-scale transport gradients, but rather by the variation, frequency and magnitude of discharge stages (and the resulting HBL-waves). The latter statement is mentioned by Van der Klis (2003) as well[1].

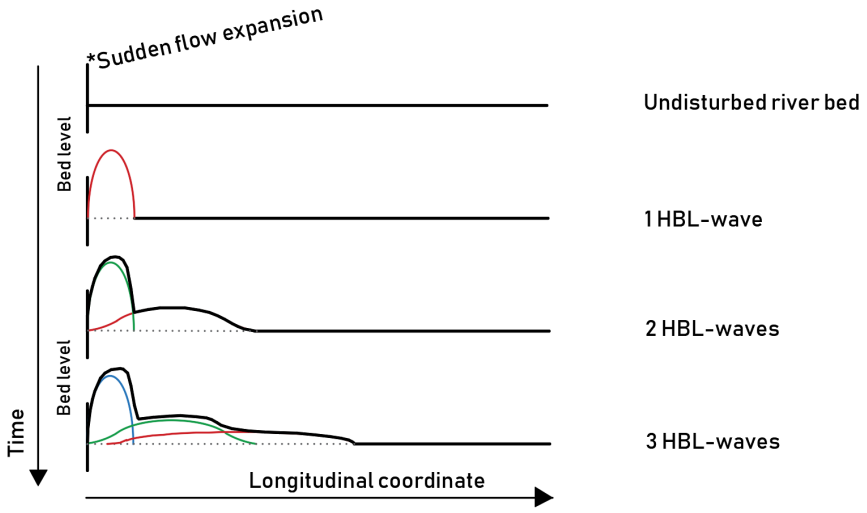

Figure 4.10: Superposition of the HBL-waves in the river bed, explaining the physics behind the development of a sedimentation zone. This sedimentation zone will be present in the dynamic equilibrium state of the river as well, since the HBL-waves will be generated continuously. These waves both propagate downstream and dampen out due to their diffusive character. The first HBL-wave is marked by a red colour at all time intervals. The second and third HBL-waves are marked by a green and blue colour respectively. The resulting superimposed bed level is marked by the solid black line. The opposite will occur in case of a sudden flow contraction. Instead of sedimentation waves, erosion waves will be generated continuously and result in a combined erosion pit on the long-term.

[1]The following link provides access to a video in which the simulated morphodynamic change of the river bed under the influence of the natural discharge time series 1971-2010 is animated: https://www.youtube.com/watch?v=vCM7nrsDwtA (uploaded at June 13, 2019).

4.3 The Monte Carlo simulations

In the previous section, the morphodynamic response to only one discharge time series results in one realisation of the bed level. However, as described in Chapter 2, future discharge series are highly unpredictable. Therefore insight on the *expected* long-term morphodynamic development and the according uncertainty is desirable. A method to obtain such information is applied in this model study. A Monte Carlo simulation with 20 synthetic discharge time series of 40 years is performed. This simulation yields a probabilistic bandwidth of the morphodynamic change consisting of 20 realisations. From this bandwidth, an average morphodynamic trend can be deduced as well as a confidence interval, representing the uncertainty in simulated morphodynamics. 18 Out of the 20 synthetic time series are constructed from the years 1971-2010, by bootstrapping years without replacement and placing them in random order. By doing so, the daily structure of the years is maintained. Besides the 18 random series, 2 extreme series are included: 1) starting with the years with the highest yearly discharge stages and ending with the years with the lowest discharge peaks, and 2) vice versa. Van Vuren (2005) states that bootstrapping from a historical database is an adequate and efficient method to generate synthetic time series that include the inherent natural variation of the river. However, it means that discharge extremes that are not observed in the historical database, will not be represented in the time series.

When performing a Monte Carlo simulation, the number of included realisations is an important consideration. After a certain number of realisations, a constant mean and standard deviation establish (Huthoff et al., 2011). An analysis is made for the development of the mean and standard deviation of the river bed to check whether the 20 randomly generated time series lead to such a constant mean and standard deviation. The development of the mean and standard deviation as a function of the number of included discharge time series is studied at the location here the largest sedimentation is observed due to the strongest negative sediment transport gradients. Two moments in time are considered: after 20 years and after 40 years. The results are presented in Figure 4.11.

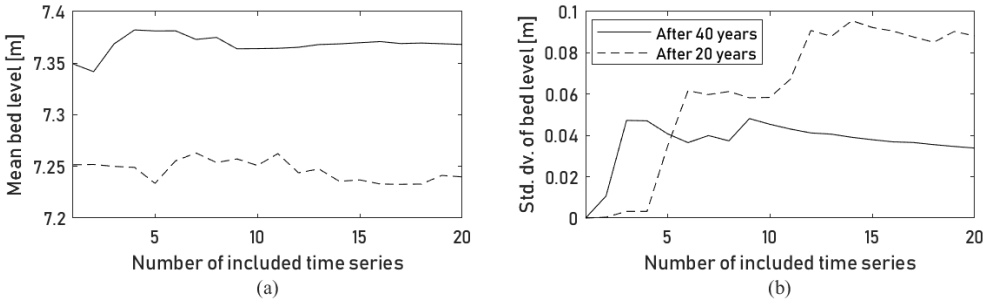

Figure 4.11: Development of **(a)** the mean and **(b)** the standard deviation of the bed level at location A after 20 and 40 years as a function of the number of included time series in the Monte Carlo simulation.

From Figure 4.11 it is clear that by including 20 time series, the mean remains fairly constant at both considered moments in time. However, the standard deviation still shows little development close to 20 simulations. This means that the standard deviation of the Monte Carlo bandwidth is less well-established than the mean. According to Huthoff et al. (2010) the development of an established standard deviation in morphodynamic development is more sensitive to singular events and therefor requires more time series to reach a fairly constant value. It is decided to continue with 20 simulations due to the limitation of

(computational) time. Moreover, it is expected that the standard deviation does not change significantly by adding more time series.

The morphodynamic state after 40 years is presented in Figure 4.12. It includes both the 20 bed level states that form the probabilistic bandwidth (gray) and the resulting bed level after imposing the observed natural discharge time series 1971-2010 (red).

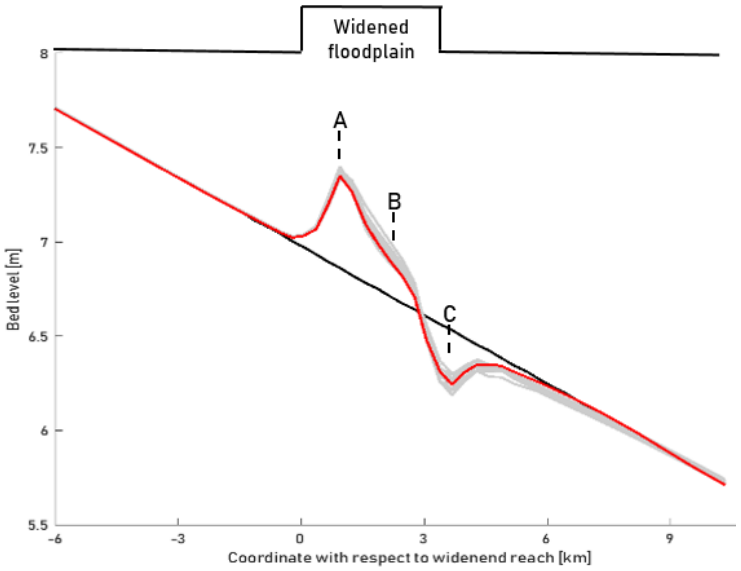

Figure 4.12: Morphodynamic state after 40 years. Including the probabilistic bandwidth from the Monte Carlo simulation (grey), and the response to the natural discharge time series 1971-2010 (red).

Figure 4.12 only represents the morphodynamic state at the end of the 20 discharge time series. For the upcoming analyses, the time development of the bed level is analysed at locations A, B and C, that are marked within Figure 4.12 as well. The time development is presented in Figure 4.13. The time development of the D_{50} of the river bed is presented in Appendix C.1. The main focus in the remaining of this thesis will be on bed level changes.

Location A

This is the zone where the largest negative sediment gradients are observed due to the expansion (and deceleration) of the flow. During discharge stages that exceed bankfull discharge, sedimentation (HBL-) waves are induced at location A due to the strong negative gradients in sediment transport. Clear examples of such HBL-waves are the sedimentation waves that are induced by the flood years 1994-1995 (blue line in Figure 4.13a). These HBL-waves propagate downstream. They show a diffusive character and are dampened by the lower discharge stages that do not exceed bankfull discharge. The lower discharge stages force the river bed back towards its initial state, since these flow stages do not experience longitudinal changes in channel width. Whether the lower discharge stages are able to fully dampen the growth of a local sedimentation hump that grows due to the continuous generation of HBL-waves, depends on the frequency, variation and duration of discharge stages, the contribution of the discharge stages to the long-term sediment transport volume and the morphological time scale of the bed (Van der Klis, 2003). In this model, an aggrading trend is observed at location A.

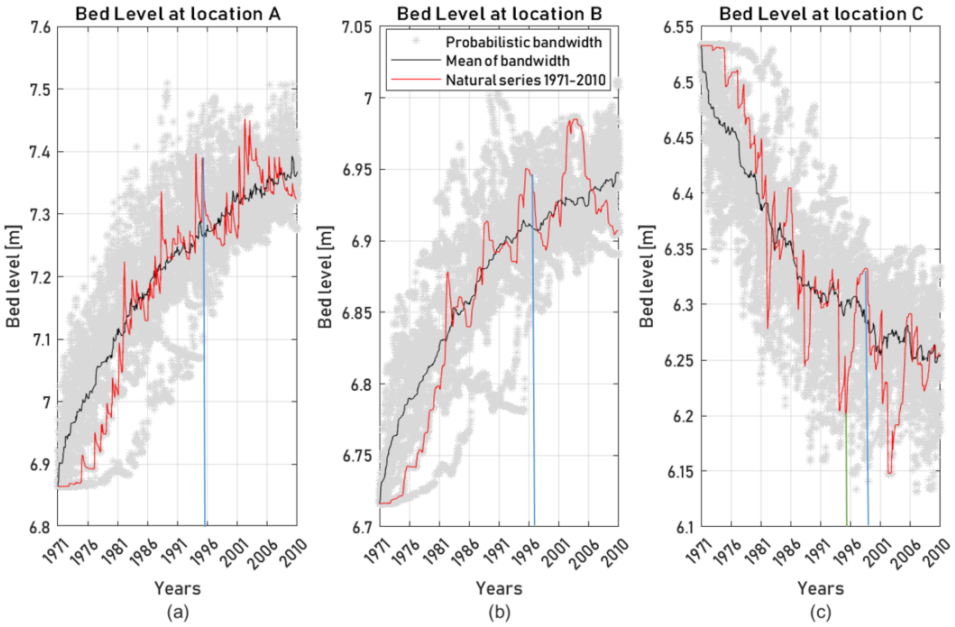

Figure 4.13: The probabilistic bandwidth that results from the 20 Monte Carlo simulations (gray), the average development of the bandwidth (black) and the time development of the bed level that follows from the natural series 1971-2010 (red) at locations **(a)** A, **(b)** B and **(c)** C

Location B

This zone is dominated by both the HBL-waves that are generated upstream at location A and more gentile, local sediment transport gradients. This zone is a combination of a hydrograph boundary layer (HBL) and a backwater segment (BWS), as discussed in Chapter 2. At location B, positive sediment gradients prevail during discharge stages above bankfull discharge, leading to local sedimentation. The same as for location A, this aggrading trend is dampened by discharge stages below bankfull discharge. The HBL-waves that are generated at location A can be observed in the time series at location B. The waves that are generated in 1994-1995 pass location B 1-2 years later (Figure 4.13b, blue line). Because of the diffusive behaviour of the bed waves, these waves are wider and have a smaller amplitude when they arrive at location B. The propagation speed of bed waves in the model will be discussed in the next section.

Location C

At location C, the flow accelerates during stages that exceed bankfull discharge. As a consequence, the river bed erodes locally during these stages and HBL waves are generated as well. The clearest examples are the two erosion shocks during 1994 and 1995 (Figure 4.13c, green line). An eroding trend can be observed. Similar to location A, the low discharge stages dampen the eroding trend and will force the morphology back to the initial state of the bed. The effect of the HBL-waves that are induced upstream of location C are still noticeable here as well. The sedimentation shock waves that are generated during 1994 and 1995 at location A (Figure 4.13c, blue line) pass location C approximately three to four years later.

4.3.1 The probabilistic bandwidth

In Figure 4.13 it can be observed that the probabilistic bandwidth at locations A and C is wider than at location B after 40 years. This suggests that the uncertainty in modelled morphodynamics is larger near zones with strong sediment gradients. This is also discussed in Section 2.4.3. A reason for this is the fact that observed fluctuations and changes in bed level at location A and C are larger compared to location B. Therefore, the resulting uncertainty can be expected to be larger at locations A and C as well.

Another notable observation is that after 25-30 years the bandwidth does not increase much and remains fairly constant. A possible explanation is the fact that the long-term discharge statistics limits the growth of the probabilistic bandwidth. According to the long-term discharge statistics, a balance exists between relatively wet and dry years. The variation of these years bounds the growth of the probabilistic bandwidth after several decades.

4.3.2 Propagation of bed waves

In Figure 4.13, the propagation of bed waves is observed. The propagation speed of these bed waves is studied here in more detail. The travelling bed waves downstream of location C become clear from Figure 4.14. The time series of the bed level development at location C and at four locations downstream of location C is plotted, each with an interval of Δx =1000 m, representing the downstream distance from location C. It is found that the bed waves downstream of point C move with a propagation speed of around $0.6 - 0.8$ km/y.

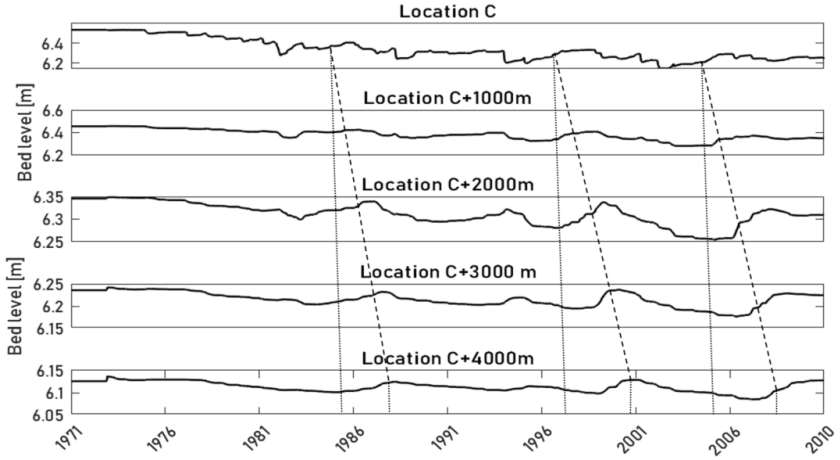

Figure 4.14: Time development of the bed level at location C and at four locations downstream of location C, each with an interval of 1000 m. The crests of propagating bed forms are connected by the black dashed lines for the different locations. From this figure, the bed celerity can be derived.

From this insight on the propagation velocity of bed level waves, an estimate of the morphodynamic time scale τ of the studied morphology can be made using the length of the widened floodplain L_w and the propagation velocity of bed level waves c_{bed}. Based on Equation 4.2, the time scale of the morphodynamic change is of the order of years to decades.

$$\tau = \frac{L_w}{c_{bed}} = O(years - decades) \tag{4.2}$$

4.3.3 A physical measure of bed level fluctuations

Short-term fluctuations can be observed around the long-term bed development in Figure 4.13. These bed level fluctuations act on time scales of years. The amplitude of these fluctuations might be of importance for the functionality of a river. Insight on the properties of these fluctuations can be gained by splitting the bed level time series into two components: the long-term trend and the fluctuations around this trend. The latter can be obtained by subtracting the long-term trend from the time series of bed level change. As an example, the following steps are conducted for the bed level response to the natural discharge time series 1971-2010 at location A: 1) The long-term trend is obtained by applying a moving average with a time window of 2 years (Figure 4.15a), such that mainly fluctuations on time scales of years are filtered out. 2) This long-term trend is subtracted from the time-development of the bed level. As a result, only fluctuations on time scales of years remain. These fluctuations are plotted in (Figure 4.15b). 3) From the resulting fluctuations in Figure 4.15b, a probability density function (PDF) can be constructed to characterise the long-term statistics of the amplitude of yearly bed level fluctuations.

The main message from Figure 4.15b is that the largest bed level fluctuations are found during the years 1983, 1988, 1994 and 1995. These are years that contain extreme discharge events. Other extreme fluctuations are found during the years 2001 and 2002. During the latter three years no extreme discharge events higher than 8500 m^3/s are observed. However, the high water events during those years had a relative long duration. This emphasises the theory from Chapter 2, where it is discussed that not only the highest discharges result in the largest morphodynamic changes, but it is rather a combination of discharge magnitude and duration.

The PDF in Figure 4.15c represents the long-term statistics of the amplitude of the bed level fluctuations and is presented in Figure 4.15c. The PDF has the nature of an exponential probability distribution which can be described by one single statistical parameter since the mean is equal to the standard deviation (Lane, 2013). Therefore, the standard deviation is selected to serve as an indicator of the long-term statistics that characterise the amplitude of the yearly bed level fluctuations. It is referred to as σ_f. It is a physical indicator of the amplitude of the fluctuations. The σ_f is expressed in the same units as the amplitudes.

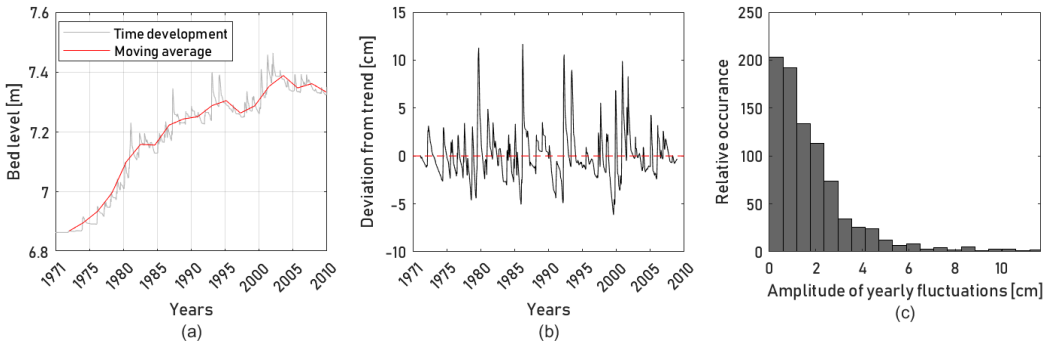

Figure 4.15: (a) Time series and the moving average of the bed level response to the natural series 1971-2010 at location A, **(b)** the bed level fluctuations around the moving average trend and **(c)** the histogram of the deviation of the bed level fluctuations around the long-term trend from which the standard deviation is derived as the physical indicator of the bed level fluctuations: $\sigma_f = 1.77$ cm.

The same procedure is executed for several locations around the reach with the widened floodplain and for all 20 realisations that follow from the Monte Carlo simulation. The resulting probabilistic bandwidth of σ_f for the 20 Monte Carlo realisations (gray), the mean of these realisations (black) and the results from the discharge time series series 1971-2010 (red) are presented in Figure 4.16. The maximum fluctuations are observed shortly after the flow expansion at the widened floodplain. A second maximum is observed just downstream of the end of the widened floodplain. These are the zones with the sharpest sediment gradients. At those zones, the HBL-waves are generated, leading to the largest fluctuations within the studied reach. These zones coincide with locations A and C. Downstream of C, the fluctuations are mainly caused by HBL-bed waves that propagate downstream. These bed waves dampen out gradually, as discussed in Section 4.2.

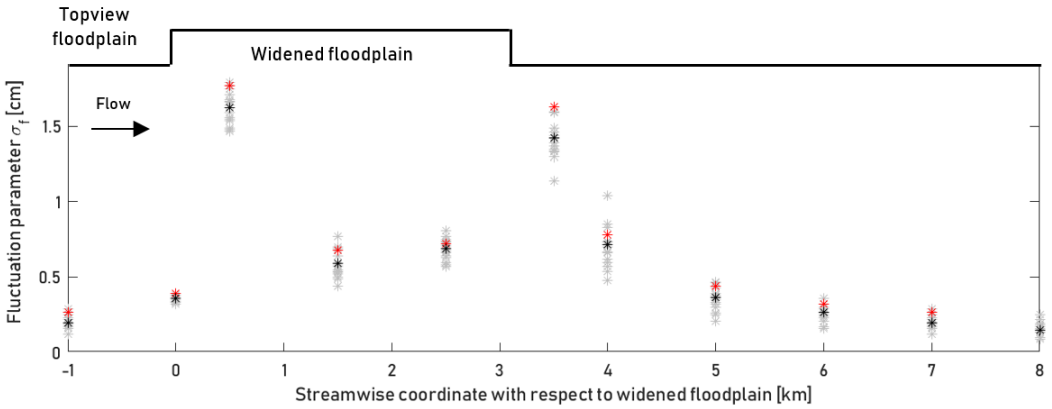

Figure 4.16: Fluctuation parameter σ_f around the reach with the widened floodplain. The results from the Monte Carlo simulations are depicted with grey dots, the black dots represent the mean of the probabilistic results and the response to the natural series 1971-2010 is represented by red dots.

4.3.4 Instantaneous bed level changes

Earlier, it was found that it is the combination of discharge magnitude and duration of a discharge stage that defines the intensity of morphodynamic change. To gain insight into this theory, the instantaneous change in bed level of each discharge stage of the piecewise constant hydrograph is evaluated. The instantaneous morphodynamic change is defined as the difference of the bed level prior to- and at the end of the steady discharge step in the hydrograph. This concept is schematised in Figure 4.17.

In this way, the net change during each specific discharge stage is evaluated. This is done for location A. Positive values indicate sedimentation, negative values depict erosion. To gain insight into the contribution of the duration of all discharge events, the dots in Figure 4.18 have a colour indication. The colour scale is based on a normalisation of the duration of a discharge stage with a specific magnitude, with respect to the maximum duration of all stages in the record that have that specific discharge magnitude.

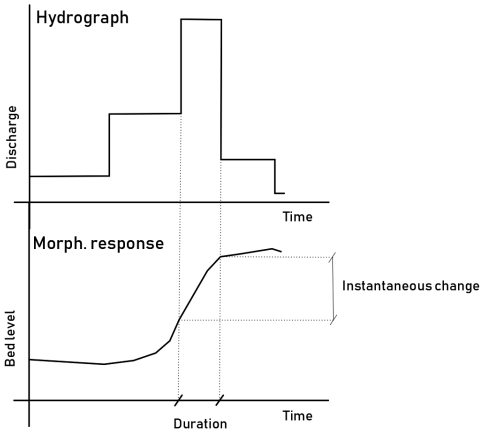

Figure 4.17: Concept behind the instantaneous change.

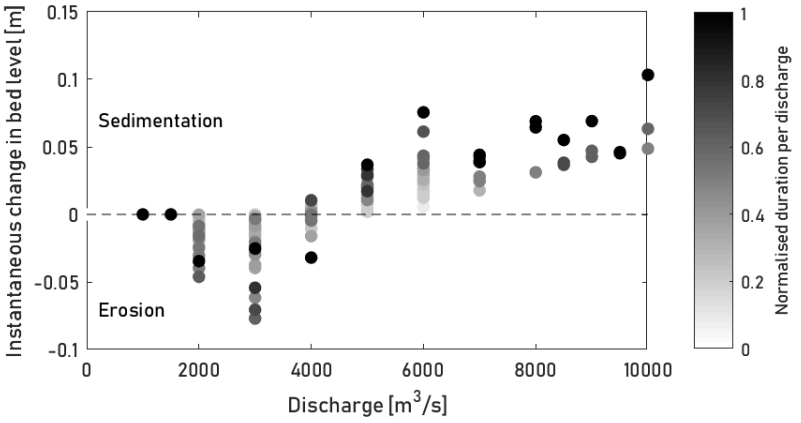

Figure 4.18: Instantaneous change for each discharge magnitude. The gray scale indicates the normalised duration per discharge level. The longer the duration of the discharge stage, the darker the dots.

The results from Figure 4.18 confirm the theory that sedimentation occurs during discharge stages that exceed bankfull discharge (Q>4000 m^3/s) and that the growth of a sedimentation zone is damped by discharge stages that do not exceed bankfull discharge (Q<4000 m^3/s).

It is found that for each individual discharge stage a wide variety of instantaneous changes can be found. In general, the discharge events of the same discharge magnitude, with a larger duration, cause a larger instantaneous change. A few exceptions can be observed. A responsible factor for this, is the influence of memory effect, which means that the instantaneous change for a discharge is also influenced by the prior morphodynamic state. The memory effect will be studied later on in this chapter.

From this analysis it is found that the most significant changes in bed level are not only observed during periods of extreme discharge magnitudes (and the associated sediment gradients), but also for medium- to high discharge stages, with a relatively long duration. This agrees with the theory by Costa and O'Connor (1995) and Wolman and Miller (1960).

The maximum instantaneous change in bed level that is observed during a discharge stage of 6000 m^3/s and 3000 m^3/s are examples of that.

Such an analysis of the instantaneous changes in bed level is less obvious for locations B and C, since at these locations not only the direct changes in bed level due to a varying discharge is experienced, but bed waves that are generated at location A pass locations B and C and affect the instantaneous bed level changes as well. These analyses are made for completeness and can be found in Appendix C.2. At location C (where the flow experiences acceleration during discharge stages that exceed bankfull discharge and resulting positive sediment gradients cause erosion in the main channel) the low discharges cause aggradation and compensate the erosion that is caused by discharge stages that exceed bankfull discharge. This opposite is observed for location A in Figure 4.18.

In Figure 4.8 it is shown that discharges lower than 1500 m^3/s do not lead to sediment transport as a result of the threshold-based Meyer-Peter Müller sediment transport model. From the results in Figure 4.18 it is confirmed that these discharge stages do not contribute to morphodynamic change. During these discharge stages, no instantaneous change is observed.

4.4 The deterministic cycled annual hydrograph (CAH)

The purpose of deterministic hydrograph time series is introduced in Chapter 3. It is considered as a *best guess* regarding a future discharge time series and aims to yield similar morphodynamic development as obtained with the mean morphodynamic trends from a Monte Carlo analysis. In this section the deterministic hydrograph will be referred to as the cycled annual hydrograph (CAH). The performance of this approach with respect to the results from the Monte Carlo simulation will be evaluated.

The CAH can be derived based on the long-term discharge statistics. The flow duration curve that is based on the discharge data set of the Dutch Upper Rhine from 1971-2010 is discretised. By doing so, the statistical mean and standard deviation are not changed. Subsequently, a symmetric annual hydrograph is constructed based on the discretised flow duration curve (Figure 4.19a). Each year, the CAH is cycled. Hence, for a simulation of 40 years, the CAH is cycled 40 times.

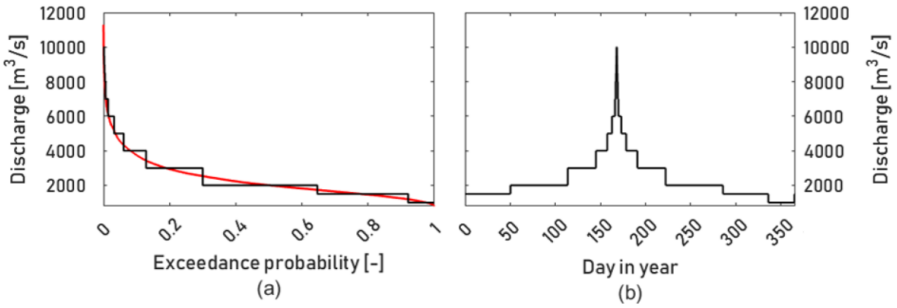

Figure 4.19: (a) The flow duration curve of the discharge data set of the Upper Dutch Rhine from 1971-2010 (red) and the discretised flow duration curve of the CAH (black); **(b)** the piecewise constant CAH [source data: GRDC, 2018].

By imposing the CAH discharge time series with similar long-term statistics as the natural discharge time series that is imposed in Section 4.2, the average sediment fluxes for all fractions are found to be similar at the upstream model boundary.

4.4.1 Long-term development

The morphodynamic state after 40 years is presented in Figure 4.20 for both the probabilistic bandwidth that yields from the 20 Monte Carlo realisations (gray) and the CAH-series (red). The resulting morphodynamics from the CAH hardly coincides with the mean development from the probabilistic bandwidth, especially at locations A and C where the largest sediment transport gradients are found and where HBL-effects are of dominant influence on the river bed development. In between locations A and C, the resulting morphodynamics falls within the probabilistic bandwidth to a larger extent. The final morphodynamic state is not indicative for the comparison of time-development as it depends on the moment of truncating the hydrograph and the last few years of the time series as will be demonstrated later in this chapter. Therefore, the morphodynamic development for the three locations A, B and C is plotted and compared to the mean time development of the probabilistic bandwidth in Figure 4.21.

From Figure 4.21 it is also clear that at locations A and C the CAH does not result in similar long-term bed level development as the mean trend from the Monte Carlo simula-

tions. Moreover, the resulting bed level development from the CAH-series tends towards a different dynamic equilibrium condition with respect to the mean trend from the probabilistic calculations, especially at locations A and C where HBL-effects are dominant. This implies that the dynamic equilibrium bed level at locations that are dominated by HBL-effects are not merely governed by the long-term discharge statistics. It is suggested that the local development of the morphology is a result of the recurrence, variation of the duration and intensity of flood and low discharge events and the HBL-waves that result from discharge series with these characteristics. The non-linear combination of HBL-waves that are caused by the CAH-series at location A and C clearly leads to a different dynamic equilibrium condition compared to the mean from the Monte Carlo analysis, in which time series are included that pursue the inherent natural variability of the discharge time series in the Upper Dutch Rhine. This natural variability is not well-represented by the current deterministic CAH-approach as one single hydrograph is cycled each year. As a consequence, the superposition of HBL-waves deviates from what is found with the natural discharge series.

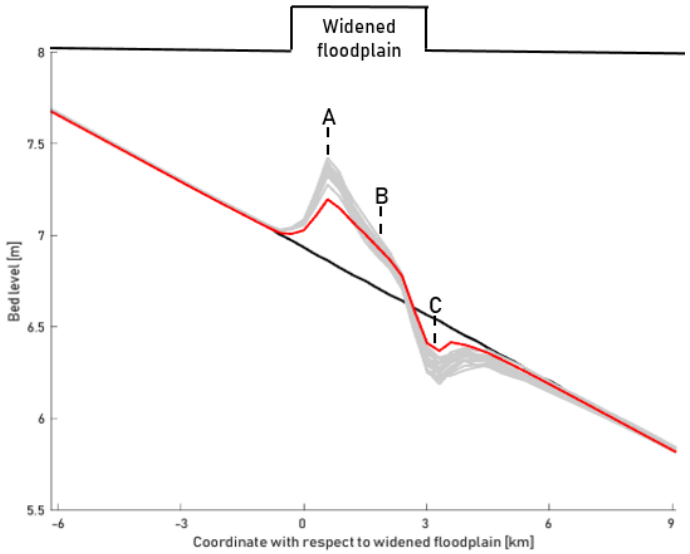

Figure 4.20: The morphodynamic state after 40 years using the CAH (red) with respect to the 20 Monte Carlo simulations (gray)

The fact that the CAH-series does not yield similar long-term bed level development at the zones with extreme sedimentation and erosion compared to the mean from the probabilistic bandwidth, is an important drawback. The zones where the river bed experiences the most sedimentation, a bottleneck might develop regarding the navigability of a river (location A). Therefore, reliable model predictions are crucial when studying the effects of river interventions. On the other hand, it is desirable to make reliable predictions of zones that experience relatively much erosion (location C) since this might amongst others induce instabilities of the surrounding soil and neighbouring structures. At location B, which is dominated by milder transport gradients and experiences relatively less influence of the HBL-effects, the resulting bed level development falls well within the probabilistic bandwidth that yields from the Monte Carlo realisations. Still, differences with respect to the mean trend from the Monte Carlo bandwidth are noticable. It was found earlier that location B experiences moderate HBL-effects that are generated at location A. This might be

the reason for the relatively small differences between the long-term bed level development that results from the CAH-series compared to the mean bed level trend from the Monte Carlo simulations.

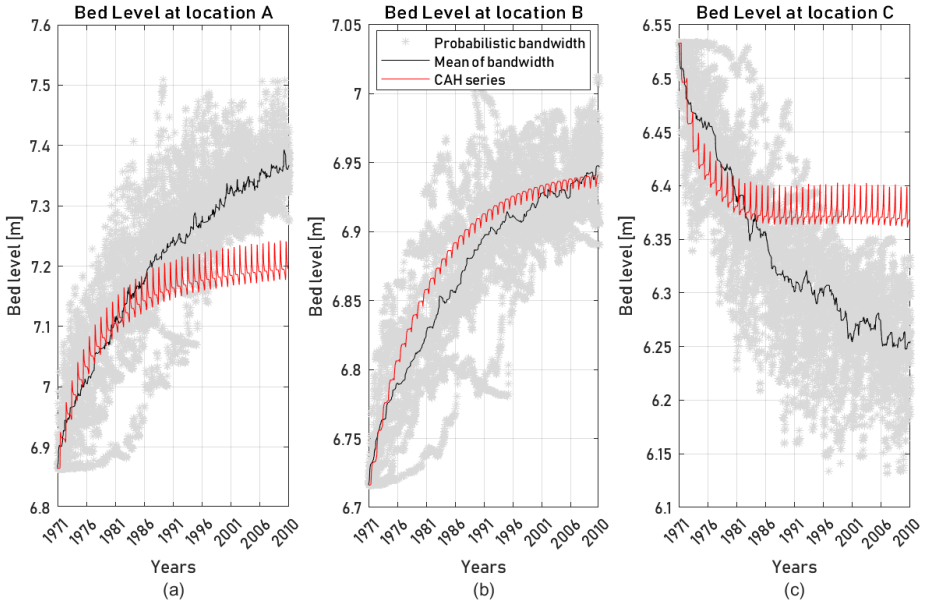

Figure 4.21: The time development of the bed level at locations **(a)** A, **(b)** B and **(c)** C, including the reference bandwidth (gray), the mean development of the Monte Carlo simulations (black) and the morphodynamic response to the CAH-series (red).

The time development of the geometric mean sediment grain size D_{50} is presented in Appendix C.3. Similar differences are observed between the mean long-term development from the Monte Carlo realisations and the morphodynamic response to the CAH-series.

4.4.2 Bed level fluctuation characteristics

Besides the long-term development, the resulting fluctuation characteristics (σ_f) around the long-term trend are examined. By simplifying a single year into a hydrograph with only one extreme discharge event per year, only fluctuations are obtained with a periodicity of one year. The fluctuations are again analysed by subtracting the mean trend from the bed level time development, as performed in Section 4.3.3. The time series, the fluctuations around the long-term trend and the hydrograph of the deviation from the mean trend are presented in Figure 4.22.

A yearly fluctuation with a maximum amplitude of 4-5 cm can be observed. This method does not have the potential to model the extreme fluctuations as observed with the natural series, even though each year a high discharge stage of 10.000 m^3/s passes. The main reason for this is the fact that the duration of extreme discharge stages is short compared to the natural series. The histogram in Figure 4.22c shows less spreading compared to the response to the natural series (see Figure 4.15c). This is caused by the fact that the CAH is characterised by a similar low- and high water period throughout the entire 40 years. As a consequence, limited variation in the fluctuations around the long-term trend can be

observed. This emphasises the importance of the variation in duration of discharge stages considering the range of fluctuation amplitudes around the long-term bed level development.

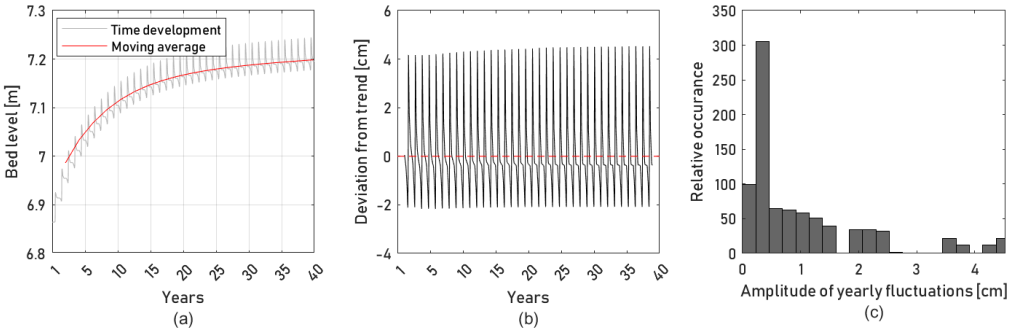

Figure 4.22: (a) Time series and the moving average of the bed level response to the CAH-series at location A; **(b)** the bed level fluctuations around the moving average trend**(c)** the histogram of the deviation of the bed level fluctuations around the long-term trend from which the standard deviation is derived as the physical indicator of the bed level fluctuations: $\sigma_f = 1.07$ cm.

The analysis of the fluctuation parameter σ_f that results from the CAH-series, in combination with the results from the 20 Monte Carlo simulations, is shown in Figure 4.23 for several locations around the widened floodplain.

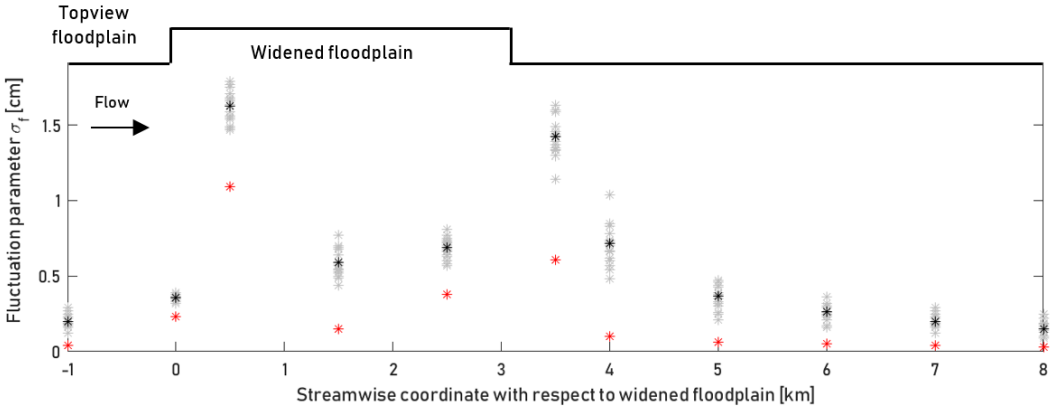

Figure 4.23: The fluctuation parameter σ_f around the reach with the widened floodplain. The probabilistic bandwidth (gray), the mean development of the Monte Carlo simulations (black) and the response to the CAH (red).

From the comparison of the fluctuation parameter σ_f, it is clear that the CAH-series is not suited for making indications of the fluctuations in the river bed at any location around the reach with the widened floodplain. Neither were any significant propagating waves observed downstream of location C. This emphasises the underprediction of bed level fluctuations and bed level waves when applying the CAH-schematisation.

Besides the simulation of long-term morphodynamic development, the CAH lacks performance with respect to the variation and amplitude of fluctuations as well, even though the long-term statistics of the discharge and the yearly periodicity are maintained. This

implies that the alternation and duration of hydrograph years is of paramount importance on morphodynamic change.

4.4.3 Instantaneous bed level changes

To study the previous findings in more detail, the instantaneous change in bed level[2] is evaluated for each discharge stage in the CAH-series. The instantaneous change in bed level for both the natural series 1971-2010 and the CAH are presented in Figure 4.24 in case of location A, where the flow suddenly expands and decelerates. The instantaneous response clearly differs between the series. Generally, the instantaneous response for each discharge value is significantly less when modelled with the CAH-series, compared to the natural series. As is stated in Section 4.3.4, such an analysis is not straightforward when applied at locations B and C. For completeness, the instantaneous response with the CAH-series at locations B and C are presented in Appendix C.4.

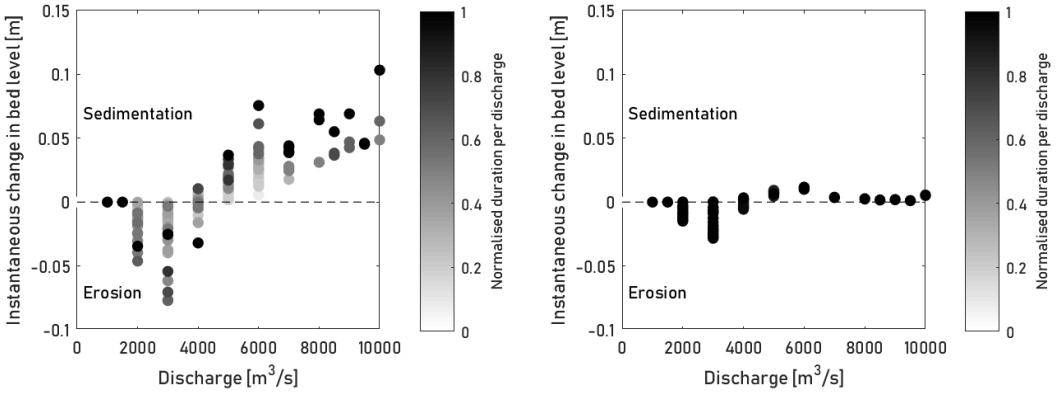

Figure 4.24: Comparison of the instantaneous change in bed level during each discharge stage of **(a)** the natural series 1971-2010 and **(b)** the CAH-series at location A.

This difference in instantaneous response does not necessarily mean that the cumulative effect of the instantaneous responses for each discharge magnitude differs as well, since the total duration of each discharge stage over the 40 years is not changed. From Figure 4.21 it can already be observed that at location A the long-term cumulative effect of all discharge stages results in a bed level difference of approximately 15 cm after 40 years, compared to the mean trend of the 20 Monte Carlo simulations. Figure 4.25 shows the cumulative contribution to bed level change per discharge magnitude for both the CAH and the probabilistic mean. This cumulative contribution is obtained by integrating all instantaneous changes for a specific discharge magnitude with respect to time.

Figure 4.25 clearly shows that the discharge stages below bankfull discharge (Q<4000 m^3/s) contribute to cumulative erosion at location A. In other words, these discharges force the river bed to its initial state, whereas discharges stages that exceed bankfull discharge induce sedimentation as a consequence of the local negative sediment transport gradients. It can be noticed that the cumulative contribution of the highest discharges remains fairly equal. In the mid to mid-high range (4000-6000 m^3/s), the CAH-series results in an underprediction of the cumulative response of these discharges. For the low-mid to mid range

[2]See Figure 4.17 for an explanation of the concept of instantaneous change in bed level.

(2500-4000 m^3/s) an overprediction of the cumulative contribution of these discharges can be observed, whereas around 2000 m^3/s the cumulative contribution is again underpredicted.

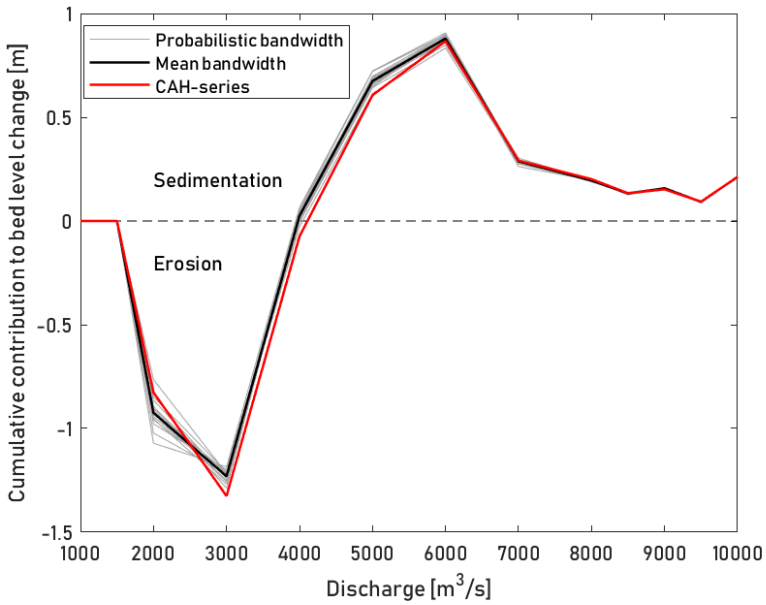

Figure 4.25: Comparison of the cumulative bed level change for each discharge value of the 20 Monte Carlo realisations (gray), the mean of the Monte Carlo simulations (black) and the CAH-series (red).

Table 4.1 gives an overview of the sum of the cumulative contribution for discharges below and above bankfull discharge for both series. From this overview, one can observe that the cumulative contribution of all discharges below bankfull discharge are slightly overpredicted. The sum of the cumulative contribution of all discharge stages above bankfull discharge is underpredicted. The total net difference is the same as observed at the end of 2010 in Figure 4.21, which is about 17 cm at location A.

Table 4.1: Comparison of the sum of the cumulative contribution to bed level change of discharge below and above bankfull discharge as well as the net cumulative effect.

Series	**Sum cum. cont.** $Q \leq Q_{bf}$	**Sum cum. cont.** $Q > Q_{bf}$	**Net change [m]**
Prob mean	-2.13 m	+2.63 m	+0.50 m
CAH	-2.22 m	+2.56 m	+0.33 m

Conclusion

The differences in long-term development for the CAH compared to the probabilistic mean are mainly dominant at locations A and C, where strong gradients in sediment transport prevail. This suggests that in zones where strong sediment transport gradients are experienced and the influence of HBL-effects is strong, the CAH-series are not suited for simulating the long-term morphodynamic development. An explanation for this mismatch is the fact that in case strong sediment transport gradients are experienced, relatively large fluctuations can be found and the (non-linear) combination of HBL-waves is paramount. Locally,

the variation of discharge sequences becomes increasingly relevant in morphodynamic development. The induced HBL-waves that result from the CAH-series are found to have a much smaller amplitude and the non-linear combination of the HBL-waves does not lead to similar dynamic equilibrium bed level states compared to the mean of the 20 Monte Carlo realisations, which account for the inherent natural variation of the river discharge. Hence, only introducing the long-term statistics with a yearly frequency seems not to be effective in modelling the morphodynamics in and around zones where strong sediment gradients and HBL-effects are experienced. This agrees with the theory by Van der Klis (2003) that the growth of the local sedimentation and erosion zones are governed by amongst others the frequency, variation (sequences) and duration of discharge events.

The CAH-series do not account for variations in sequences and duration of discharge events, neither does it account for any variation in short- and long-term sequences. With the aim of finding an improved deterministic hydrograph schematisation, important features that define variability in discharge are studied in the upcoming sections of this chapter.

4.5 The importance of short-term sequences

This section evaluates the impact of reducing the daily structures within a yearly hydrograph into simplified, symmetric, yearly hydrographs with a single yearly maximum event. As a consequence, fluctuations that result from short-term daily sequences are neglected. The aim is to study the contribution of intra-annual sequences that occur on time scales that are smaller than one year to long-term bed level development. A reason for modifying time series that way, is the fact that in general the number of discharge steps in a year decreases. Hence this reduces the computational time. Moreover, no methods for maintaining daily structures in a year have to be accounted for. As a reference, the measured discharge time series 1971-2010 is used. Besides this natural series, a series is introduced in which the daily structure is modified into symmetrical yearly hydrographs with only one extreme discharge event, similar to the approach by Ottevanger et al. (2015). The sequence of the years 1971-2010 and the yearly statistics is not changed in the modified series. This procedure is schematised in Figure 4.26.

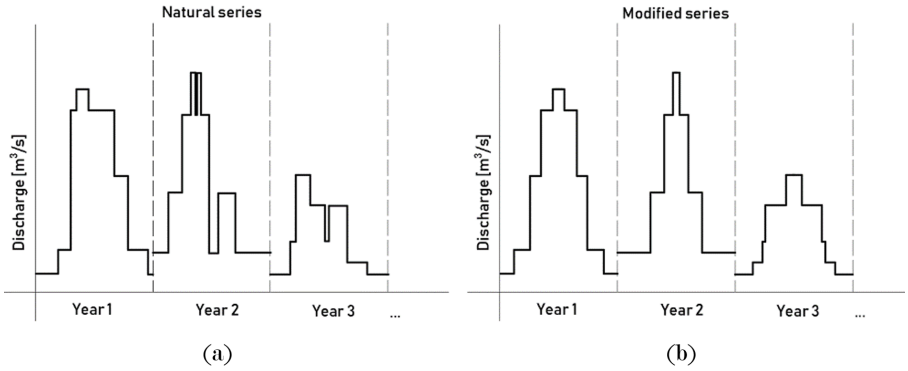

Figure 4.26: Schematic of **(a)** the natural series in which the daily structures are maintained and **(b)** the modified hydrograph in which the years are represented by symmetric hydrographs.

By reorganising the natural years into simplified yearly hydrographs, the duration of the discharge stages differs from the durations in the natural series. Figure 4.27 shows that the duration of stages with a relatively low discharge generally increases (but the total duration of each discharge magnitude in a year is conserved).

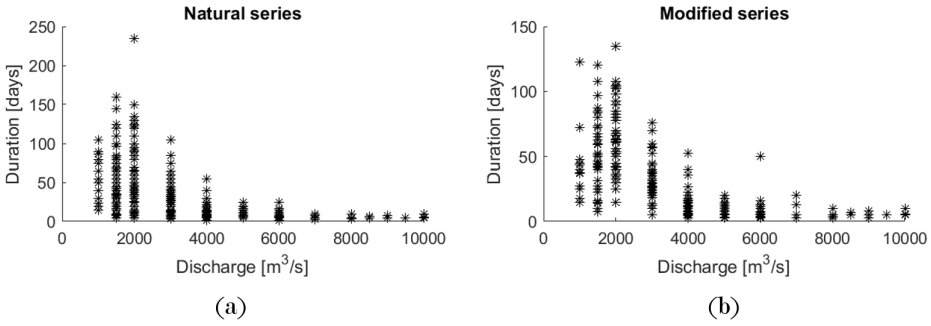

Figure 4.27: Discharge stages versus duration of the discharge stages for **(a)** the natural series 1971-2010 and **(b)** the modified hydrograph series.

The main reason for this is that the lowest discharge stages occur more frequently in a year than the events with a relatively high discharge, whereas the extremest discharge events occur mostly once a year. On the other hand, the duration of high discharge stages is hardly changed due to the fact that these stages occur mostly once in a year when observing the natural discharge time series. Consequently, by modifying the years into symmetrical hydrographs with one flood event, mainly the duration of the low to mid regime of discharges is affected. The redistribution of discharge stages is expected to change the balance between the (restoring) lower discharge stages and the discharge stages that exceed bankfull discharge and hence the sedimentation and erosion trends of the bed at location A and C respectively.

Long-term development

The long-term development at locations A, B and C for both the natural and the modified discharge time series is studied. In Figure 4.28, it is observed that for all three locations, the long-term development of the bed level does not differ significantly. At the end of the series, the difference in bed level between the two time series is the largest at location A and C. This difference is of the order of several centimeters for this conceptual study. Due to the reorganisation of discharge stages within a year, the difference in timing of the extreme discharge events causes a deviation between the two time series at each moment in time.

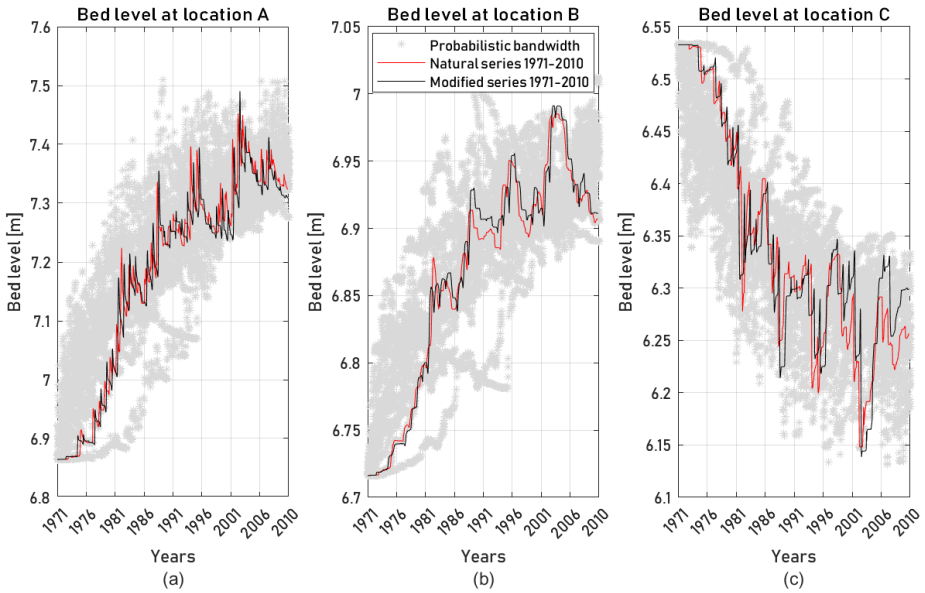

Figure 4.28: Time series of the bed level development at locations **(a)** A, **(b)** B and **(c)** C for the probabilistic bandwidth (gray), natural series 1971-2010 (red) and the modified series (black).

The long-term trends of the bed level development are compared for both the natural and the modified series. These long-term trends are again obtained by computing a moving average. The difference between the long-term trends from the natural and the modified series is presented in Figure 4.29. The difference grows gradually in time, but can still be considered relatively small compared to the total bed level change, as it is in the order of several centimeters.

The difference in long-term trends is larger at locations A and C, compared to location B. Again, this suggests that the morphodynamics at zones with sharp sediment gradients (and hence more influence of HBL-effects and increased non-linear interaction between the river discharge and morphodynamics) is governed by both the long-term statistics and the variation and duration of discharge events.

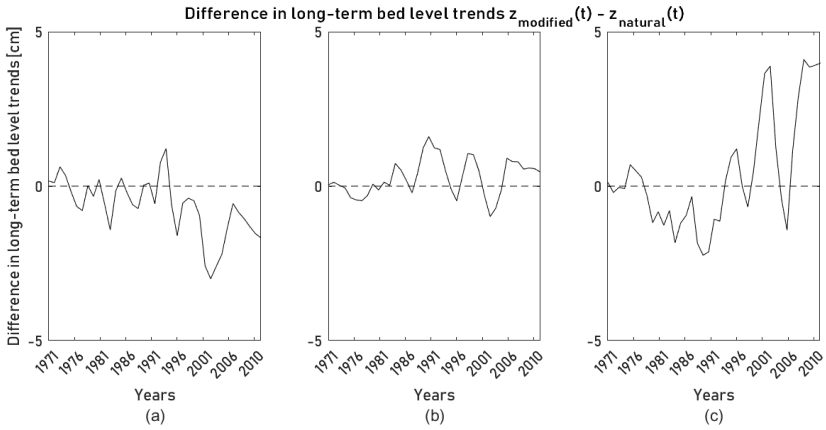

Figure 4.29: Difference in long-term bed level trends between the modified series and the natural series 1971-2010 at location **(a)** A, **(b)** B and **(c)** C.

Bed level fluctuation characteristics

The extent to which the simplification of the hydrograph affects the statistics of the bed level fluctuations is evaluated by studying the fluctuation parameter σ_f. The comparison of the σ_f for the natural and the modified hydrograph series is presented in Figure 4.30. It reveals that the modified hydrograph overpredicts the fluctuations mainly at location A (in the acceleration zone) by approximately 10%. At almost all other locations, the fluctuation intensity is hardly affected. From this, it can be concluded that by simplifying the natural series into simplified, symmetrical hydrographs, similar (HBL-) fluctuations are induced compared to the natural discharge series.

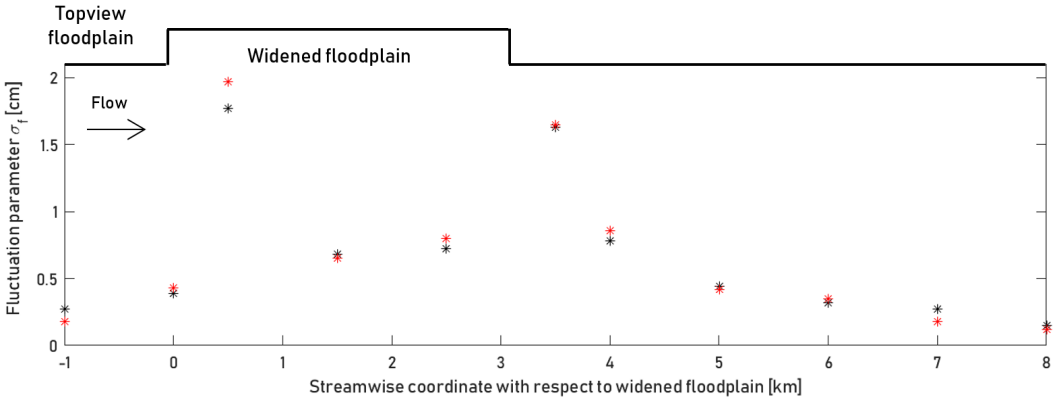

Figure 4.30: The fluctuation parameter σ_f for the natural (black) and simplified (red) series.

Instantaneous bed level changes

By simplifying the natural series into the modified hydrographs, the duration of each individual discharge stage changes. However, the total duration of each discharge stages in a year remains unchanged. In Figure 4.31, the instantaneous response for each discrete discharge at location A is presented for both series.

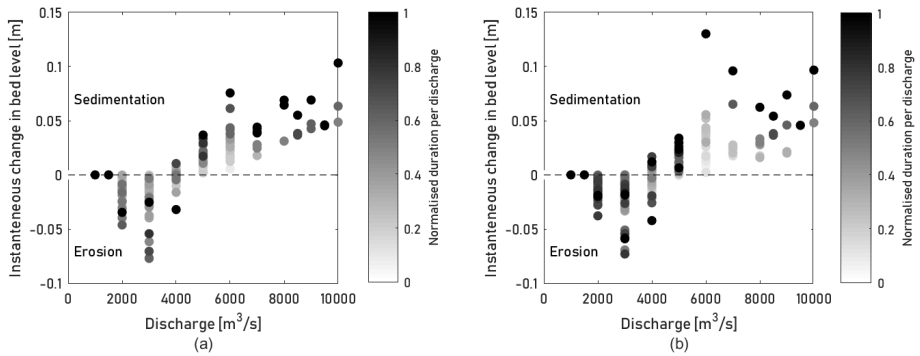

Figure 4.31: Comparison of the instantaneous response at location A for **(a)** the natural and **(b)** the modified series.

From Figure 4.31, it is clear that for the modified series in general, a larger instantaneous response is observed for the mid-high discharge regimes. For both the natural and the modified time series, the cumulative instantaneous change for each discharge magnitude is presented in Figure 4.32.

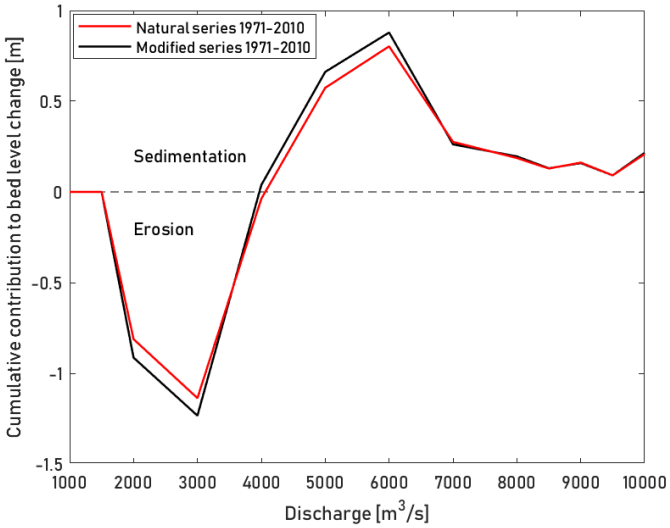

Figure 4.32: Comparison of the cumulative contribution to bed level change for all discharges magnitudes for the natural (red) and modified (black) discharge series.

It can be observed that the modification of the hydrograph leads to a cumulative contribution of the low-mid to mid-high discharges that is slightly overestimated, mainly as a

consequence of the increase of duration of these discharges. The cumulative contribution of the highest discharges is not affected significantly. This is no surprise: when observing the natural discharge time series, discharge events above 6000 m^3/s occur hardly more than once per year. Hence, merging the duration of these discharges within a year hardly results in a different duration than the duration of the event in case of the natural series.

The sum of the cumulative contribution of the discharges below bankfull discharge, the discharge above bankfull discharge and the cumulative change for total discharge range are compared in Table 4.2. Considering the modified series, the overprediction of the contribution of discharges below bankfull discharge apparently compensates for the overpredicted cumulative contribution of the discharges above bankfull discharge and result in small difference in net cumulative change of 4 cm. This is the change that is observed at the end of 2010 at location A in Figure 4.28.

Table 4.2: Comparison of the sum of the cumulative contribution of discharge below and above bankfull discharge as well as the net cumulative effect.

Series	**Cum. cont.** $Q \leq Q_{bf}$	**Cum. cont.** $Q > Q_{bf}$	**Net change [m]**
Natural series	$-1.99m$	$+2.43m$	$+0.44m$
Modified series	$-2.10m$	$+2.59m$	$+0.48m$

It is not straightforward to draw conclusions on the instantaneous change at locations B and C since these are disturbed by bed waves that are generated at location A. Still, for completeness, a similar analysis was conducted for locations B and C. These can be found in Appendix C.5.

4.6 The persistence of the memory effect

In Chapter 2, the memory effect is introduced. It is stated that the morphodynamic state at a moment in time is the cumulative effect of historical flow events. It is discussed that this memory effect has a fading character. The persistence of this memory effect is discussed here as it might have important implications on the construction of discharge time series.

To increase insight on the persistence of the memory effect, two different discharge time series are imposed. For both series, the natural series 1971-2010 is used as a starting point. The years 1976-1985 are placed in a different order for both series. After 1985, the two series are equal up until the end of the simulation. The two series are presented in Figure 4.33. The red dashed lines depict the time window in which the years are reorganised. The daily structure within the years is maintained.

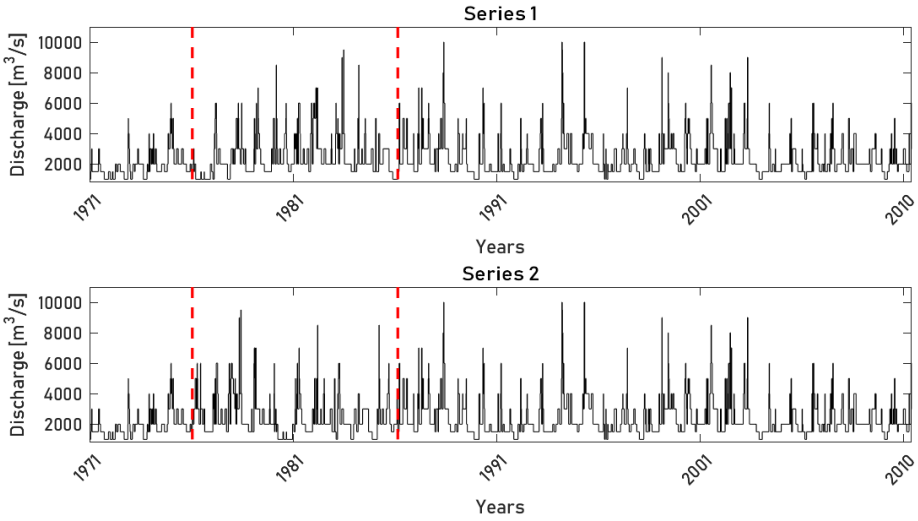

Figure 4.33: Comparison of two time series that are used for studying the influence of the memory effect. The red dashed lines indicate the time window in which the years are reorganised.

The bed level time development of both series at locations A, B and C is presented in the first column of Figure 4.34. The memory effect is evaluated in terms of the difference between the two series ($\Delta z(t) = z_{series2}(t) - z_{series1}(t)$). This difference is presented in the second column of Figure 4.34. To increase insight on the fading character of the memory effect per location, the third column represents the difference in bed level, yet normalised with respect to the maximum observed difference in bed level within the time window. Any difference in morphodynamic state later than 1985, can be addressed as the memory effect.

Before discussing the memory effect, a relatively large momentary difference in bed level between the two series that can be observed inside the time window of rearranged years is observed. This difference is in the order of 10 cm, which is of the same order of magnitude as the bed level change after 40 years of simulation time. This implies that in case a time series is imposed on the model, the final year(s) and the moment of truncating the hydrograph have a dominant influence on the model results if only the end state of the simulation is considered. The final state of the long-term mean trend, or the average morphodynamic state of the last few years might be more indicative.

To show the dependency of the memory effect on its location, the effect is studied at the three locations A, B and C. At location A, the memory effect decreases with time and approaches the zero-difference line after several decades. At location B, the fading of the historical memory persists shorter compared to location A. Regarding location B, the momentary differences inside the time window are smaller and the final different state of the bed level is smaller at the end of 1985 compared to location A. At location C, the memory effect has a similar influence. The time it takes for the memory effect to diminish is comparable to location A, where relatively large bed level changes are found compared to location B. At location C, a small wave is observed right after 1985. This means that the memory effect at a specific location also consist of propagating waves. To study this wave-type of memory effect, two other time series are compared and the memory effect is studied. Similar to the time series in Figure 4.33, two time series are imposed in which the years in between 1986-1996 are reorganised. The results are presented in Figure 4.35.

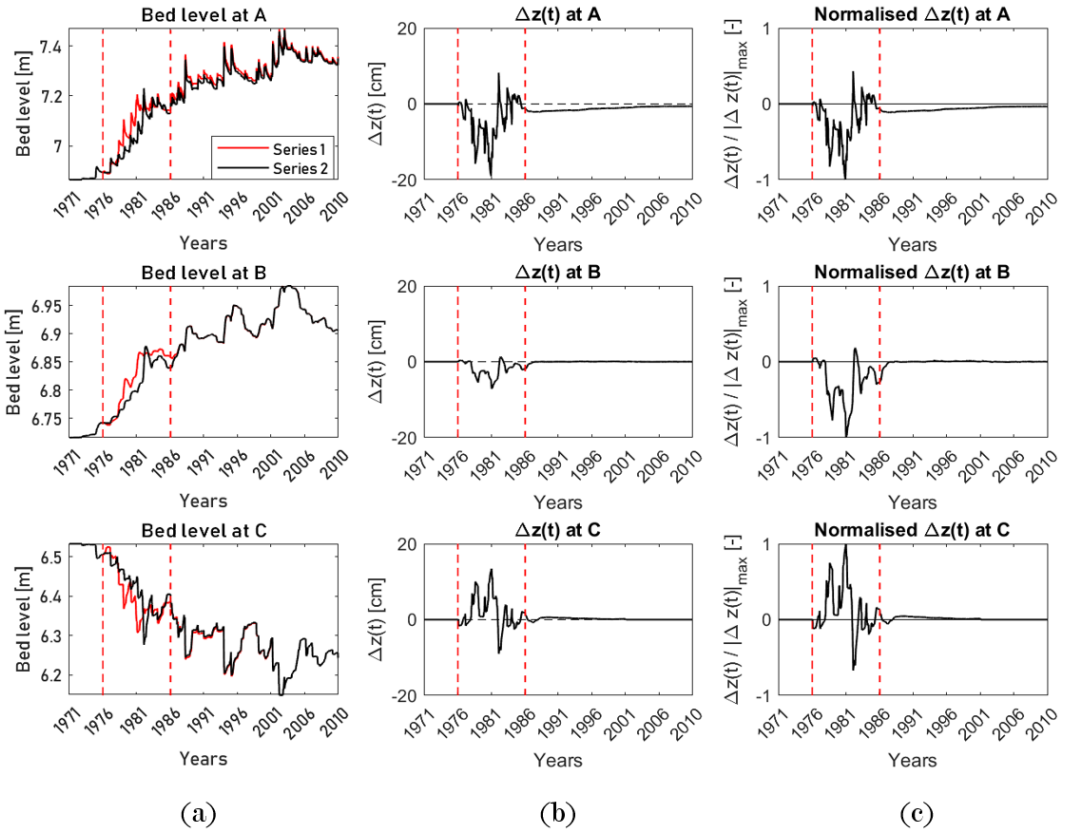

Figure 4.34: Overview of **(a)** the time development of the bed level, **(b)** the momentary difference between the two series and **(c)** the difference normalised with the maximum difference that was observed at that location. The time window in between which the years were reorganised is depicted by the vertical red dashed lines. They mark the period 1976-1986.

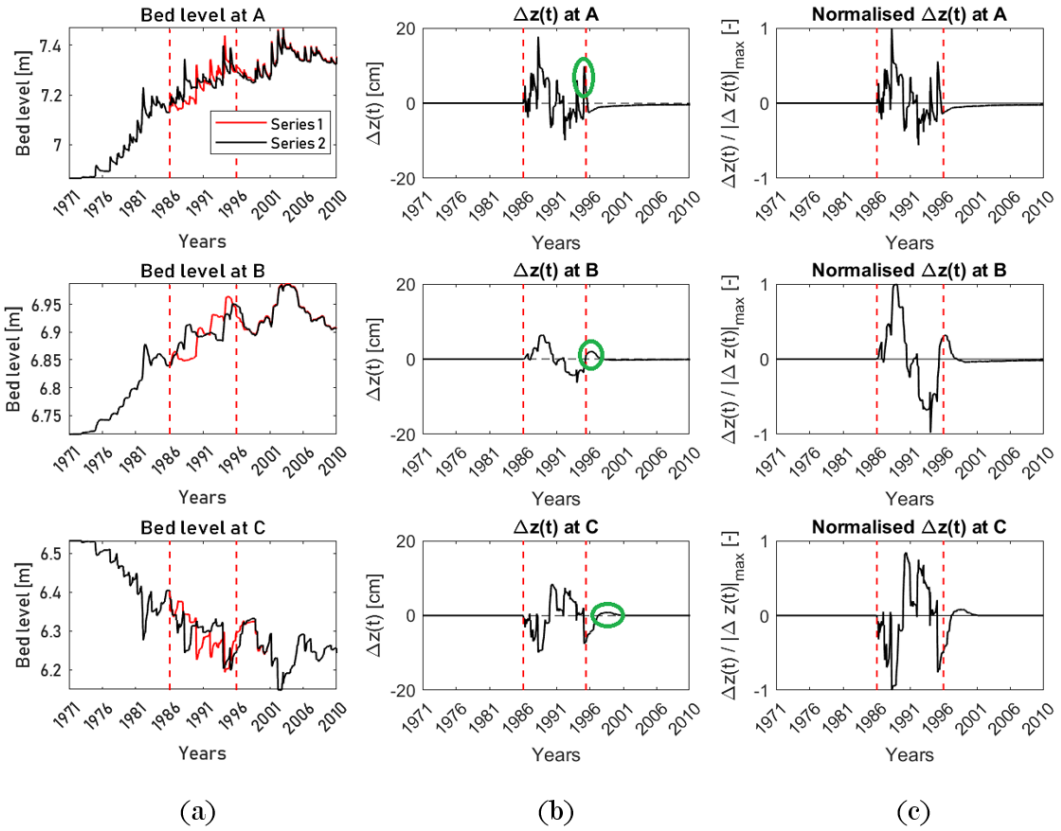

Figure 4.35: Overview of **(a)** the time development of the bed level, **(b)** the momentary difference between the two series and **(c)** the difference normalised with the maximum difference that was observed at that location. The time window in between which the years were reorganised is depicted by the vertical red dashed lines. They mark the period 1986-1996. The propagating wave that is noticable in the memory effect at locations B and C is marked with the green circle in the second column.

In the results that are presented in Figure 4.35 similar conclusions can be drawn as from Figure 4.35. However, at locations B and C, a more clear wave pattern can be noticed in the memory effect in Figure 4.35 compared to Figure 4.35. This wave is marked by a green circle and is present at location A just before the time window in which the years are reorganised ends. A significant difference in bed level is not observed at the end of the time window in the analysis in Figure 4.35. Therefore, a wave is hardly observed in the memory effect at locations B and C in Figure 4.35. With the analysis from Figure 4.35 it is shown that the memory effect consists of local adjustments and passing bed waves.

At all three locations, it is clear that after approximately 5-10 years the memory effect is hardly noticable in terms of the difference in observed bed level. The fading behaviour (or the *decaying signature of historical events*) as mathematically described by Pickup and Rieger (1979) is demonstrated here. The memory proves to be a complex combination of several physical properties of the system. From the present analyses, it is suggested that the memory effect at a certain location depends on the following factors:

- The relative difference in local morphodynamic state at the end of the time window in which the years are reorganised;

- The time scale of the considered morphodynamic feature;
- The distance between the observed locations and the location where upstream bed waves are generated, and hence the (geometric) complexity of the modelled river;
- The propagation velocity of bed waves;
- The diffusive nature of bed waves.

If the modelled morphodynamics shows a rapidly fading memory effect, this might have important implications on the creating of long-term discharge time series. The rapid decrease and the relatively small contribution of the memory effect implies that, in that case, the final morphodynamic state of the simulation is mainly dominated by the last years of the simulation. This means that it would be questionable what is the relevance of generating complex long-term hydrograph time series when the final morphodynamic state is dominated by the last hydrograph years. A conceptual application of this theory will be given in Chapter 7.

4.7 The influence of excluding discharge extremes

Cutting off the extreme discharge peaks in a hydrograph series is sometimes considered in order to save computational time (e.g. in Ottevanger et al., 2015). The maximum discharges are excluded by cutting of the extremes and representing them by the threshold discharge above which the extremes are omitted. This procedure is illustrated in Figure 4.36. In this section, the effect of this procedure on morphodynamic change is examined. This is demonstrated by omitting extreme discharge events and comparing the resulting morphodynamics to the response to the natural series 1971-2010.

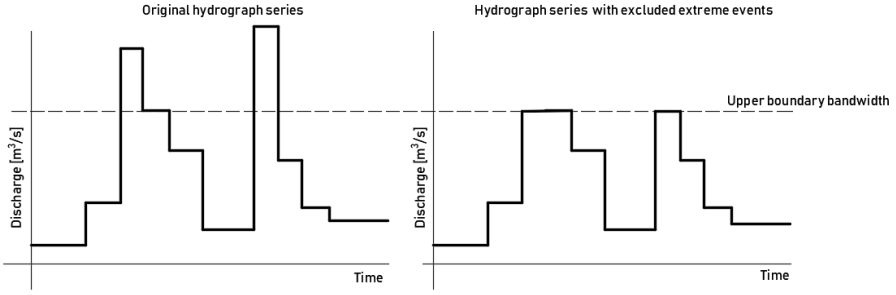

Figure 4.36: Schematic of the original hydrograph and the hydrograph with omitted extreme events

In this section, the natural discharge time series has been reduced up to an upper discharge boundary of 8.000 and 9.000 m^3/s. The resulting statistics of the time series are summarised in Table 4.3. The long-term mean of the discharge is hardly affected by excluding discharge events above this boundary. The standard deviation is more sensitive to reducing the upper tail of the probability density distribution. Omitting the upper tail of the discharge PDF impacts the long-term statistics of the sediment transport differently due to the non-linear interaction of river discharge and sediment transport[3]. It was found that the resulting yearly averaged sediment transport is not affected significantly either as a consequence of omitting the upper tail of the PDF up to 8.000 m^3/s.

Table 4.3: Statistical properties of the probabilistic collection of the different series

Bandwidth	**Mean Q** $[m^3/s]$	**Std.dv. Q** $[m^3/s]$	**Mean S** $[m^3/s]$	**Exc. prob.**
$1.000 - 10.000$	2332.0	1236.5	$8.36e-6$	$4.1e-4$
$1.000 - 9.000$	2330.4	1226.3	$8.28e-6$	$1.6e-3$
$1.000 - 8.000$	2326.0	1206.5	$8.23e-6$	$2.8e-3$

Long-term development

The resulting morphodynamic response of the time series with excluded discharge extremes are compared to the response to the natural series 1971-2010, by subtracting the original series from the modified series with excluded extremes (new-old). The difference between the

[3]This study is roughly based on the geometry, sediment and discharge characteristics of the Dutch Upper Rhine. Frings et al. (2015) found a yearly averaged bedload sediment flux of 0.700 Mt/a $\approx 1.1 - 1.3e-5$ m^3/s, based on field measurements, mass balances and an estimated mass density of the bed. Without any calibration, the model calculates a total bed sediment flux of 8.36e-6 m^3/s for the discharge time series with a discharge range of 1000-10000 m^3/s. This is reasonably close to the findings by Frings et al. (2015).

series is shown in Figure 4.37. The difference in bed level is defined as $\Delta z(t) = z_{modified}(t) - z_{original}(t)$. The figure focusses on the years 1976-1998 as during these years, several extreme discharge events occurred.

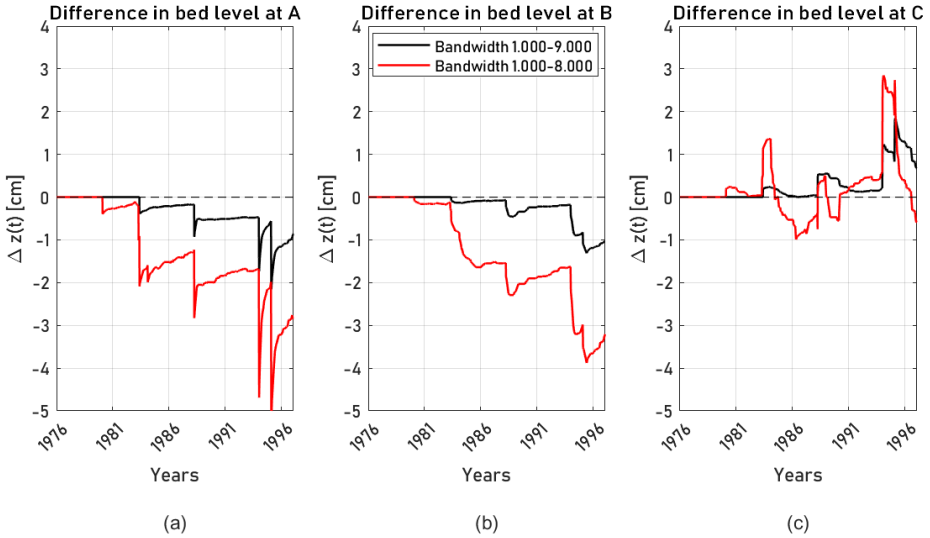

Figure 4.37: Difference of the morphodynamic time development of the bed level from the series with exclued extremes (denoted with the upper boundary of the considered discharge bandwidth), compared to the natural series with a bandwidth of 1.000-10.000 m^3/s (new-old).

The first extreme event that exceeds 8.000 m^3/s passes in 1979. The first time 9.000 m^3/s is exceeded, occurs in 1983. Each time an extreme is cut-off and replaced by the reduced upper limit, the bed level difference suddenly increases. After this sudden difference, a similar process takes place as for the memory effect. Hence, not only the direct impact of extremes are absent, but the memory of these extremes is missing as well. This difference manifests itself in terms of a bed wave of *missing* extremes. Therefore, the differences in bed level in C are more complex. A bed wave due to the *missing* extremes and the according memory at A travels downstream and reaches B and C eventually.

Earlier, it was stated that the local rising trend at location A is caused by the fact that the lower discharges, in combination with their duration and the according morphodynamic time scale, were not able to dampen the growth of this sedimentation hump that was induced by the discharge stages that exceed bankfull discharge. By excluding extreme events above the defined upper boundaries in the series, the growth of the sedimentation hump at location A is limited compared to the natural series. This can be observed by means of the negative difference at location A.

At the zone where the flow experiences sudden acceleration (location C), for the same reason, one might expect that excluding extreme events would lead to a limited eroding trend compared to the original series (hence a positive difference). However, the bed level development at location C is much more complex due to bed waves of *missing* extremes that propagate downstream and affect the development at location C. Still, sudden differences in bed level can be observed at location C, especially in the years 1979, 1983 and 1994.

CHAPTER 5

An improved deterministic hydrograph schematisation

In this chapter, an improved deterministic hydrograph schematisation is aimed for, based on the main findings from Chapter 4. This chapter consists of two main parts: 1) a recap of the weaknesses of the deterministic cycled annual hydrograph (CAH), a demonstration of how the improved hydrograph schematisation is obtained and how it can be constructed (Section 5.1) and 2) a demonstration of the resulting improvements in terms of long-term bed level development, yearly bed level fluctuations and a rough indication of the uncertainty in simulated morphodynamics (Section 5.2-5.6).

5.1 Constructing multiple cycled annual hydrographs (MCAH)

Chapter 4 shows a comparison of the morphodynamic change that results from a probabilistic Monte Carlo simulation and the morphodynamic response that follows from the CAH. The weakness of the latter method proves to be the absence of variation in intensity of discharge events and the absence of variation in long-term hydrograph sequences. Differences in long-term morphodynamic development between the two methods is especially observed around the zones that experience relatively strong sediment transport gradients and large fluctuations that are mainly the result of hydrograph boundary layer (HBL-) effects.

Another important finding of Chapter 4 is that by simplifying yearly hydrographs into symmetric hydrographs, similar long-term morphodynamic development and fluctuations are observed on time scales of years to decades, compared to the natural series. These results are used to find an improved deterministic hydrograph schematisation. With this updated method, the variability of duration of discharge stages and yearly high water events is to be preserved to a larger extent. A way to establish this, is by introducing the multiple cycled annual hydrographs (MCAH-) method instead of the CAH-approach.

First, a method to increase the number of cycled annual hydrographs will be discussed. Based on the long-term daily discharge measurements, an approach is introduced in which hydrograph years with similar statistical properties can be characterised by a single clas-

sification parameter. Two classification parameters are considered. The first parameter is the yearly maximum discharge. This parameter is relatively easy to obtain from long-term discharge measurements. Moreover, the yearly maximum discharge is an important contributor to the yearly fluctuations. A statistical analysis is conducted for the discharge time series of 1901-2010 at Lobith. For each year, the mean discharge and the standard deviation of that year were obtained and compared to the yearly extreme discharges. The analysis yields a positive correlation of the yearly extreme discharge and the yearly mean discharge ($\rho = 0.67$), but even a stronger correlation with the yearly standard deviation of discharge observations ($\rho = 0.91$), as Figure 5.1 illustrates.

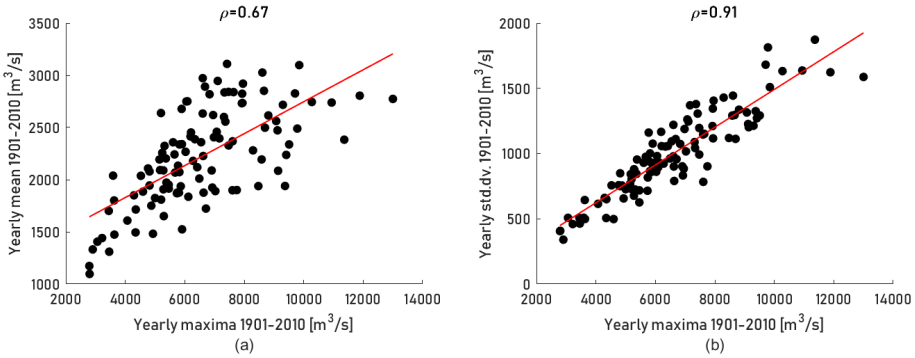

Figure 5.1: Correlations between **(a)** the yearly maximum discharge with respect to the yearly mean discharge and **(b)** the yearly maximum discharge and the yearly standard deviation of the discharge. Both for the years 1901-2010 at Lobith. The red lines represent the linear regression lines through the plotted points [source data: GRDC, 2018].

Besides the yearly maxima, the yearly mean discharge is considered as well to serve as a classification parameter. It is found that the correlation of the yearly mean with the yearly standard deviation of a year is weaker ($\rho = 0.71$) compared to the correlation with the yearly maximum discharge. Therefore it is decided to classify the years based on the yearly maxima of the historical record 1971-2010.

As a next step, threshold levels have to be defined that segregate classes of years with similar statistical characteristics. The years in such a class have a maximum discharge that falls in between two threshold levels. In this study, threshold discharges are defined such that each class contains an equal number of years from the historical discharge data set. How the years relate to the classes and threshold levels, is schematised in Figure 5.2 for the case of three classes with two thresholds levels at 5000 m^3/s and 7000 m^3/s. The impact of the number of classes on the simulated long-term morphodynamic change will be discussed later on.

Step by step, the following procedure is executed to obtain the MCAHs: 1) importing a historical data set of discharge observations; 2) finding the yearly maximum discharge for each year in the historical data set; 3) classes of years are formed by comparing the yearly maximum discharges to threshold levels. Each class contains the years of which the yearly maximum discharges falls within two discharge threshold levels. The discharge threshold levels are defined such, that each class contains an (approximately) equal number of years from the historical dataset; 4) the yearly hydrographs that belong to the same class are combined into a discharge duration curve for that class. Based on the flow duration curve of a class, the statistically representative hydrograph can be constructed in a similar way as for the deterministic CAH for each class.

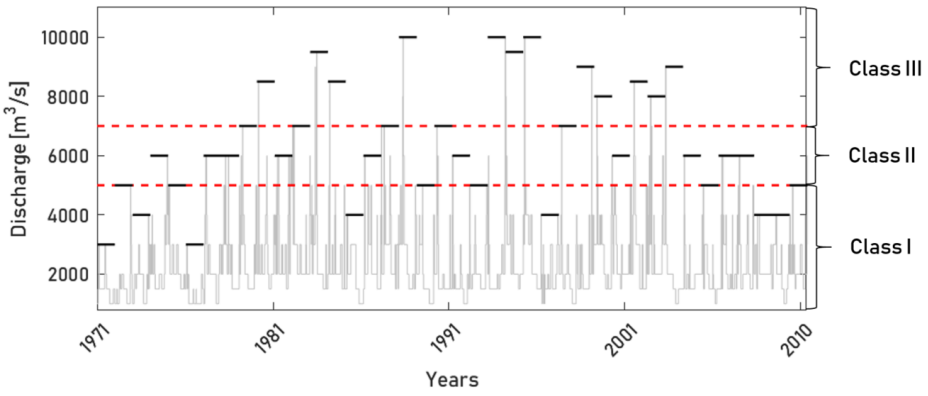

Figure 5.2: Classification of the years of the historical discharge record (gray), by comparing the maximum yearly discharge stages (black lines) with respect to the discharge thresholds (dashed red lines). Each class contains an equal number of years.

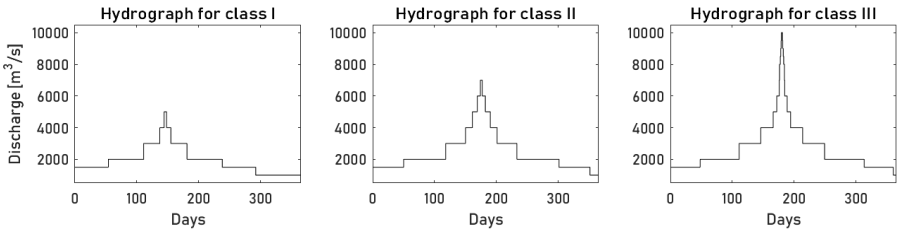

Figure 5.3: The hydrographs that are based on the flow duration curves of classes I, II and III from Figure 5.2.

Using the multiple cycled annual hydrographs (MCAH; one for each class), artificial time series can be constructed. The occurrence of each MCAH in the artificial time series must correspond to the relative occurrence of the years that are included in the according class. This is necessary in order to maintain the long-term statistics of the discharge record. Since no correlation among subsequent years is observed in Chapter 2 in case of the river Rhine, the long-term hydrograph time series is obtained by spreading the MCAHs equally over the time domain, such that their occurrence is well-spread. An example for a series with three MCAHs is presented in Figure 5.4.

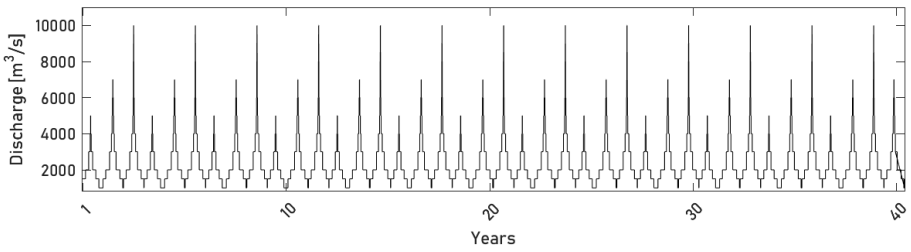

Figure 5.4: The artificial time series with the three MCAHs from Figure 5.3.

5.2 Tested series

The morphodynamics will be studied for a selection of test cases using different numbers of classes (MCAHs). The cases that are studied in the upcoming sections are summarised in Table 5.1.

Table 5.1: Considered number of classes (MCAHs) and the threshold that define the classes of years.

Series	**Number of classes/MCAHs**	**Threshold discharges** [m^3/s]
Ser0	1	CAH-series
Ser1	2	6000
Ser2	3	5000, 7000
Ser3	4	5000, 6000, 8500
Ser4	5	4000, 5000, 6000, 7000
Ser5	6	4000, 5000, 6000, 7000, 8500
Ser7	40	Reorganised natural series

Ser7 is an extreme series in which all the years of the natural 1971-2010 discharge record are represented by symmetric hydrographs with a single high water event. This is the series that was discussed in Section 4.5. For the series that is used here, the years are reorganised such that the years with discharge extremes and the years with relatively low discharge maxima are more or less equally spread over the 40 years of simulation time.

5.3 Long-term development

The morphodynamic state after 40 years is presented in Figure 5.5a and 5.5b for the different series from Table 5.1. Due to clarity, the results are spread over two separate figures. The cases with 1-3 classes are presented in Figure 5.5a. The cases with 4-6 are presented in Figure 5.5b.

From the comparison of the morphodynamic states after 40 years, it turns out that increasing the number of MCAHs improves the performance of the deterministic discharge time series compared to the CAH-series. Mainly by increasing the number of MCAHs from 1 up to 4, the morphodynamic development with respect to the probabilistic bandwidth improves. When the number of classes is increased further, the difference between the final states of the series is not significant, as can be observed in Figure 5.5b.

By studying the influence of long-term sequences in Section 4.6, it is concluded that the morphodynamic state at the end of the simulation should not be considered as fully indicative for the long-term development of the river bed, since the final hydrograph years and the moment of truncating the hydrograph have a significant influence on the morphodynamic state at the end of the simulation. Therefore, the morphodynamic time development of the bed level, as well as the according long-term trends are studied at location A, B and C. A selection of the results is presented here. The morphodynamic development of the bed level that results from the deterministic discharge series with 2, 4 and 6 MCAHs is shown in Figure 5.6 - 5.8. In order to compare the bed level development from the MCAH-series to the CAH-series, the bed level response to the CAH-series is plotted as well in each figure. The analyses for the D_{50} of the river bed can be found in Appendix D. Similar improvement can be observed in simulating the long-term development of the D_{50} of the river bed in case the MCAH-series are imposed in the model.

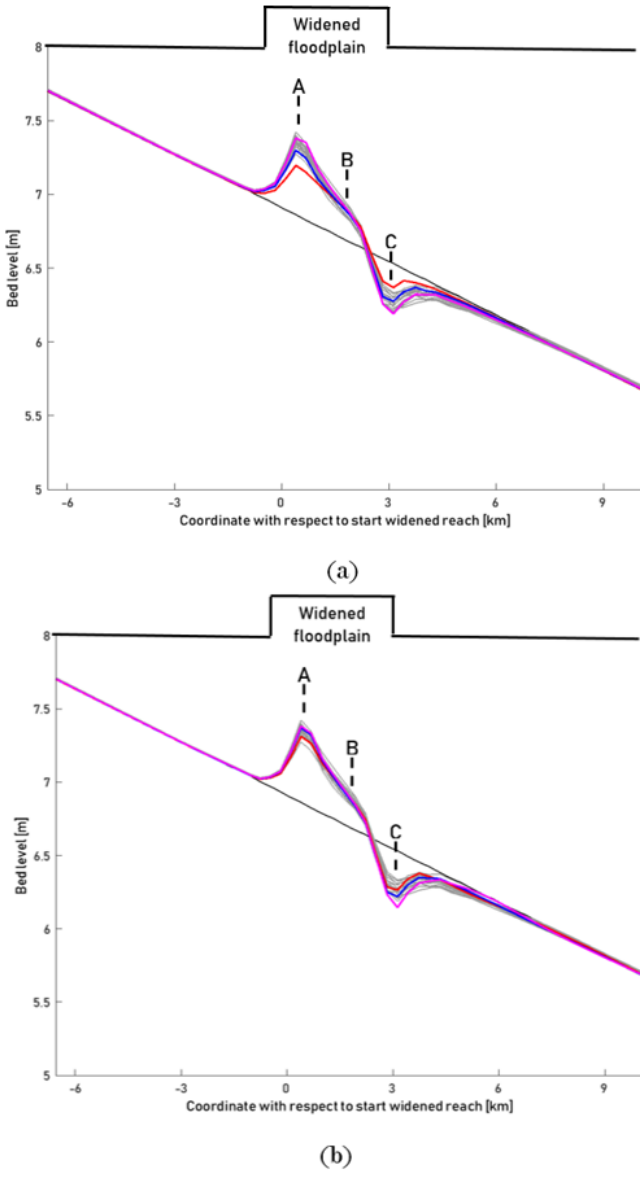

Figure 5.5: Morphodynamic state after 40 years with an increasing number of classes. **(a)** 1 CAH (red), 2 MCAHs (blue), 3 MCAHs (purple), the Monte Carlo bandwidth (gray) and the initial state of the river bed (black); and **(b)** 4 MCAHs (red), 5 MCAHs (blue), 6 MCAHs (purple), the reference bandwidth (gray) and the initial state of the riverbed (black).

From Figures 5.5- 5.8, it becomes clear that by imposing the MCAH-series, the long-term development of the bed level and of the D_{50} is much closer to the mean development from the Monte Carlo analysis. The more MCAHs are included in the time series, the more natural variability in discharge stages is included in the discharge time series and the more variation among yearly hydrographs is present. The upcoming sections focus on the increase in performance of the MCAH-series for an increasing number of MCAHs.

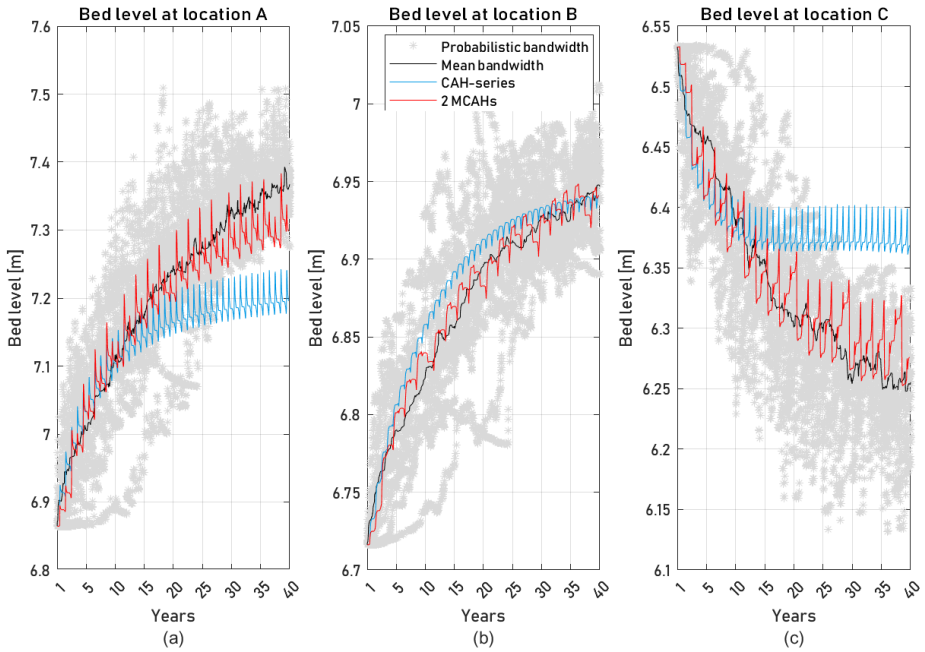

Figure 5.6: Time series for the case of 2 MCAHs with a threshold at 6000 m^3/s at location **(a)** A, **(b)** B and **(c)** C.

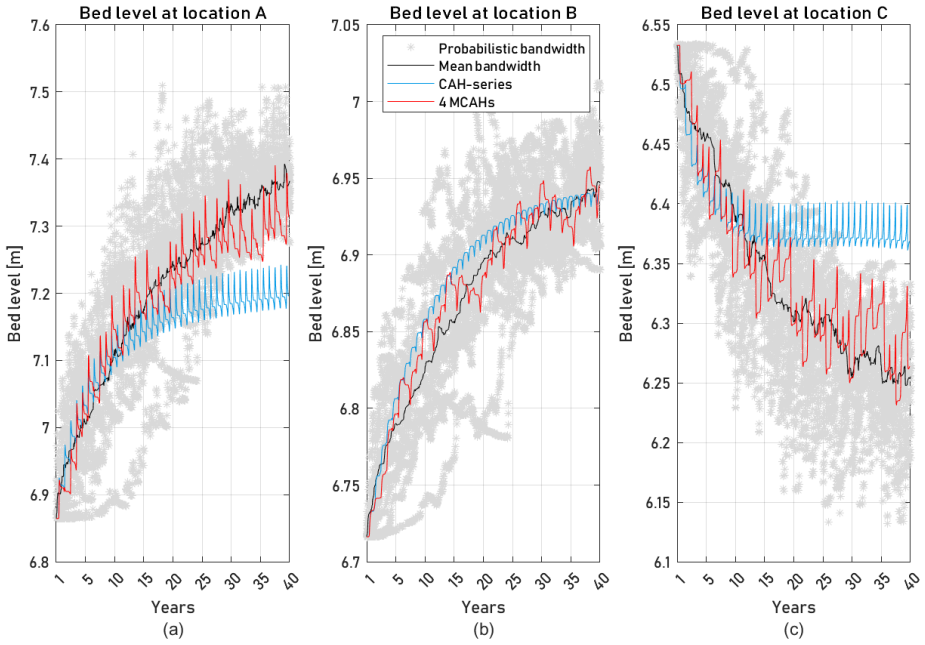

Figure 5.7: Time series for the case of 4 MCAHs with a threshold at 5000 m^3/s, 6000 m^3/s and 8500 m^3/s at location **(a)** A, **(b)** B and **(c)** C.

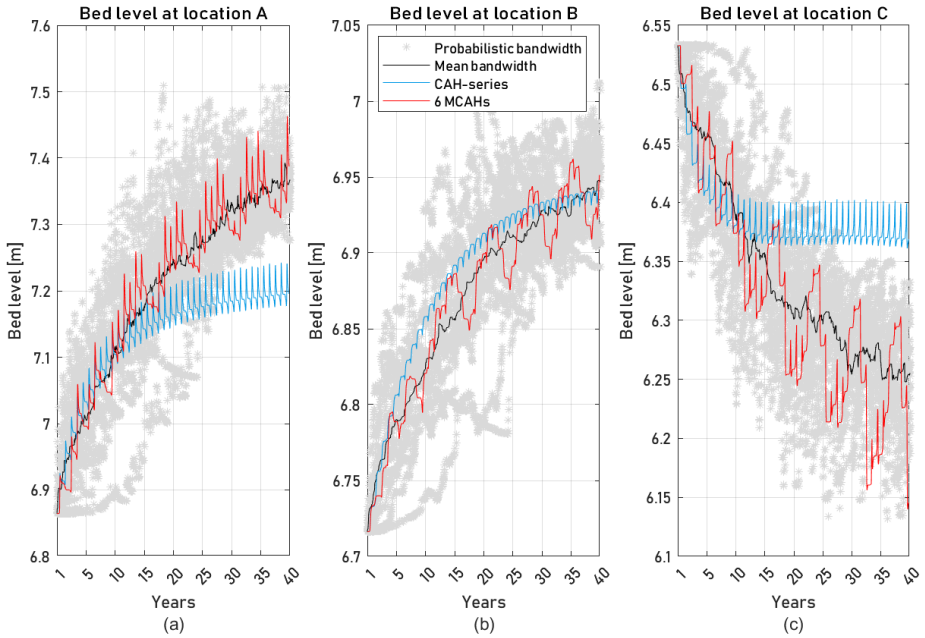

Figure 5.8: Time series for the case of 6 MCAHs with a threshold at 4000 m^3/s, 5000 m^3/s, 6000 m^3/s, 7000 m^3/s and 8500 m^3/s at location **(a)** A, **(b)** B and **(c)** C.

5.4 Improvements with respect to long-term bed level trends

In order to compare the long-term bed level trend from the Monte Carlo simulations to the long-term bed level development that results from the MCAH-series, long-term trends are fitted through the bed level development that results from the MCAH-series. The fitted trends are shown in Figure 5.9 for the bed level response to 1 (CAH), 2 and 5 MCAHs.

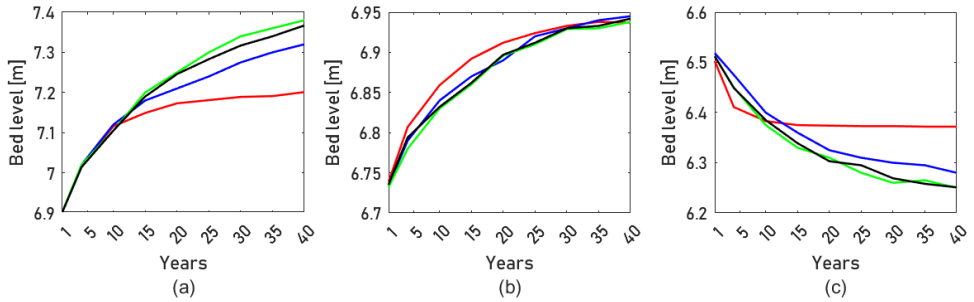

Figure 5.9: The fitted long-term trends for the bed level response to the discharge time series with 1 MCAH (CAH) (red), 2 MCAHs (blue), 5 MCAHs (green) and the mean bed level trend from the Monte Carlo simulations (black) at locations **(a)** A, **(b)** B and **(c)** C.

To get insight on the performance of the included number of hydrographs in the MCAH-method with respect to the long-term trends compared to the mean trend from the Monte

Carlo simulations, an analysis of the root mean square error (RMSE) is made. This indicator is often used to make estimations of the difference between long-term trends. In this case, it is a measure of the deviation of the long-term trend in bed level from the deterministic discharge time series with respect to the mean trend from the Monte Carlo simulations. An advantage of this method is the fact that the RMSE is expressed in terms of the same units as the measured quantity itself (Holmes, 2000).

The RMSE for the different series is presented in Figure 5.10. On the horizontal axis, the number of MCAHs is plotted that are used to construct the deterministic hydrograph series. On the vertical left axes, the RMSE is presented. On the vertical right axes, the RMSE is expressed in terms of the percentage of the RMSE that was found with the CAH-series, which is in fact the MCAH-method with one single class. Therefore, for one class, the error RMSE equals 100%.

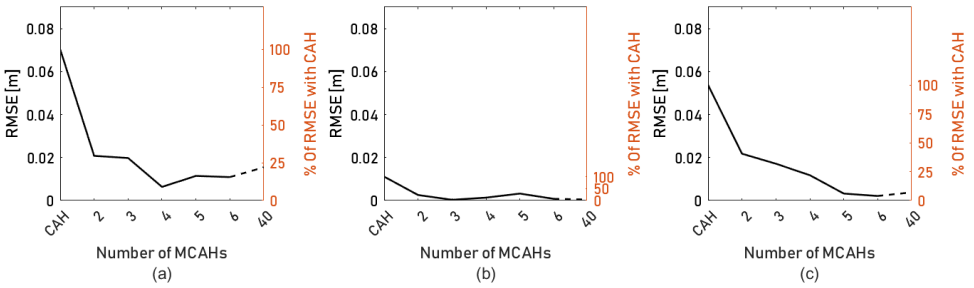

Figure 5.10: The RMSE for the different number of hydrographs in the MCAH-approach at locations **(a)** A, **(b)** B and **(c)** C.

For the CAH-series, the RMSE at location B is one order of magnitude smaller than the RMSE at locations A and C. As is demonstrated in Section 4.4, the CAH-series results in long-term bed level development that deviates from the mean trends from the Monte Carlo analysis, especially at the zones where the strongest sediment transport gradients are observed and where HBL-waves have a large influence on the bed level development: around locations A and C. This explains the large difference in RMSE at locations B for the CAH-series compared to locations A and C.

As can be observed in Figure 5.10, a significant decrease in RMSE can be observed at locations A and C by using the MCAH-series. Already after imposing discharge time series that consist of 4 to 5 different MCAHs, the RMSE reduces to approximately $20 - 25\%$ of the initial RMSE that was found with the CAH-method. A possible cause for the fact that the RMSE does not reduce significantly after increasing the number of hydrograph classes, is the simplification that is made when constructing the MCAHs. In Chapter 4 it is shown that by simplifying the natural hydrograph into symmetrical hydrographs, a small difference can be observed in the modelled long-term morphodynamics with respect to the result from the natural series. This error is encapsulated in the RMSE as well.

From Figure 5.10 it is clear that the RMSE is time-dependent, as the differences between the trends from the MCAH-method and the mean from the Monte Carlo simulations varies in time. To study this in quantitative way, the RMSE is evaluated for the fitted long-term trends from Figure 5.10 for each interval of 10 years during the 40 years of simulation time. The result is presented in Figure 5.11.

Especially at locations A and C, the series with few MCAHs lead to different equilibrium conditions compared to the probabilistic mean trend and consequently, the RMSE grows in

time. As is discussed in Section 4.2, the equilibrium bed level at locations A and C is dependent on the variation in duration and intensity of discharge events. By imposing the MCAH-series, this natural variation is pursued to a larger extent compared to the CAH-series. Consequently, the equilibrium condition of the river bed that result from the MCAH-series is much closer to the result from the Monte Carlo simulations. The series that include 4-5 MCAHs show a smaller RMSE that is almost constant during the entire 40 years. This means that the long-term bed level development is close to the mean bed level from the Monte Carlo simulations during the entire 40 years of the simulation and leads to similar (dynamic) equilibrium conditions.

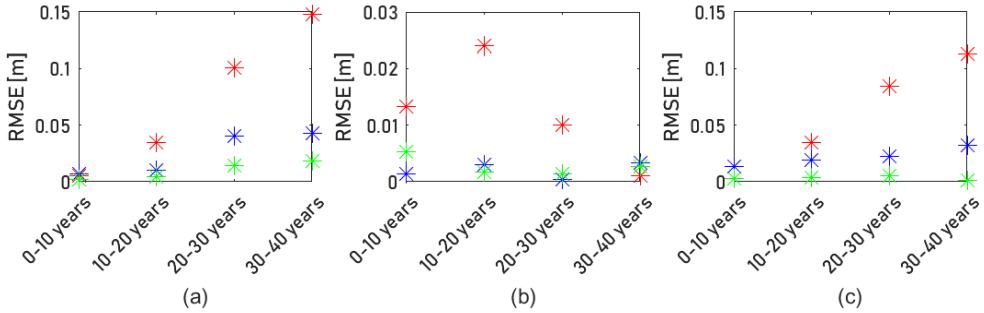

Figure 5.11: RMSE for intervals of 10 years in the 40 years of simulation time for the fitted long-term trends from Figure 5.10 compared to the mean bed level trend from the Monte Carlo calculations. The RMSE is evaluated for the series with 1 MCAH (CAH) (red), 2 MCAHs (blue) and 5 MCAHs (green) at locations **(a)** A, **(b)** B and **(c)** C.

5.5 Bed level fluctuation characteristics

The fluctuation parameter σ_f for the deterministic MCAH-approach is compared to the mean observations from the Monte Carlo simulations as well. The results for the series with 1, 2 and 5 MCAHs is presented in Figure 5.12.

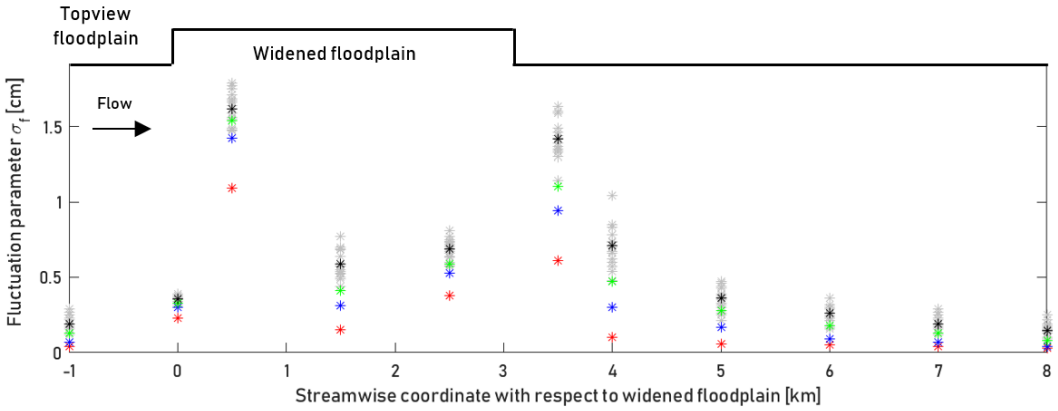

Figure 5.12: The fluctuation parameter σ_f for the Monte Carlo bandwidth (gray), the mean of the Monte Carlo simulations (black), 1 CAH (red), 2 MCAHs (blue) and 5 MCAHs (green).

The classification of historical hydrograph years, leads to MCAHs that represent the

yearly statistical parameters of the hydrograph years for the specific class. Years with similar low and high water events are combined into a single hydrograph that represents the class. The variation of years and the nature of extreme events in the deterministic series becomes closer to those of the natural series, for an increasing number of classes. As a result, the bed level fluctuations that result from the MCAH-series are closer to the natural series, compared to the response from the CAH-series.

5.6 A rough indication of uncertainty in future morphodynamics

Besides the fact that increasing the number of cycled annual hydrographs results in an improved performance in terms of long-term morphodynamic development and bed level fluctuation characteristics, it also allows for another feature. By conveniently constructing discharge time series out of the MCAHs, a rough (preliminary) indication can be obtained with respect to the uncertainty in future morphodynamics without the need for generating many randomly generated synthetic series in case of a Monte Carlo simulation. The construction of *extreme* long-term discharge sequences is considered to serve for this purpose.

Assume three MCAHs Y_1, Y_2 and Y_3. The extreme sequences are composed by grouping all similar MCAHs and placing the groups in all possible orders. This means that for the case with three MCAHs, 3! = 6 extreme hydrograph time series can be constructed[1]. The extreme series are demonstrated below, assuming that the MCAHs Y_1, Y_2 and Y_3 occur m, n and p times respectively. The presented series are schematised in Figure 5.13.

$$
\begin{aligned}
&(1) Y_{1;1}..Y_{1;m} - Y_{2;1}..Y_{2;n} - Y_{3;1}..Y_{3;p}\\
&(2) Y_{1;1}..Y_{1;m} - Y_{3;1}..Y_{3;p} - Y_{2;1}..Y_{2;n}\\
&(3) Y_{2;1}..Y_{2;n} - Y_{1;1}..Y_{1;m} - Y_{3;1}..Y_{3;p}\\
&(4) Y_{2;1}..Y_{2;n} - Y_{3;1}..Y_{3;p} - Y_{1;1}..Y_{1;m}\\
&(5) Y_{3;1}..Y_{3;p} - Y_{1;1}..Y_{1;m} - Y_{2;1}..Y_{2;n}\\
&(6) Y_{3;1}..Y_{3;p} - Y_{2;1}..Y_{2;n} - Y_{1;1}..Y_{1;m}
\end{aligned}
$$

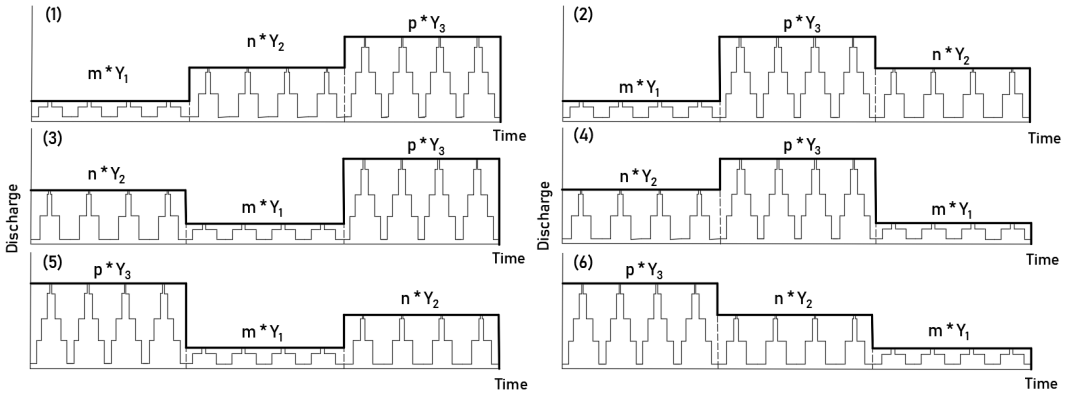

Figure 5.13: Schematisation of the extreme series that are constructed out three MCAHs: Y_1, Y_2 and Y_3. These years occur m, n and p times respectively in each extreme series.

[1] The number of extreme series that can be constructed from n MCAHs is $n!$. Hence in case four MCAHs are used, the number of extreme series would be 4! = 24.

To check whether the extreme series result in morphodynamic changes that cover a similar probabilistic bandwidth as obtained from the Monte Carlo simulations, the contours of the bandwidth of morphodynamic change from the extreme series are compared to the results from the Monte Carlo simulations. The contour of the bandwidth represents the envelope of possible morphodynamic realisations from all included discharge time series. Hence, this is not the same as a 90%-confidence interval. Whether these extreme sequences yield an estimation of the envelope of possible morphodynamic changes can be simulated from the extreme MCAH discharge series, is investigated for several cases varying from 2 to 4 MCAH-classes. The resulting contour of the bandwidth is presented in Figure 5.14.

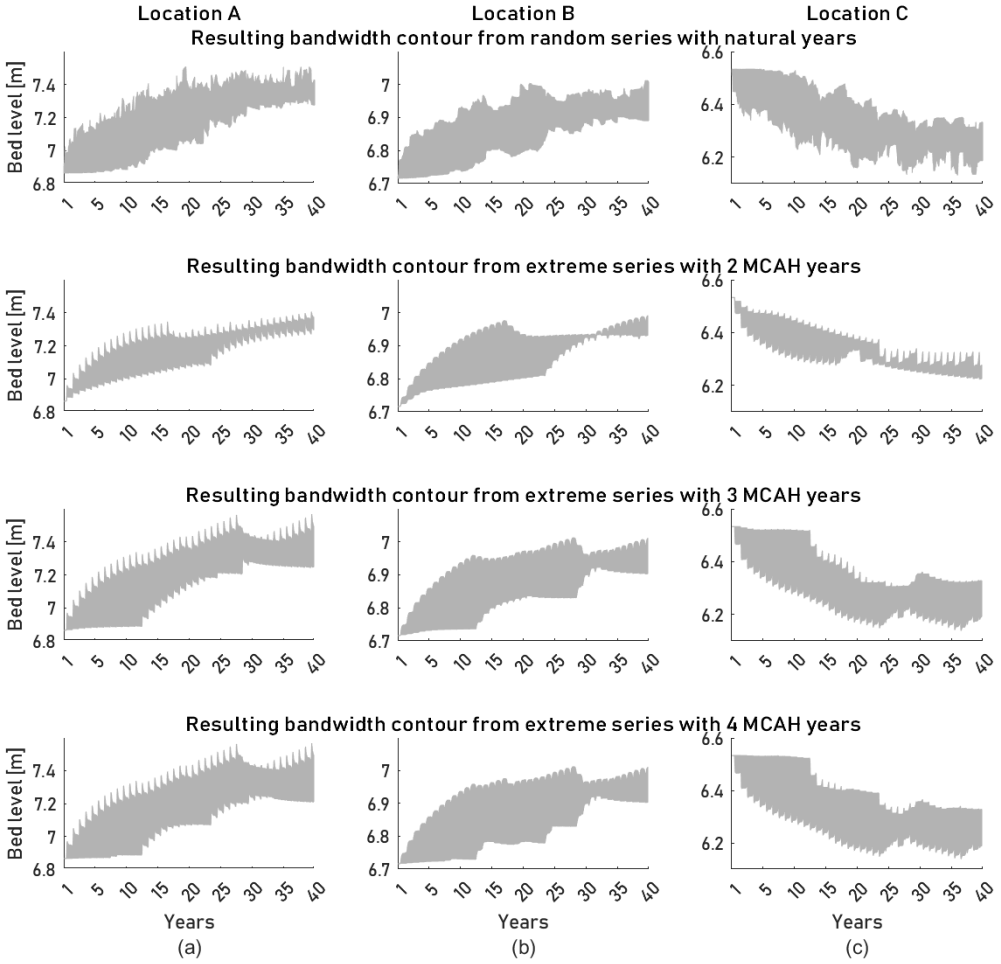

Figure 5.14: Comparison of the contours of the bandwidth from the Monte Carlo simulations (first row) and the series with two to four MCAH-classes (second up to fourth row) for locations **(a)** A, **(b)** B and **(c)** C.

When only two MCAHs are used (and hence only 2! = 2 extreme series can be constructed), the envelope of the change in bed level shows poor similarities with the envelope

from the Monte Carlo bandwidth at all three locations A, B and C. For an increasing number of MCAHs, the extreme series yield a reasonable indication of the envelope of morphodynamic response compared to the results from the probabilistic series. Especially during the first years and at the end of the time series, the bandwidth contours from the Monte Carlo simulations show significant similarities with the contours of the bandwidth from the extreme MCAH discharge time series.

The contours of the bandwidth that follow from the envelope of extreme discharge time series give a rough indication of the uncertainty around the expected long-term trend compared to the Monte Carlo simulations. The advantage of the introduced approach is the fact that a relatively small number of time series leads to a similar (rough) indication of uncertainty in future morphodynamics. This might support preliminary estimations of uncertainty that is associated with morphodynamic response to, for instance, river interventions.

Closing remark on the classification parameter

In this final section, a finding is discussed that is not tested or considered in the model study throughout this chapter. However, this finding might contribute to increased performance of the deterministic hydrograph time series. Therefore, it is briefly addressed here.

In Section 5.1 two classification parameters are considered that characterise the discharge statistics of historical years. Besides the yearly maxima ('mean of the wettest day in a year[2]') or the yearly mean ('mean of the 365 wettest days in a year), another classification parameter is found to be promising. In order to demonstrate this, an analysis is made for the correlation between the yearly mean discharge, maximum discharge and standard deviation with respect to the *mean discharge of the n wettest days of the year*. The results are presented in Figure 5.15.

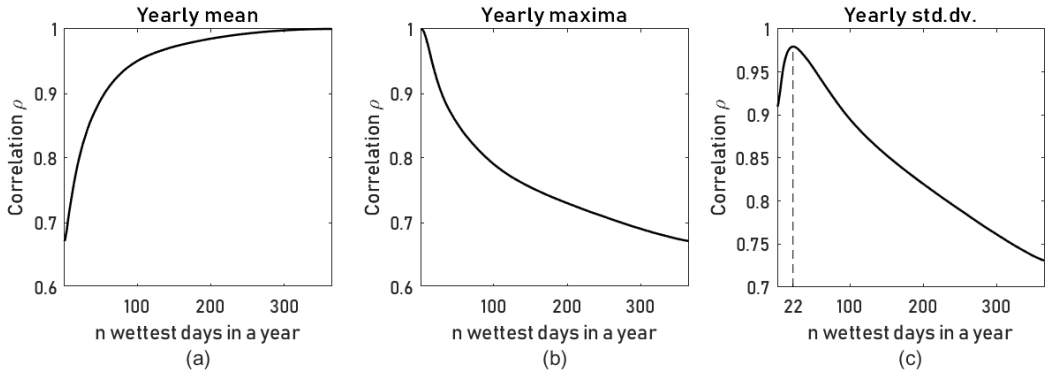

Figure 5.15: The correlation between the mean of the n wettest days in a year and **(a)** the yearly mean, **(b)** the yearly maxima and **(c)** the yearly standard deviation, for the years 1901-2010 as measured at Lobith [source data: GRDC, 2018].

Figure 5.15a shows the correlation between the yearly mean discharge and the mean discharge of the n wettest days in a year. It is obvious that $\rho = 1$ when the mean discharge of the 365 wettest days of a year is compared to the yearly mean discharge (n=365). A similar theory applies to Figure 5.15b. In case the yearly discharge maxima are compared to

[2]The wettest day in a year is the day during which the highest discharge magnitude is registered in that year.

the mean discharge of the wettest day in the year (n=1), $\rho = 1$. The correlation gradually decreases to $\rho = 0.64$ which is the same as the correlation in Figure 5.15a in case the mean discharge of the 1 wettest day is compared to the yearly mean discharge (n=365, see Section 5.1). It becomes interesting when Figure 5.15c is observed. The correlation between the mean discharge of the n wettest days in a year with the yearly standard deviation increases to a maximum of $\rho = 0.98$ when the mean discharge of the 22 wettest days in a year (n=22) is compared to the yearly standard deviation. This correlation is remarkably strong. The main reason for this strong correlation, is the fact that most periods of high water in a year have a duration of approximately 22 days. Consequently, the high water periods in a year contribute significantly to the yearly standard deviation and cause a strong correlation.

By considering the mean discharge of the 22 wettest days in a year as the classification parameter for statistical characteristics of a historical year of discharge observations, the correlation with the yearly mean discharge and the yearly standard deviation increases to 0.8 and 0.98 respectively (Figure 5.15). The correlation with the yearly maxima reduces to $\rho = 0.93$, which is still a strong correlation. Whether this would (significantly) improve the deterministic MCAH-method as proposed in this chapter, is not studied further.

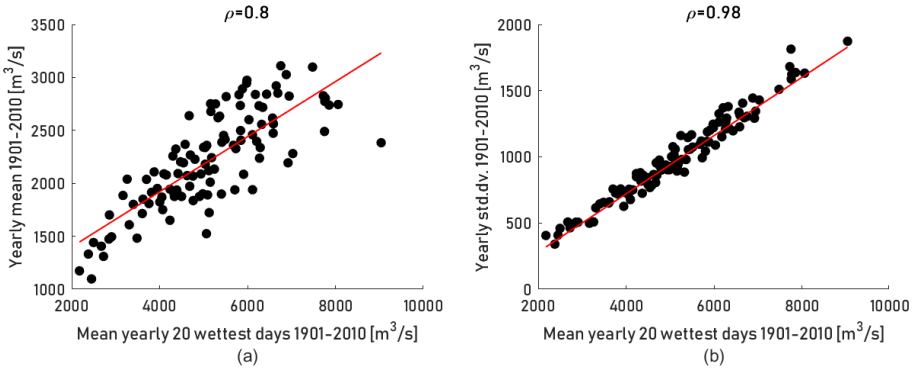

Figure 5.16: Correlation between **(a)** the mean discharge of the yearly 22 wettest days with respect to the yearly mean discharge and **(b)** the mean discharge of the yearly 22 wettest days and the yearly standard deviation. Both for the years 1901-2010 at Lobith. The red line represents a linear regression through the points [source data: GRDC, 2018].

CHAPTER 6

Discussion

Throughout this study, a conceptual model is used in which a typical Room for the River intervention is selected to serve as a case study. The model parameters, such as the discharge data, the geometrical layout and sediment characteristics are roughly based on the Dutch Upper Rhine. The most important considerations and assumptions are elaborated here. The extent to which these decisions have affected the model results is discussed here as well. Moreover, the generality of the main findings will be addressed in this chapter.

Two-dimensional morphodynamics

The purpose of this study is to investigate the impact of discharge variability on longitudinal morphodynamic processes in a conceptual way. These processes are mainly governed by longitudinal gradients in sediment transport. Many other morphodynamics processes prevail when studying two-dimensional morphodynamic such as the morphodynamics in river bends and at bifurcations. As the natural variation of river discharge is an important factor when simulating these morphodynamic features, it is expected that the proposed multiple cycled annual hydrograph (MCAH-) schematisation leads to increased model performance with respect to the cycled annual hydrograph (CAH-) schematisation. However, it is recommended to study the effects of the proposed hydrograph schematisation on two-dimensional morphodynamic changes as well in future studies as these processes are governed by complex flow patterns.

Model efficiency

The conceptual model that is used in this study consists of a strongly idealised two-dimensional domain decomposition that represents a river of which the floodplain is locally widened. This enables the horizontal expansion and contraction of the flow around the reach with the widened floodplain. This contributes to the distribution of river discharge over the main channel and the floodplain. As a consequence of the horizontal flow expansion and contraction and the associated adaptation length of the flow, smoother morphodynamic change is observed in the model results compared to a theoretical one-dimensional analysis in which

the flow velocity is assumed to be uniform throughout the flow cross-section. The model schematisation is however too coarse to account for other complex flow structures such as recirculation and spiral flow. It is expected that the latter two flow features do not significantly impact the studied longitudinal morphodynamics, as these features mainly affect lateral morphodynamic changes.

Even though the model accounts for (limited) two-dimensional flow features, the morphodynamics in the active channel is purely longitudinal, as the active channel is only one grid cell wide. Therefore, it is arguable whether the two-dimensional domain decomposition has a significant contribution to the findings in this thesis. The main disadvantage of a two-dimensional model representation is the increase of simulation time. Even though it is not expected that the model results would have been significantly different with a one-dimensional model representation (since (strong) sediment gradients are still observed around the sudden spatial changes in flow cross-section, as observed in the one-dimensional analysis), the two-dimensional domain decomposition aims to produce model results that are closer to what would be found with practical two-dimensional models such as the *Duurzame Vaarwegen Rijndelta* (DVR-) model that is introduced in Chapter 3. It is also selected in order to increase the link between research and practical application of the proposed hydrograph schematisation in this thesis.

Extension to more complex morphodynamic models

In Chapter 1 and 2 of this thesis it is mentioned that in case multiple large-scale river interventions are executed, the morphodynamic response might become a combination of the effects of all these measures. In this study, the morphodynamic response to a single intervention is considered. Therefore it is questionable whether the obtained results are applicable to more extensive models that include multiple measures. The difficulty of combined interaction of bed level changes is already experienced within the conceptual model. Downstream of the widened floodplain, local bed waves interact with bed waves that are generated upstream and that propagate through the river system. In Chapter 4 and 5 it is shown that the MCAH-method results in simulated morphodynamics that is close to the findings from the Monte Carlo simulations at all studied locations in the conceptual model. Hence, improvement in model performance is also observed downstream of the widened floodplain. This increases the confidence that the MCAH hydrograph schematisation is useful for more extended morphodynamic models as well.

The applicability to other river interventions

It is also expected that the findings from this study are representative for similar river interventions that include the change of local conveyance area or roughness of the river. These (sudden) changes cause (strong) sediment gradients similar as found with this conceptual study. It is not necessarily the specific intervention itself that leads to the morphodynamic change, but rather the resulting (strong) sediment transport gradients.

The widened floodplain is modelled as a sharp spatial transition in cross-sectional area. In reality, these transitions are often smoother (for example the widened floodplain at Voorsterklei and Cortenoever). This means that, in reality, the sediment transport gradients are expected to be not as strong as observed in the case study. The model study considers an extreme scenario.

Hydrograph discretisation

The influence of the number of discrete discharge steps in the hydrograph is not part of this study. A relatively large number of steps is chosen to fulfill the statement by Wiersma (1997) that a discretisation of the discharge time series into piecewise constant hydrographs results in similar morphodynamics compared to the natural series, at least, if *not too coarse*. Since in Wiersma (1997) or in other available literature no statement is made about what is actually meant by *not too coarse*, a relatively large number of discrete discharge levels is defined in the conceptual study: 13. This has an important consequence on the simulation time. In Chapter 3, it is discussed that the more discrete steps are included, the more computational time is required. Therefore, the number of discrete discharge steps in the hydrograph is a factor that needs attention in future research. Computational time might be saved.

Generality of the used discharge data set

40 Years of daily discharge measurements of the Dutch Upper Rhine are used to construct the discharge time series amongst others for the Monte Carlo simulations. In Chapter 2 it is found that after several decades, the statistical parameters that describe the long-term statistics (the mean and the standard deviation) do not change significantly by adding more years of data. Still, as is demonstrated in Chapter 4 and 5, the long-terms statistics is not the only characteristic that governs morphodynamic change. Especially at zones that experience strong sediment gradients and where the influence of HBL-waves is dominant, yearly hydrograph sequences prove to be of importance as well. This means that the selection of 40 years other than 1971-2010, might have resulted in slightly different morphodynamic realisations. The difference in long-term morphodynamic development is however not expected to be significant as it is believed that the inherent natural variation in river flow is not significantly different for a selection of other discharge years than the 1971-2010 observations.

The importance of yearly seasonality

In Chapter 2 it is demonstrated that a yearly periodicity dominates the seasonality in the lower section of the river Rhine. This finding led to the simplified discharge hydrographs with a one-yearly flooding event. However, it is also shown that in some parts of the river Rhine (around Kaub-Andernach), the seasonal periodicity shows on average two (mild) flood peaks per year as a consequence of both geological and meteorological factors (see Chapter 2, Figure 2.3). It is expected that the simplification into yearly hydrographs with one flood event will result in larger inaccuracies when applied to river systems that are not dominated by such a clear, yearly periodicity. A possibility could be to simplify the yearly hydrographs into hydrographs with two (different) flood events. This is however not part of this study, but might be recommended for future research.

For setting up the proposed deterministic MCAH discharge time series, a classification parameter is introduced that categorises years with similar statistical characteristics. The yearly maximum discharge is used, since it shows significant correlation with the yearly mean and standard deviation. This correlation is found for the daily discharge observations from 1901-2010 at Lobith, which show a dominant yearly periodicity. It is however questionable whether this classification parameter would be effective in case of the river discharge does not show a dominant yearly periodicity. Therefore, an analysis is made of the correlation between the yearly maximum discharge and the yearly mean and standard deviation of the discharge measurements at the observation station in Kaub, where on average two (milder)

flood events are observed in one year. It appears that the correlations are similar for this station ($\rho = 0.68$ for the yearly mean and $\rho = 0.87$ for the yearly standard deviation). This means that the classification parameter would have been applicable for a classification of the years as measured at Kaub as well.

The MCAHs as input for a Monte Carlo simulation

In Chapter 3 several methods are discussed how synthetic discharge time series can be constructed. These synthetic time series can be used as input for a Monte Carlo simulation. The MCAHs could be used for this purpose as well. Whether this would result in similar Monte Carlo results compared to the applied bootrap method is not addressed in this study. It is recommended to study the potential of a Monte Carlo simulation using randomly generated series out of the MCAHs. It would be convenient to use the MCAHs for this purpose as no complex methods are required to generate artificial hydrographs that contain daily structures (e.g. Huthoff et al., 2010; Van Vuren et al., 2015).

Climate change

For the MCAH-method, a historical data set is used. This means that the hydrograph schematisation for future simulations is based on historical data. However, trends in climate change influence the flow regime of the river on the long-term (e.g. Emmanouil, 2017; Yossef and Sloff, 2012). Depending on the presence and severity of those trends, the MCAH-method might not represent the long-term future flow statistics of the river. This is not a complexity for the MCAH-method only, but this is a general complication in river modelling. As is discussed in Chapter 2, the limited knowledge about climate change is therefore a source of uncertainty as well.

CHAPTER 7

Conclusion: A synthesis and recommendations for the future schematisation of discharge time series

The main objective of this study is to increase insight on the performance of the deterministic cycled annual hydrograph (CAH-) schematisation compared to the results from a probabilistic Monte Carlo approach. This insight is used to propose an improved deterministic hydrograph schematisation that meets the results from the Monte Carlo simulation to a larger extent. The main findings and answers to the research questions are elaborated here. The findings are translated into recommendations for the river engineering practice.

The implication of variable river discharge on river morphology

The impact of discharge variability on river morphodynamics can be distinguished into three zones: 1) Hydrograph boundary layer (HBL); 2) the quasi-normal flow segment (QNFS) and 3) the backwater segment (BWS). A conceptual study is evaluated in which a typical Room for the River intervention is modelled: a reach with a widened floodplain. It is found that not only the long-term statistics of the river discharge governs the morphodynamic change. This is observed mainly for the zones that experience dominant influence of HBL-waves. The local morphology in the HBL-zone is to a large extent dependent on the combined intensity and influence of bed waves that are continuously generated under the influence of a variable river discharge. This implies that the (long-term) sequence of hydrograph years is of paramount importance when simulating the future development of the the river bed at zones where the HBL-influence is significant. However, due to a lack of dependency and correlation among subsequent hydrograph years, constructing future discharge series is a complicated task.

The Monte Carlo analysis

The limited predictability of future river discharge series is a source of uncertainty in simulated morphodynamics. A Monte Carlo simulation is carried out to study the time development of longitudinal morphodynamic changes. Three locations are considered around the

reach with the widened floodplain: in the zone where the flow expands (location A), where the flow contracts (location C) and in between these zones (location B). Locations A and C are zones where strong sediment transport gradients are observed and where HBL-effects are of large influence. At location B, the HBL-influence is smaller and milder sediment transport gradients can be observed. By conducting a Monte Carlo simulation with 20 realisations, it is found that the largest uncertainty can be observed in the zones that experience the largest influence of bed level fluctuations and where the influence of HBL-waves is dominant.

The deterministic cycled annual hydrograph (CAH-) series

The morphodynamic response to the deterministic cycled annual hydrograph (CAH) is compared to the results from the Monte Carlo simulations. The CAH is a representation of the long-term statistics, imposed by means of a single, yearly hydrograph. It is aimed for to be the *best guess* with respect to a future discharge time series that leads to a similar long-term trend as obtained from the Monte Carlo realisations. However, the long-term development show poor similarities with the long-term trend from the Monte Carlo simulations, especially in the zones where the flow contracts and expands and where the most extreme sedimentation and erosion are expected respectively. At those locations, the HBL-effects are the most pronounced. This implies that the trends towards a new dynamic equilibrium at locations that are dominated by strong sediment transport gradients and HBL-effects are not merely governed by the long-term discharge statistics. It is supposed that at those locations, the long-term morphodynamic development is the result of the variation in duration and intensity of flood and draught sequences as well. This feature is not well-represented by the current deterministic CAH-approach. The lack of variation of discharge events and the absence of varying yearly sequences is appointed to be the main weakness of the deterministic CAH-method.

The poor performance in simulating the morphodynamic change at the zones where extreme sedimentation and erosion are observed is an important drawback of the CAH-method. At zones where the river bed experiences the most sedimentation (location A), a bottleneck might develop regarding the navigability of a river. Therefore, a reliable model prediction of these zones that experience extreme sedimentation is of large importance when evaluating the future impact of river interventions. On the other hand, it is desirable to make reliable predictions of zones that experience relatively much erosion (location C) since this might amongst others induce instabilities of the surrounding soil and neighbouring structures.

The importance of short-term sequences

In order to propose an improved deterministic hydrograph schematisation and to find a convenient strategy for schematising discharge time series, the importance of short-term (intra-annual) daily sequences of the variable river discharge is evaluated considering long-term morphodynamic change. The contribution of intra-annual short-term sequences to simulated morphodynamics is studied by comparing the morphodynamic response to the natural discharge series to a hydrograph series in which all years are simplified into symmetrical hydrographs with one flood event per year. The influence of daily structures proves to be of no significant influence on the morphodynamic response on the studied time scales of years up to decades. The long-term trends are similar at all locations, but the relative difference increases incrementally in time and results in a difference in the order of centimeters at the end of the 40 years of simulation at locations A and C. The yearly dominant

fluctuations around the long-term bed level trend are also found to be similar to the natural series. The simplification removes fluctuations that occur on smaller time scales than one year. Therefore, for the modelling of morphodynamics on smaller time scales, this method is expected to be too much simplified.

The influence of long-term sequences

In this study, the concept of the memory effect is used to demonstrate the importance of including long-term (yearly) sequences in discharge time series. The fading character of the memory effect in the river bed, or the *decaying signature* of historical events, is evaluated. The memory at each location is found to be a combination of local changes and the passage of bed waves that are generated upstream of the observed location. The convective and diffusive behaviour of these bed waves depends on the flow and sediment flux characteristics of the river. This implies that the memory effect is dependent on the studied case and river. In this conceptual study, the memory effect is reduced by an order of magnitude after approximately 5-10 years at all considered locations. The findings have important implications on the interpretation of morphodynamic change in river systems. It means that the final state of the morphodynamic simulation is mainly determined by the last 5-10 hydrograph years. Another interesting finding is the fact that using only the final state of a model simulation seems not to be fully indicative for the long-term morphodynamics, since it depends on the final stages of the hydrograph, as well as on the last years of the simulation. Therefore, it is recommended to consider the average morphodynamic development during the last few years rather than interpreting merely the final morphodynamic state of the simulation.

An improved deterministic approach

An improved deterministic method is proposed in which multiple cycled annual hydrographs (MCAHs) are combined into long-term deterministic discharge time series. The MCAHs are based on the classification of years with similar yearly discharge statistics. More detail on classifying the years from a historical discharge data set and the method how to construct the MCAH discharge time series can be found in Chapter 5. The number of defined classes (and hence the number of MCAHs) has influence on the long-term morphodynamic development and affects the performance of the deterministic hydrograph time series, compared to the Monte Carlo simulations.

As a performance indicator for the MCAH discharge time series considering the long-term morphodynamic trends, the root mean square error (RMSE) is evaluated. Already by defining 3-4 classes (and the according MCAHs), a significant reduction of the RMSE with respect to the long-term bed level trend from the Monte Carlo analysis can be obtained. The RMSE does not reduce significantly for a further increase in classes or MCAHs. This means that for 4-5 classes, the MCAH series represents the essential inherent natural variation of the river discharge. Moreover, the bed level fluctuations around the long-term trend are similar to those that result from the natural series in case of 5-6 MCAHs. At last, it is shown that by creating extreme sequences out of 3-4 MCAHs, a rough indication can be given on the uncertainty in simulated morphodynamics that is comparable to the Monte Carlo simulations.

Combining the deterministic and probabilistic model approaches

Finally, a conceptual idea about a combined model approach is discussed. It combines multiple findings from this study. It is found that the probabilistic bandwidth stagnates after several decades of simulation at all studied locations after a number of decades. This is mainly the result of the long-terms statistics of the river discharge, which limits the occurrence of wet and dry discharge years in long-term discharge time series. It is also shown that, with the use of a well-considered deterministic hydrograph schematisation, the long-term bed level trend from the Monte Carlo analysis can be approached with one single (MCAH-) discharge time series. Based on this knowledge, a Monte Carlo approach with reduced computational effort is proposed. A Monte Carlo simulation can be used to simulate the uncertainty bandwidth up to the point where it is observed that the uncertainty does not increase further. Simultaneously, the deterministic discharge time series is run for the entire simulation time. As the probabilistic bandwidth remains fairly constant after a certain period, the bandwidth can be extrapolated around the long-term development as calculated with the deterministic series. This model approach is illustrated in Figure 7.1.

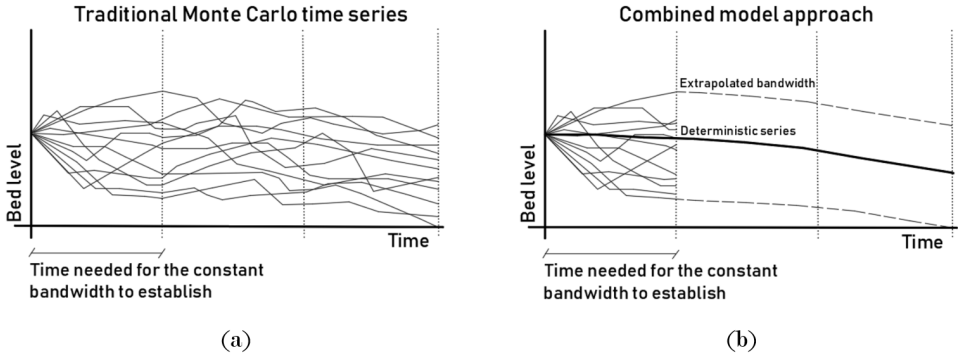

Figure 7.1: Schematic of **(a)** the traditional Monte Carlo concept and **(b)** the conceptual model approach that combines the long-term morphodynamic development that yields from the improved deterministic hydrograph schematisation and the constant bandwidth from Monte Carlo simulation with reduced simulation length.

There are two important requirements for this theory: 1) The probabilistic bandwidth must stagnate (this is observed after approximately 30-35 years in the case study); and 2) the deterministic series must be an accurate approximation of the average development of the Monte Carlo series. The latter requirement is not satisfied with the conventional CAH-method. This emphasises the value of the introduced MCAH schematisation strategy in this study. It is recommended to study the possibilities of this combined model approach as computational time can be saved with this approach.

References

Arkesteijn, L., Labeur, R., Chavarrias, V., and Blom, A. (2018a). The morphodynamic steady state of a river in its normal flow and backwater segments. *Journal of Geophysical Research: Earth Surface* (under review).

Arkesteijn, L., Labeur, R., and Blom, A. (2018b). From time series to probability density functions at the boundaries in morphodynamic modelling. *NCR Book of abstracts*.

BfG - Sedimentdatenbank SedDB (2016)

Blom, A. (2016, October). Bed degradation in the Rhine River. Online source: *http://flows platform.nl* (4. January, 2019).

Blom, A., Arkesteijn, L., Chavarrias, V., and Viparelli, E. (2017). The equilibrium alluvial river under variable flow and its channel-forming discharge. *Journal of Geophysical Research: Earth Surface*, Vol. 122, pp. 1924-1948. doi: 10.1002/2017JF004213.

Bolla Pittaluga, M., Luchi, R., Seminara, G. (2014). On the equilibrium profile of river beds. *Journal of Geophysical Research: Earth Surface*, Vol. 119, pp. 317-332. doi: 10.1002/2013JF002806

Bowers, M., Tung, W., and Gao, J. (2012). On the distributions of seasonal river flows: Lognormal or power law?. *Water Resources Research*, Vol. 48, W05536. doi: 0043-1397/12/2011WR011308.

Buffington, J. (2012). Chapter 32: Changes in Channel Morphology Over Human Time Scales. In M. Church, P. Biron, and A. Roy, Gravel-bed Rivers: Processes, Tools, Environments. First Edition. John Wiley and Sons, Ltd.

Chow, V. (1954). The log-probability law and its engineering application. *Proceedings of the American Society of Civil Engineerings*, Vol. 80, No. 11, pp. 1-25.

Copeland, R., Biedenharn, D., and Fischenich, J. (2000). Channel-Forming discharge. U.S. Army Corps of Engineers, Technical Note ERDC/CHL CHETN-VIII-5.

Costa, J., and O'Connor, J. (1995). Geomorphically effective floods. In J. Costa, A. Miller, K. Potter, and P. Wilcock, Natural and Anthropogenic Influences in Fluvial Geomorphology (pp. 45-56). Washington, DC: American Geophysical Union.

Crosato, A. (2008). Analysis and modelling of river meandering. [PhD thesis TU Delft].

De Vries, M. (1965). Considerations about non-steady bed-load transport in open channels. I.A.H.R. Leningrand, Russia.

De Vries, M. (1974). Sedimenttransport (collegedictaat f10). Delft, The Netherlands: Technische Hogeschool Delft: Afdeling der Weg- en Waterbouwkunde.

De Vries, M. (1993). *Use of models for river problems*, pp. 85. UNESCO

Dimitriadis, P. (2017). Hurst-Kolmogorov dynamics in hydroclimatic processes and in the microscale of turbulence. [PhD thesis National Technical University of Athens].

Doyle, M., and Shields, C. (2008). An alternative measure of discharge effectiveness. *Earth Surface Processes and Landforms*, Vol. 33, pp. 308-316. doi:10.1002/esp.1543

Emmanouil, I. (2017). Morphodynamic trends in the freely flowing Rhine. Additional MSc thesis [TU Delft]

Exner, F.M. (1925). Über die Weschelwerkung zwischen Wasser und Geschiebe in Flüssen. *Akademie der Wissenschaften in Wien. Mathematischen Naturwissenschaftliche Klasse*, Vol. 134, No. 2a, pp. 165-204.

Frings, R., Banhold, K., Evers, I. (2015). Sedimentbalanz des Oberen Reindeltas für den Zeiträum 1991-2010. Rapport 2015.019, Institut für Wasserbau und Wasserwirtschaft, RWTH Aachen, Germany

Frings, R., Doring, R., Beckhausen, C., Schüttrumpf, H., and Vollmer, S. (2014). Fluvial sediment budget of a modern, restrained river: The lower reach of the Rhine in Germany. *Catena*, Vol. 122, pp. 91-102. doi: 10.1016/j.geomorph.2013.08.035

Global Runoff Data Center (2018). Online source: *https://www.bafg.de/GRDC/* (1. October, 2018)

Hegnauer, M., Beersma, J., Van den Boogaard, H., Buishand, T., and Passchier, R. (2014). Generator of Rainfall and Discharge Extremes (GRADE) for the Rhine and Meuse basins: Final report of GRADE 2.0. Delft: Deltares, 1209424-004-ZWS-0018.

Holmes, S. (2000). RMS Error. Online source: http://statweb.stanford.edu (2. May, 2019)

Hurst, H. (1951). Long Term Storage Capacity of Reservoirs. *Transactions of the American Society of Civil Engineers*, Vol. 116. pp. 770-799.

Huthoff, F., Van Vuren, S., Barneveld, H.J. and Scheel, F. (2010). On the importance of discharge variability in the morphodynamic modelling of rivers. In K. Koll, A. Dittrich, J. Aberle, and P. Geisenhainer (eds.). *River Flow 2010 Proceedings of the International Conference on Fluvial Hydraulics, 8-10 September 2010, Braunschweig.* pp. 985-991. Karlsruhe, Bundesanstalt für Wasserbau.

Jansen, P. (1997). Principles of River Engineering. Delft, The Netherlands: VSSD. ISBN 978-90-6562-146-7.

Lane, D. (2013). Introduction to statistics: An interactive eBook. Online source: *http://onlinestatbook.com/2/index.html* (28. November, 2018).

Montanari, A. (2012). Hydrology of the Po River: looking for changing patterns in river disharge. *Hydrology and Earth System Sciences*, Vol. 16, No. 10, pp. 3739-3747. doi: 10.5194/hess-16-3739-2012

Mosselman, E. and Sloff, C.J. (2008). The importance of floods for bed topography and bed sediment composition: numerical modelling of Rhine bifurcation at Pannerden. In Habersack, H., Piégay, H. and Rinaldi, M. (eds). *Gravel-Bed Rivers VI: From Process Understanding to River Restoration.* Elsevier B.V. ISBN 978-0-444-52861-2

Nittrouer, J., Shaw, J., Lamb, M., and Mohring, D. (2011). Spatial and temporal trends for water-flow velocity and bed-material sediment transport in the lower Mississippi River. *Geological Society of America*, Vol. 124, No. 3/4, pp. 400-414, doi: 10.1130/B30497.1.

NL Rijnpatent (2018). Online source: *https://www.rijnpatent.nl/* (6. January, 2019).

Ottevanger, W., Giri, S., and Sloff, C. (2015). Sustainable Fairway Rhinedelta II: Effects of yearly bed stabilisation nourishments, Delta Program measures and training walls. Deltares.

Parker, G. (2004). 1D Sediment Transport Morphodynamics, With Applications of Rivers and Turbidity Currents [E-book]. Minneapolis, USA.

Parker, G., Hassan, M., and Wilcock, P. (2008). Adjustment of the bed surface size distribution of gravel-bed rivers in response to cycled hydrographs. In A. Habersack, H. Piégay, and M. Rinaldi ed., Gravel-Bed Rivers VI: From Process Understanding to River Restoration (pp. 241-285). New York: Elsevier.

Pickup, G. and Rieger, W.A. (1979). A conceptual model of the relationship between channel characteristics and discharge. *Earth Surface Processes*, Vol. 4, pp. 37-42. doi: 0360-1 269/79/0104-OO37

Pizzuto, J. (1994). Channel adjustments to changing discharges, Powder River, Montana. *Geological Society of American Bulletin*, Vol. 106, No. 11, pp. 1494-1501. doi: 10.1130/0016-7606(1994)106(1494:CATCDP)2.3.CO;2

Poff, N., Allan, J., Bain, M., Karr, J., Presegaard, K., Richter, B., . . . Stromberg, J. (1997). The natural flow regime. *BioScience*, Vol. 47, No. 11, pp. 769-784. doi: 10.2307/1313099

Proust, S., Rivière, N., Bousmar, D., Paquier, A., Zech, Y., Morel., R (2006). Flow in compound channel with abrupt floodplain contraction. *Journal of Hydraulic Engineering*, Vol. 132, No. 9. pp.958-970. doi: 10.1061(ASCE)0733-9429(2006)132:9(958).

Ray, S., Biswas, N. and Roy, P.C. (2012). Investigation of Newotnian Fluid Flow through a Two-dimensional Sudden Expansion and Sudden Contraction Flow Passage. *International Journal of Engineering Research and Development*, Vol. 1, No. 12, pp.1-9.

Ribbering, J.S. (1987). Mathematical modelling of one-dimensional morphological changes in rivers with non-uniform sediment. [PhD thesis TU Delft]

Ruimte voor de Rivier (2018). Online source: *https://www.ruimtevoorderivier.nl/ over-ons/* (28. October, 2018).

Sloff, C.J. (2011). DVR toolbox for sediment management in the Rhine delta. *Proc. Internationales Wasserbau Symposium Aachen 2011*

Sloff, C.J., Van der Sligte, R., Ottevanger, W. (2014). Morfologische Pakketsom Waal, Morfologische effecten Ruimte-voor-de-Riviermaatregelen. Delft, The Netherlands. Deltares.

Stall, J., and Fok, Y. (1967). Discharge as related to stream system morphology. Symposium on river morphology - General Assembly of Bern, (pp. 224-235). Bern, Switzerland.

Struiksma, N., Olesen, K., Flokstra, C. and De Vriend, H. (1985). Bed deformation in in curved alluvial channels. *Journal of Hydraulic Research*, Vol. 23, No. 1, pp.57-79

Suzuki, K. (1976). On the propagation of a disturbance in the bed composition of an open channel. Delft, The Netherlands: Delft University of Technology .

USGS (2018). Online source: *https://earthexplorer.usgs.gov/* (6. January, 2019).

Van Asselt, M.B.A. and Rotmans, J. (2002). Uncertainty in integrated assessment modelling. From positivism to pluralism. *Climate Change*, Vol. 54. pp. 75-105

Van den Houten, G., Hartong, H., Bartelds, A., Filius, P. (2010) Handboek 'Debieten in open waterlopen' geactualiseerd. *H2O-magazine*, Vol. 7, Koninklijk Nederlands Waternetwerk

Van Denderen, R.P. (2014). Bed level changes in the Waal during floods. [MSc thesis TU Delft].

Van der Klis, H. (2003). Uncertainty analysis applied to numerical models for river bed morphology. [PhD thesis TU Delft].

Van Gelder, P., Kuzmin, V. and Visser, P. (2000). Analysis and statistical forecasting of trends in riverh discharges under uncertain climate changes. In Tönsmann, F. and Koch, M. (eds.). *Int. Symposium on River Flood Defence*, Vol. 1, pp. D13-D22. Kassel, Germany.

Van Heijningen, B. (2017). Influence of discharge cycle length on morphodynamic behavior. [BSc thesis TU Delft].

Van Vuren, S. (2005). Stochastic modelling of river morphodynamics. [PhD thesis TU Delft].

Van Vuren, S., Mosselman, E., Sloff, C., and Vermeulen, B. (2006). Voorspelinstrument Duurzame Vaarwegen: Initiele modelbouw en demonstratieberekeningen [in Dutch]. Delft, The Netherlands: WL Delft Hydraulics.

Van Vuren, S., Paarlberg, A., and Havinga, H. (2015). The aftermath of "Room for the River" and restoration works: Coping with excessive maintenance dredging. *Journal of Hydro-environmental Research*, Vol. 9, No.2, pp. 1-15.

Wiersma, F.E. (1997). The modelling of submerged vanes. [MSc thesis TU Delft].

Wilcock, P., and Crowe, J. (2003). Surface-based Transport Model for Mixed-Sized Sediment. *Journal of Hydraulic Engineering*, Vol. 129, No. 2, pp. 120-128.

Wolman, M., and Miller, J. (1960). Magnitude and Frequency of Forces in Geomorphic Processes. *The Journal of Geology*, Vol. 68, pp. 54-74. doi: 10.1086/626637

Wong and Parker (2006). Reanalysis and Correction of Bed-Load Relation in Meyer-Peter and Müller Using their Own Database. *Journal of Hydraulic Engineering*. Vol. 132, No. 11, pp. 1159-1168. doi: 10.1061/(ASCE)0733-9429(2006)132:11(1159)

Yossef, M., Jagers, H.R.A., Van Vuren, S. and Sieben, A. (2008). Innovative techniques in modelling large-scale river morphology.

Yossef, M., and Sloff, C.J. (2012). Detailed Modelling of River Morphological Response to Climate Change Scenarios. Conference paper.

Nomenclature

Symbol	Unit	Description
b	[-]	Degree of non-linearity in $s = s(u)$
C	$[\sqrt{m}/s]$	Chezy rougness coefficient
c_{bed}	$[m/s]$	Propagation velocity of bed level waves
c_{mix}	$[m/s]$	Propagation velocity of bed sediment composition waves
$d(x)$	$[m]$	Water depth
d_e	$[m]$	Equilibrium water depth
D_{50}	$[m]$	Geometric mean grainsize diameter
δ	$[m]$	Active layer thickness
ϵ	[-]	Porosity of river bed
Fr	[-]	Froude number
g	$[m/s^2]$	Gravitational acceleration
i_b	$[m/m]$	Initial bed slope
i_{be}	$[m/m]$	Equilibrium bed slope
λw	$[m]$	Flow adaptation length
L_w	$[m]$	Length widened floodplain
μ	[-]	Ratio average grain size bedload to average grain size active layer
Q	$[m^3/s]$	Water discharge
Q_{bf}	$[m^3/s]$	Bankfull discharge
ρ	[-]	Correlation between two parameters
$s(x)$	$[m^2/s]$	Total volumetric streamwise sediment transport per unit width
$S(x)$	$[m^3/s]$	Total volumetric streamwise sediment transport
σ_f	$[m]$	Fluctuation parameter
τ	$[s]$	Morphological time scale
$u(x)$	$[m/s]$	Longitudinal flow velocity
Δx	$[m]$	Longitudinal spatial interval
z_0	$[m]$	Initial bed level
z_{eq}	$[m]$	Equilibrium bed level
$z(t)$	$[m]$	Momentary bed level
$\Delta z(t)$	$[m]$	Momentary difference in bed level

Abbrevation	Description
BWS	Backwater segment
CAH	Cycled annual hydrograph
CDF	Cumulative density function
DVR	Duurzame Vaardiepte Rijndelta
GRDC	Global Runoff Data Center
HBL	Hydrograph boundary layer
MCAH	Multiple cycled annual hydrographs
PDF	Probability density function
QNFS	Quasi normal flow segment
RfR	Room for the River
RMSE	Root mean square error
std.dv.	Standard deviation

Appendices

APPENDIX A

Establishment of the mean and standard deviation of the long-term discharge statistics at Lobith

The same procedure as performed in Section 2.2.3 is executed, but now starting from the year 2010 backwards to 1901. Again, both the mean and the standard deviation tend towards a fairly constant value already after several decades.

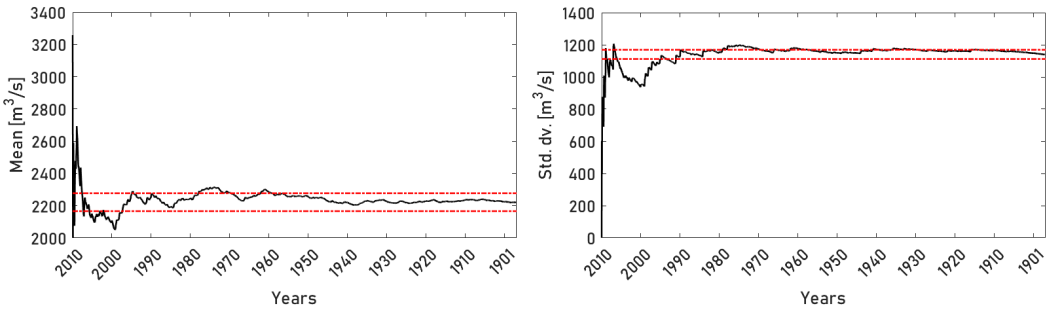

Figure A.1: **(a)** Establishment of the mean and the **(b)** standard deviation of the discharge series at Lobith (black solid line) with respect to the 5% interval around the long-term value for the series 2010-1901 (red dashed line) [source data: GRDC, 2018].

APPENDIX B

Hydrodynamics and sediment transport in the model

B.1 Depth and velocity distribution over the main channel and floodplain

Figure B.1 illustrates the depth averaged velocity and the water depth at both the floodplain and inside the main channel. The conditions previal in the normal flow zone far upstream of the reach with the widened floodplain.

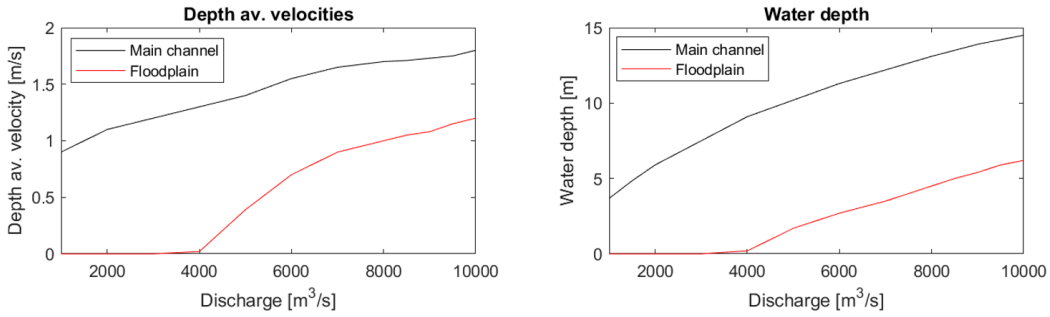

(a) (b)

Figure B.1: **(a)** Velocity distribution over the main channel and the floodplains and **(b)** the water depth in the main channel and at the floodplain for all discrete discharge stages.

B.2 Initial backwater effects

Figure D.3 shows the backwater effects for extreme discharges that are induced by the widened floodplain. Also for the extreme discharges, relatively mild backwaters are initiated, resulting in negligible erosion upstream of the reach with the widened floodplain.

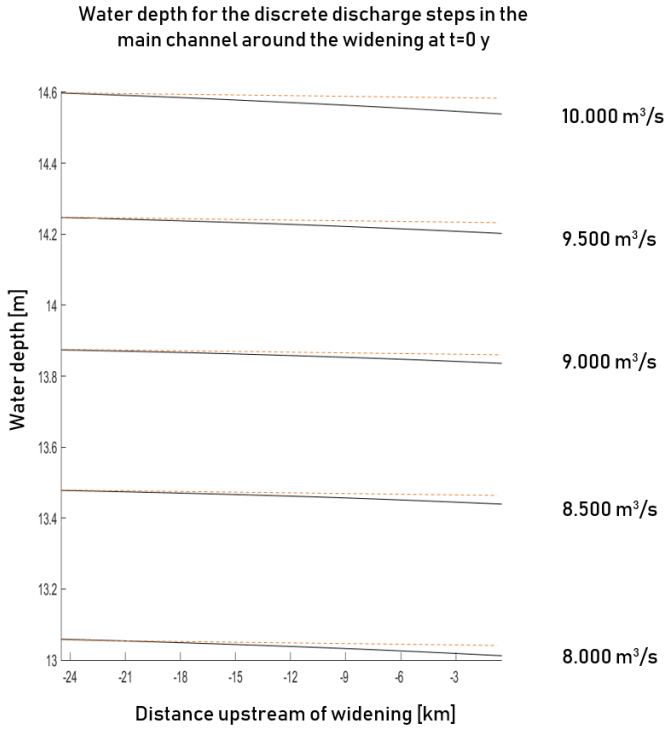

Figure B.2: Backwater effects upstream of the widening for the most extreme discharges.

B.3 Velocity field for a discharge stage of Q=6000m^3/s

In Figures B.3- B.4 the velocity fields are presented for a constant discharge of 6000 m^3/s. The figures show a top view of the velocity fields around the reach with the widened floodplain. The horizontal extraction and contraction of the flow can be observed by means of the flow velocity vectors.

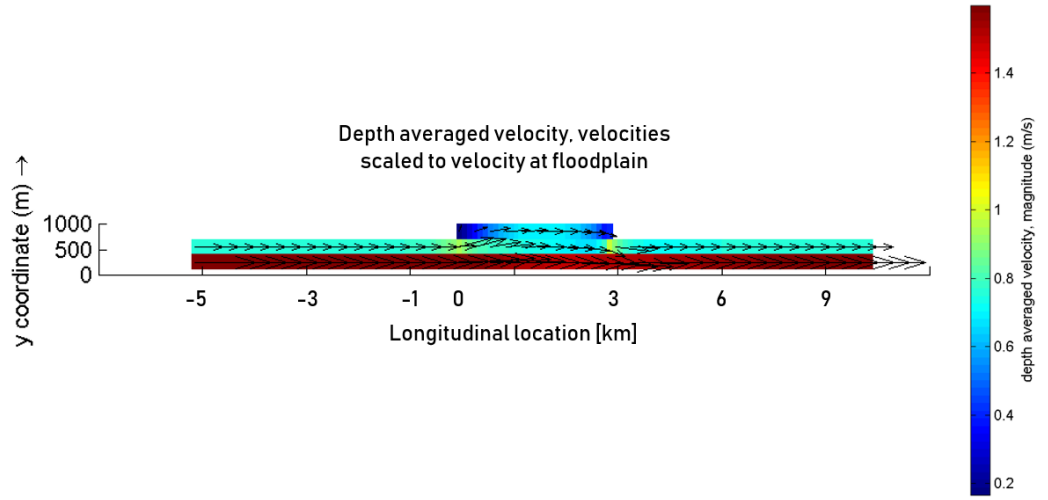

Figure B.3: Velocity field around the widened floodplain, colors scaled to velocities at the floodplains for a steady discharge of Q=6000m^3/s.

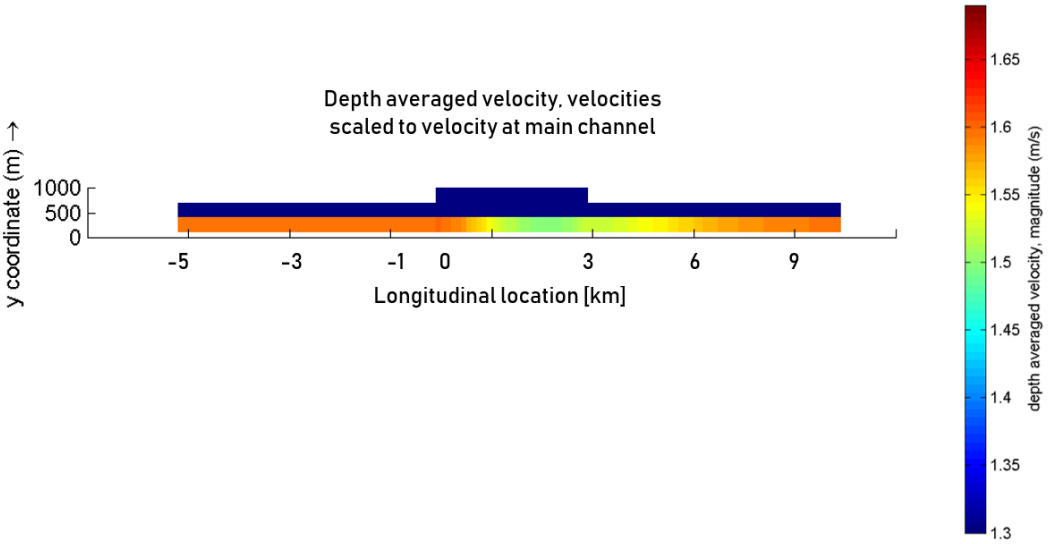

Figure B.4: Velocity field around the widened floodplain, colors scaled to velocities in the main channel for a steady discharge of Q=6000m^3/s.

B.4 Bed level changes with different longitudinal grid sizes

Figure B.5 shows a comparison of the bed level changes that are calculated with the numerical model. They represent the bed level change for imposing a steady discharge of 6000 m^3/s for one year. The computed bed level changes are similar.

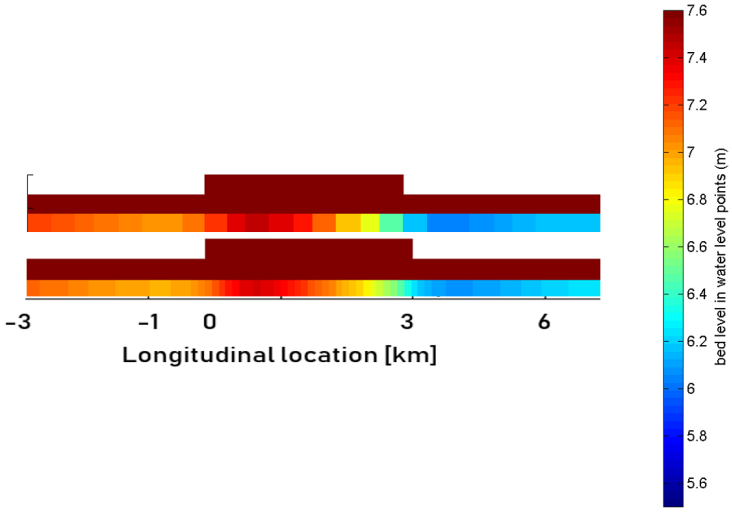

Figure B.5: Computed bed level with a longitudinal grid cell size of 300 m (top) and 100 m (bottom).

B.5 Sediment transport for all discrete discharge stages

The longitudinal bed sediment transport for four discharge magnitudes are presented during the first year (Figure B.6a) and after 40 years (Figure B.6b).

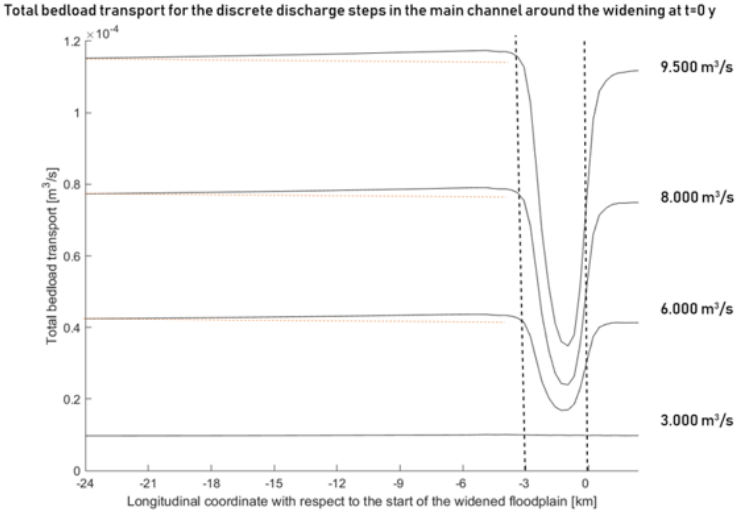

(a)

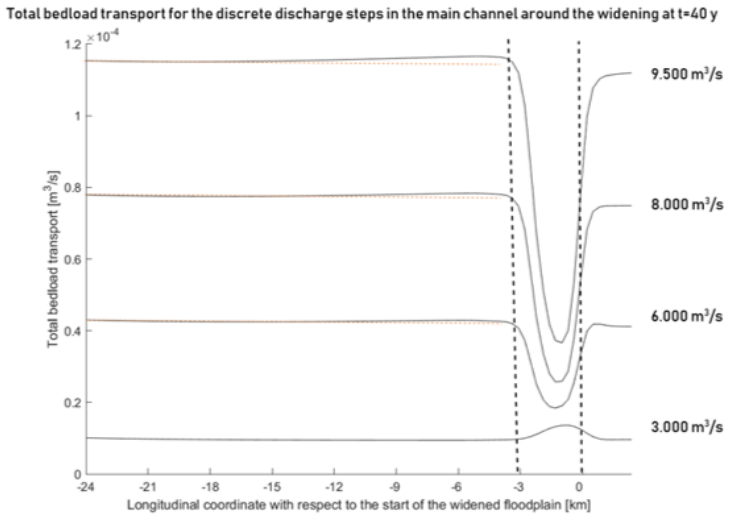

(b)

Figure B.6: Bed load transport **(a)** initially and **(b)** after 40 years. The vertical dashed lines represent the location of the widened floodplain.

APPENDIX C

Morphodynamic changes in the model

C.1 Time development of the D_{50} for the natural discharge series 1971-2010

Figure C.1 shows the time development of the D_{50} of the river bed at the studied locations.

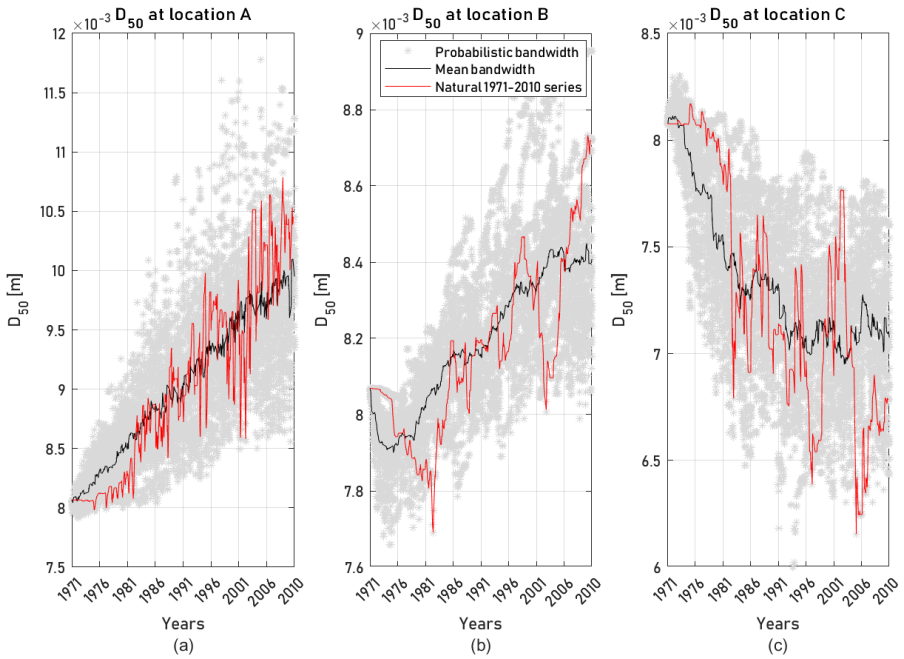

Figure C.1: The time development of the D_{50} of the bed sediment at locations **(a)** A, **(b)** B and **(c)** C for the Monte Carlo realisations (gray), the mean of the probabilistic bandwidth (black) and the natural 1971-2010 discharge time series (red).

At locations A and B, a coarsening trend is observed. M. Tewolde (personal communication, June 6., 2019) states that a possible cause for this coarsening trend is the fact that the future equilibrium flow velocity at the reach with the widened floodplain (that belongs to the future equilibrium bed conditions and sediment flux) will be lower compared to the equilibrium flow velocity in the river prior to when the river intervention was installed. Consequently, the relative mobility difference of the fine and coarse sediment fractions of the bed sediment increases and relatively much fine material is transported. As a result, the river bed coarsenes whereas sedimentation is observed. At location C, other effects might become important that decrease the mobility difference between coarse and fine fractions: the hiding effect. Hiding effects make the coarse grains easier to be transported and decreases the mobility of the finer grains in the bed sediment mixture (Wilcock and Crowe, 2003). This effect possibly contributes to the observed trends as well. Modelling with mixed sediments proves to be an extremely complicated task. Sloff (personal communication, June 4., 2019) states that these trends in bed sediment composition, in combination with the observed trends in bed level are observed in practical models as well. Similar observations are found in model simulations by Tewolde. A clear, complete scientific explanation is however still not found.

C.2 Instantaneous bed level changes at B and C with the natural discharge series 1971-2010

The instantaneous response at locations B and C is disturbed by the bed waves that are generated at location A and approach locations B and C with a certain time lag. They are therefore not considered further and are presented in Figure C.2 here only for completeness.

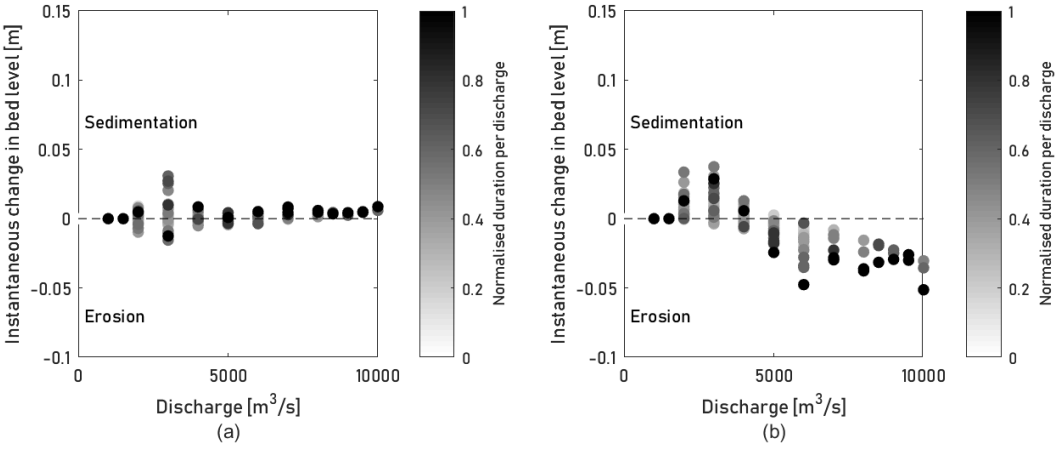

Figure C.2: Instantaneous bed level change at locations **(b)** B and **(c)** C for the natural series of 1971-2010.

C.3 Time development of the D_{50} for the CAH-series

Similar differences can be noticed in long-term bed level development for the D_{50} of the bed sediment at all three locations. The results are presented in Figure C.3.

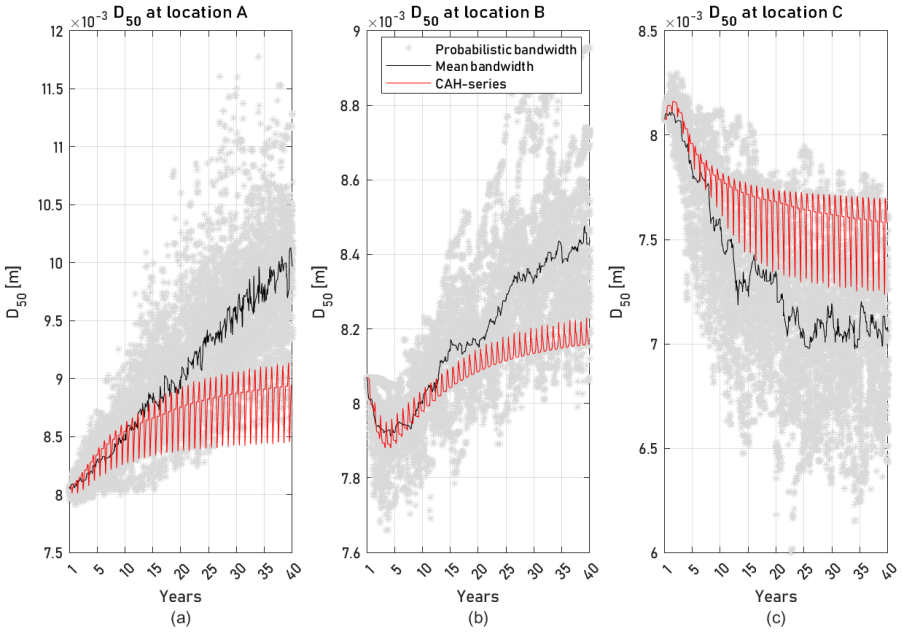

Figure C.3: The time development of the D_{50} of the bed sediment at locations **(a)** A, **(b)** B and **(c)** C for the Monte Carlo realisations (gray), the mean of the probabilistic bandwidth (black) and the CAH series.

C.4 Instantaneous bed level changes at B and C with the CAH-series

The instantaneous bed level changes are presented in Figure C.4. The analysis is disturbed by bed level waves that are generated upstream of the considered locations.

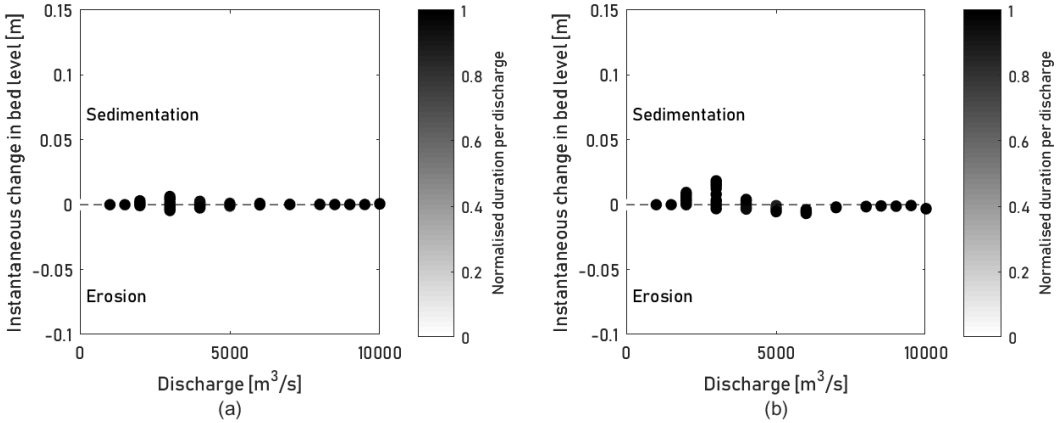

Figure C.4: Instantaneous change at locations **(b)** B and **(c)** C using the CAH-series.

Cumulative intantaneous response at location B with the CAH-series

The analyes of the cumulative instantaneous change for all discharges are added for completeness as the analyses are disturbed by bed waves that are generated upstream in case of the CAH-series. The results are presented in Figure C.5. The integrated change for discharge stages below and above bankfull discharge is presented in Table C.1.

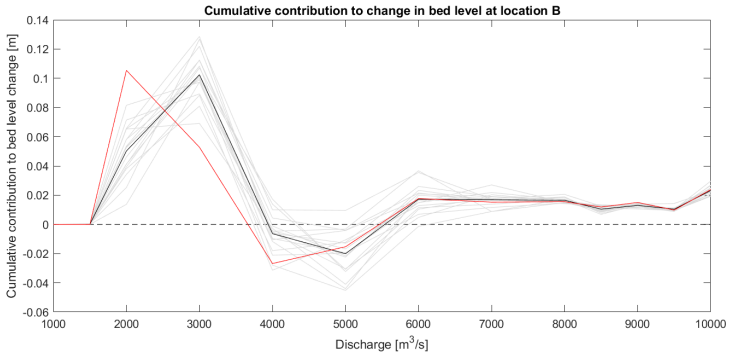

Figure C.5: Cumulative instantaneous response at location B for the mean of the probabilistic series (black) and the CAH-series (red). The according properties are given in Table C.1.

Table C.1: Comparison of the sum of the cumulative contribution of discharge below and above bankfull discharge as well as the net cumulative effect at location B.

Series	**Sum cum. cont.** $Q \leq Q_{bf}$	**Sum cum. cont.** $Q > Q_{bf}$	**Net change [m]**
Prob. series	$+0.15m$	$+0.09m$	$+0.23m$
SAYH series	$+0.13m$	$+0.09m$	$+0.22m$

Cumulative intantaneous response at location C with the CAH-series

The same is shown for location C in Figure C.6 and Table C.2.

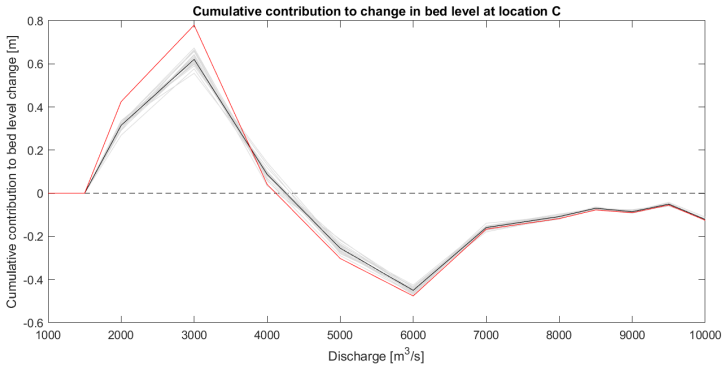

Figure C.6: Cumulative instantaneous response at location C for the mean of the probabilistic series (black) and the CAH-series (red). The according properties are given in Table C.2.

Table C.2: Comparison of the sum of the cumulative contribution of discharge below and above bankfull discharge as well as the net cumulative effect at location C.

Series	**Sum cum. cont.** $Q \leq Q_{bf}$	**Sum cum. cont.** $Q > Q_{bf}$	**Net change [m]**
Prob. series	$+1.02m$	$-1.3m$	$-0.27m$
SAYH series	$+1.25m$	$-1.41m$	$-0.16m$

C.5 Instantaneous bed level changes for the modified symmetric hydrograph series

The instantaneous bed level changes are presented in Figure C.7. The analysis is disturbed by bed level waves that are generated upstream of the considered locations. They are added for completeness.

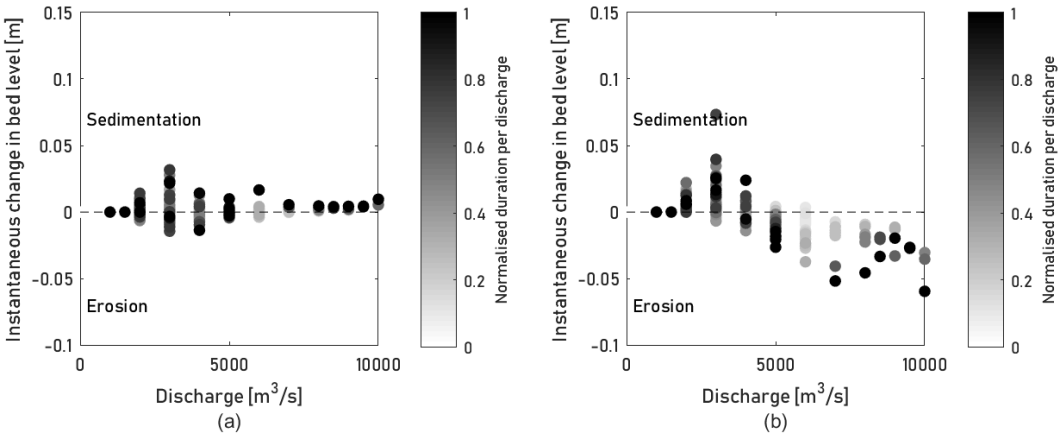

Figure C.7: Instantaneous change at locations **(b)** B and **(c)** C using the modified, symmetric hydrograph series from 1971-2010.

Cumulative intantaneous response at location B

The analyes of the cumulative instantaneous change for all discharges are added for completeness as the analyses are disturbed by bed waves that are generated upstream. The results are presented in Figure C.8. The integrated change for discharge stages below and above bankfull discharge is presented in Table C.3.

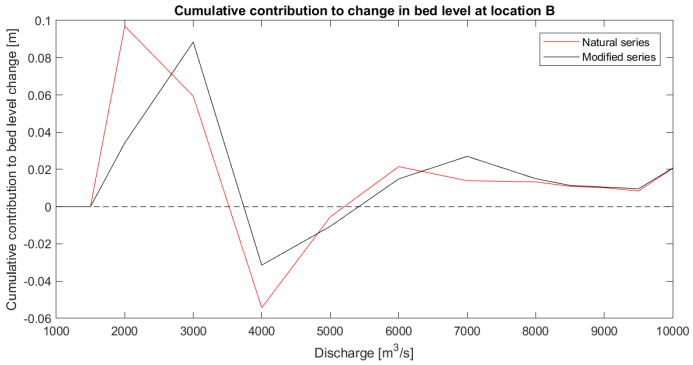

Figure C.8: Cumulative instantaneous response at location B for the natural series 1971-2010 (red) and the modified series in which the years have been simplified into yearly, assymetric hydrographs (black). The according properties are given in Table C.3.

Table C.3: Comparison of the sum of the cumulative contribution of discharge below and above bankfull discharge as well as the net cumulative effect.

Series	**Cum. cont.** $Q \leq Q_{bf}$	**Cum. cont.** $Q > Q_{bf}$	**Net change [m]**
Natural series	$+0.10m$	$+0.09m$	$+0.19m$
Modified series	$+0.09m$	$+0.10m$	$+0.19m$

Cumulative intantaneous response at location C

The same is done for location C. The results are presented in Figure C.9 and Table C.4.

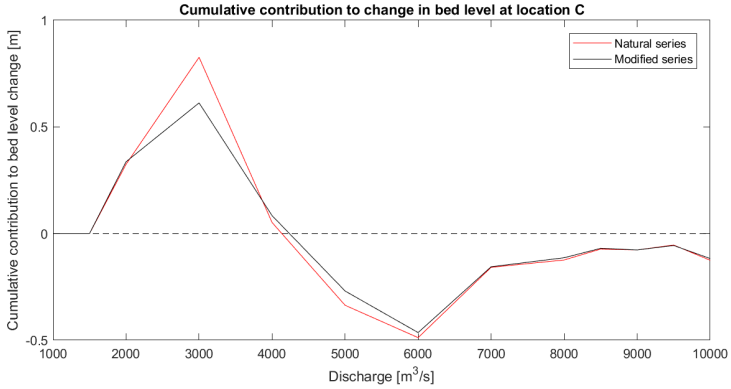

Figure C.9: Cumulative instantaneous response at location C for the natural series 1971-2010 (red) and the modified series in which the years have been simplified into yearly, assymetric hydrographs (black). The according properties are given in Table C.4.

Table C.4: Comparison of the sum of the cumulative contribution of discharge below and above bankfull discharge as well as the net cumulative effect.

Series	**Cum. cont.** $Q \leq Q_{bf}$	**Cum. cont.** $Q > Q_{bf}$	**Net change [m]**
Natural series	$+1.20m$	$-1.44m$	$-0.23m$
Modified series	$+1.03m$	$-1.32m$	$-0.29m$

APPENDIX D

Results from the MCAH-series

D Time development of the D_{50} for 2, 4 and 6 MCAHs

In the following figures, the long-term development of the D_{50} of the river bed is presented for series with 2, 4 and 6 MCAHs. In each figure, the morphodynamic response to the CAH-series presented as well in order to demonstrate the improvements that are made with the MCAH-series.

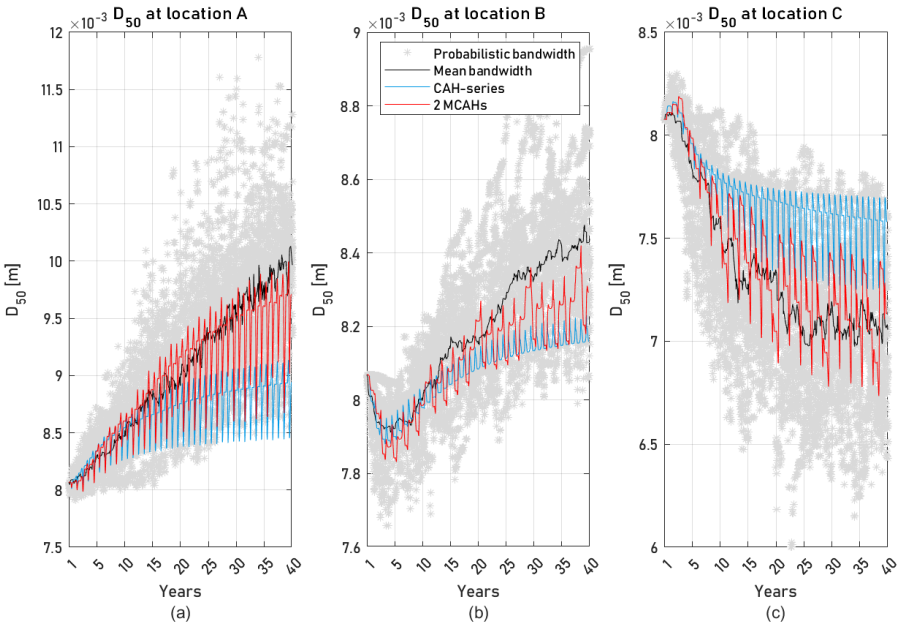

Figure D.1: Time development of the D_{50} of the river bed at locations **(a)** A, **(b)** B and **(c)** C using 2 MCAHs (red) compared to the mean development from the Monte Carlo realisations (gray). The response to the CAH-series is presented as well (blue).

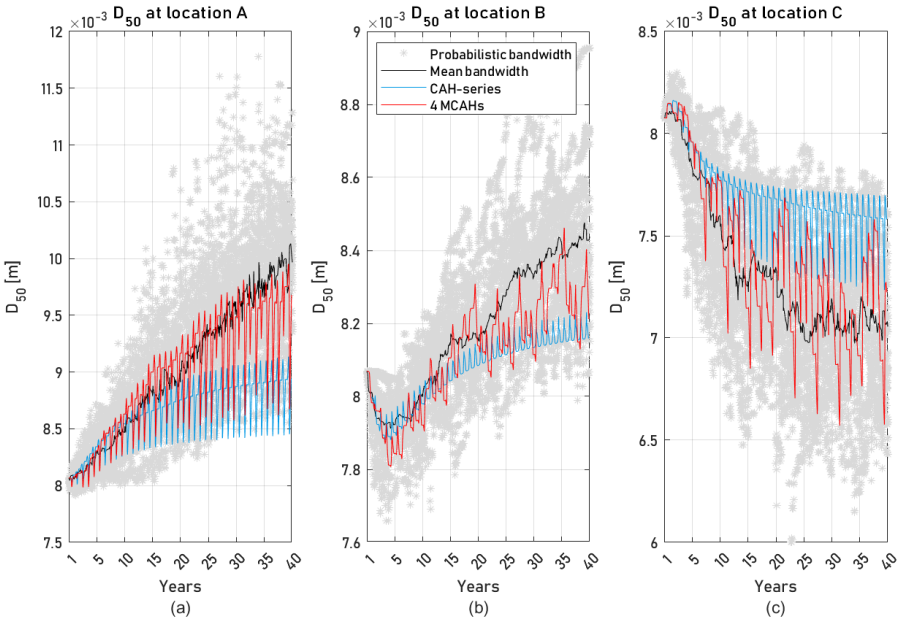

Figure D.2: Time development of the D_{50} of the river bed at locations **(a)** A, **(b)** B and **(c)** C using 4 MCAHs (red) compared to the mean development from the Monte Carlo realisations (gray). The response to the CAH-series is presented as well (blue).

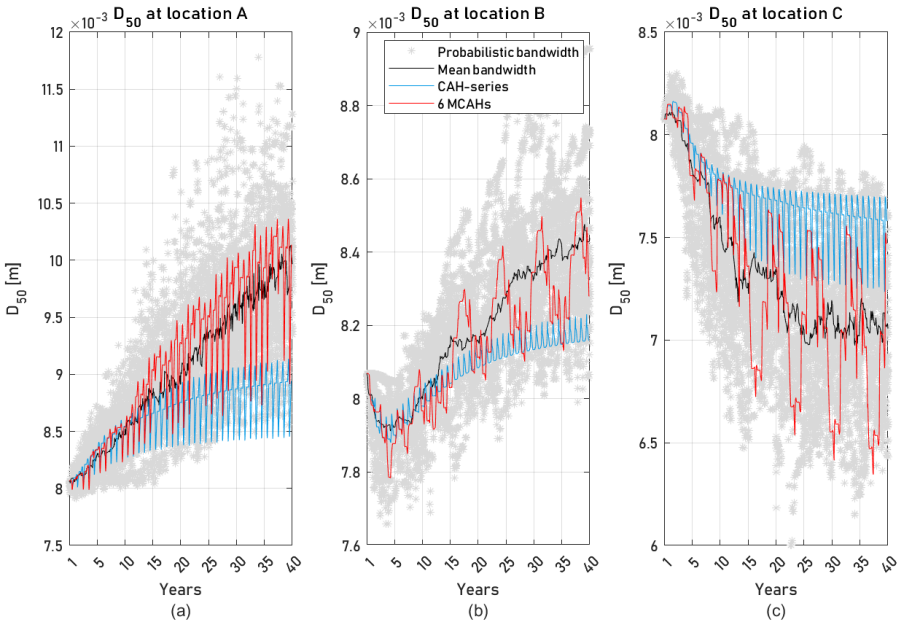

Figure D.3: Time development of the D_{50} of the river bed at locations **(a)** A, **(b)** B and **(c)** C using 6 MCAHs (red) compared to the mean development from the Monte Carlo realisations (gray). The response to the CAH-series is presented as well (blue).

Notes

TU Delft